UNCLASSIFIED

AD NUMBER

AD911532

NEW LIMITATION CHANGE

TO

Approved for public release, distribution unlimited

FROM

Distribution authorized to U.S. Gov't. agencies only; Test and Evaluation; MAY 1973. Other requests shall be referred to Air Force Flight Dynamic Laboratory, Wright-Patterson AFB, OH 45433.

AUTHORITY

AFFDL ltr, 27 Aug 1979

THIS PAGE IS UNCLASSIFIED

THIS REPORT HAS BEEN DELIMITED
AND CLEARED FOR PUBLIC RELEASE
UNDER DOD DIRECTIVE 5200.20 AND
NO RESTRICTIONS ARE IMPOSED UPON
ITS USE AND DISCLOSURE.

DISTRIBUTION STATEMENT A

APPROVED FOR PUBLIC RELEASE;
DISTRIBUTION UNLIMITED.

AFFDL-TR-72-138
Volume I

AD 911532

AEROACOUSTIC LOADS ASSOCIATED WITH HIGH BETA RE-ENTRY VEHICLES

L. E. CHAUMP, A. MARTELLUCCI, A. MONFORT

GENERAL ELECTRIC COMPANY

TECHNICAL REPORT AFFDL-TR-72-138, VOLUME I

MAY 1973

D D C
RECEIVED
JUL 10 1973
B

Distribution limited to U.S. Government agencies only; test and evaluation, statement applied 28 November 1972. Other requests for this document must be referred to AF Flight Dynamics Laboratory, (FY), Wright-Patterson AFB, Ohio 45433.

AIR FORCE FLIGHT DYNAMICS LABORATORY
AIR FORCE SYSTEMS COMMAND
WRIGHT-PATTERSON AIR FORCE BASE, OHIO

NOTICE

When Government drawings, specifications, or other data are used for any purpose other than in connection with a definitely related Government procurement operation, the United States Government thereby incurs no responsibility nor any obligation whatsoever; and the fact that the government may have formulated, furnished, or in any way supplied the said drawings, specifications, or other data, is not to be regarded by implication or otherwise as in any manner licensing the holder or any other person or corporation, or conveying any rights or permission to manufacture, use, or sell any patented invention that may in any way be related thereto.

Copies of this report should not be returned unless return is required by security considerations, contractual obligations, or notice on a specific document.
AIR FORCE/56780/29 June 1973 — 150

AEROACOUSTIC LOADS ASSOCIATED WITH HIGH BETA RE-ENTRY VEHICLES

L. E. CHAUMP, A. MARTELLUCCI, A. MONFORT

GENERAL ELECTRIC COMPANY

Distribution limited to U.S. Government agencies only; test and evaluation, statement applied 28 November 1972. Other requests for this document must be referred to AF Flight Dynamics Laboratory, (FY), Wright-Patterson AFB, Ohio 45433.

FOREWORD

This report was prepared by the General Electric Company, Re-entry and Environmental Systems Division, Philadelphia, Pennsylvania under Contract F33615-71-C-1245. This contract was sponsored by the Air Force Flight Dynamics Laboratory under Project 1471 "Aero-Acoustic Problems in Flight Vehicles", Task 147102 "Aero-Acoustic". Mr. D. L. Smith of AFFDL/FYA was the Project Engineer.

This report consists of two volumes. Volume I summarizes the complete results of the effort and Volume II contains the experimental data from which the final results were determined.

The authors gratefully acknowledge the assistance of D. L. Smith and R. D. Talmadge of AFFDL/FYA for their efforts in data reduction; D. Rogers and F. George for model instrumentation and wind tunnel support; and J. Howe and C. Parks for their assistance in data analysis.

The report concludes the work on Contract F33615-71-C-1245 which covered a period from February 1971 to January 1973. The manuscript was released by the authors for publication on 29 September 1972.

This report has been reviewed and is approved.

WALTER J. MYKYTOW
Asst. for Research & Technology
Vehicle Dynamics Division
AF Flight Dynamics Laboratory

ABSTRACT

Conical shaped vehicles with high ballistic coefficients are subjected during re-entry, to intense fluctuating air pressures which result in high internal sound and vibration levels. As a result of these high vibration levels, internal components can be adversely affected. In order to insure reliability, vibration test criteria are predicted based on limited experimental data at high Mach numbers and generally result in conservatism of the design. This program using prior experimental data and high Mach number data obtained in the present contract, reviews existing analytical expressions necessary to define aeroacoustic loads associated with high beta re-entry vehicles and recommends analytical expressions for transitional, fully developed turbulent, separated and base flow.

TABLE OF CONTENTS

PRECEDING PAGE BLANK-NOT FILMED

Section	Title	Page
I	INTRODUCTION	1
II	CONCLUSIONS AND RECOMMENDATIONS	2
	1. ATTACHED TURBULENT BOUNDARY LAYER	2
	2. TRANSITIONAL BOUNDARY LAYER FLOW	3
	3. SEPARATED FLOW	3
	4. BASE FLOW	4
III	PRIOR EXPERIMENTAL DATA REVIEW	6
	1. ATTACHED TURBULENT BOUNDARY LAYER FLOW	6
	a. Acoustic Magnitude	6
	b. Acoustic Power Spectral Density	6
	c. Cross Correlation Functions	6
	d. Convection Velocity	14
	2. TRANSITIONAL BOUNDARY LAYER FLOW	18
	a. Acoustic Magnitude	18
	b. Acoustic Power Spectral Density	20
	3. SEPARATED FLOW	22
	a. Acoustic Magnitude	22
	b. Acoustic Power Spectral Density	23
	c. Cross Correlation Functions	31
	d. Convection Velocity	31
	4. BASE FLOW	31
	a. Base Flow Acoustic Intensity and Spectra	35
IV	PRIOR PREDICTION METHODS REVIEW	40
	1. ATTACHED TURBULENT BOUNDARY LAYER FLOW	40
	a. Acoustic Magnitude	40
	b. Acoustic Power Spectral Density	41
	c. Cross-Correlation Functions	44
	d. Convection Velocity	50
	2. SEPARATED FLOW	51
	a. Acoustic Magnitude	51
	b. Acoustic Power Spectral Density	53
	c. Cross-Correlation Function	55

TABLE OF CONTENTS (Continued)

Section	Title	Page
	3. BASE FLOW	57
	a. Acoustic Magnitude	58
	b. Acoustic Power Spectral Density	59
	c. Cross Correlation	60
V	SUMMARY OF TEST RESULTS	62
	1. ACOUSTIC MAGNITUDE	62
	2. POWER SPECTRAL DENSITY	64
	3. CROSS CORRELATION FUNCTIONS	76
	4. CONVECTION VELOCITY	76
VI	PREDICTION METHODS REFINEMENT	79
	1. ATTACHED TURBULENT BOUNDARY LAYER FLOW	79
	a. Acoustic Magnitude	79
	b. Acoustic Power Spectral Density	82
	c. Cross-Correlation Functions	86
	d. Convection Velocity	88
	2. TRANSITIONAL BOUNDARY LAYER FLOW	88
	a. Acoustic Magnitude	90
	b. Acoustic Power Spectral Density	93
	c. Cross Correlation Functions	100
	d. Convection Velocity	101
	3. BASE FLOW	101
	a. Acoustic Magnitude	101
	b. Acoustic Power Spectral Density and Correlation Function	102
VII	REFERENCES	106
APPENDIX	ENGINEERING RELATIONS/GRAPHS FOR THE DETERMINATION OF LOCAL FLOW PROPERTIES ON SHARP BODIES	A-1

LIST OF ILLUSTRATIONS

Figure	Title	Page
1	Root Mean Square Pressure Fluctuation Vs. Mach Number for Attached Turbulent Flow	7
2	Normalized Power Spectra of Pressure Fluctuation for $M_\infty < 1$	8
3	Normalized Power Spectra of Pressure Fluctuation for $M_\infty > 1$ Using δ^* as Normalizing Parameter	9
4	Normalized Power Spectra of Pressure Fluctuation for $M_\infty > 1$ Using δ as Normalizing Parameter	10
5	Narrow Band Longitudinal Space Correlation Coefficient for Attached Turbulent Flow	11
6	Narrow Band Lateral Space Correlation Coefficient for Attached Turbulent Flow(11)	12
7	Narrow Band Space-Time Correlation Coefficients for Attached Turbulent Flow(11)	13
8	Asymptotic Values of Narrow Band Pressure Coefficients for Attached Turbulent Flow	15
9	Longitudinal Broad Band Space Time Correlation for Attached Turbulent Flow	16
10	Lateral Broad Band Space-Time Correlation for Attached Turbulent Flow	17
11	Variation of Broad Band Convection Velocity With Separation Distance	17
12	Variation of Narrow Band Convection Velocity With Frequency for Various Separation Distances	18
13	Root Mean Square Pressure Fluctuations Peak Value Represents Transitional Flow	19
14	Root Mean Square Pressure Fluctuations Vs. Free Stream Mach Number	20
15	Transitional Flow Spectral Distribution Obtained in Wind Tunnel Experiments	21
16	Comparison of Transition and Turbulent Flow Pressure Spectra Measured in Flight	21
17	Comparison of Acceleration Spectra Measured in Transitional and Fully Turbulent Flow	22
18	Overall Acoustic Magnitude Vs. Local Mach Number for Expansion Induced Separated Flow(1)	23
19	Overall Acoustic Magnitude Vs. Free Stream Mach Number for Separated Flow Upstream of Compression Corners(1)	24
20	Acoustic Magnitude Distribution Representing Shock Separation and Reattachment	25
21	Normalized (Using δ) Pressure Spectra Representative of Separated Flow (Prel. Data Taken from Ref. 16 With Permission From NASA Ames)	26

LIST OF ILLUSTRATIONS (Continued)

Figure	Title	Page
22	Normalized (Using $S-X_s$) Pressure Spectra Representative of Separated Flow (Preliminary Data Taken From Ref. 16 With Permission From NASA Ames)	27
23	Comparison of Normalization Technique for Separated Flow Spectra	28
24	Comparison of Expansion and Compression Induced Separated Flow Spectra(5)	29
25	Comparison of Power Spectra for Shock-Wave Oscillation Induced by Two and Three Dimensional Protuberances(1)	30
26	Normalized Narrow Band Longitudinal Cross Spectra for Separated Flow(14)	32
27	Coherence Function for Attached and Separated Flow(4)	33
28	Broad Band Space Correlation Function for Attached and Separated Flow(4)	34
29	Correlation of Pressure Fluctuations Between Shock Wave and Adjacent Attached and Separated(1) Flow	35
30	Narrow Band Convection Velocities in Separated Flow Vs. Strouhal Number(4)	36
31	Narrow Band Convection Velocities Using Separation Distance as Normal (Preliminary Data Taken from Ref. 16 With Permission from NASA Ames)	37
32	Typical Unnormalized Narrow Band Convection Velocity for Separated Flow (Preliminary Data Taken from Ref. 16 With Permission From NASA Ames)	38
33	Typical Spectral Distribution in Base Flow (Subsonic)	39
34	Comparison of Overall Acoustic Magnitude Prediction Methods to Experimental Data	42
35	Comparison of Normalized Power Spectra Prediction Methods to Experimental Data	45
36	Comparison of Lowson's Normalized Power Spectra (Using δ) to Experimental Data	46
37	Comparison of Frequency Dependent Narrow Band Long. Space Correlation Coefficient with Analytical Expression	47
38	Comparison of Frequency Dependent Narrow Band Lat. Space Correlation Coefficient with Analytical Expression	48
39	Comparison of Spatial Dependent Long. and Lat. Correlation with Analytical Expressions	49
40	Comparison of Overall Acoustic Magnitude for Separated Flow With Analytical Predictions	52
41	Comparison of Overall Acoustic Magnitude at the Point of Flow Separation With Analytical Predictions	53

LIST OF ILLUSTRATIONS (Continued)

Figure	Title	Page
42	Comparison of Separated Flow Power Spectra With Analytical Expression	54
43	Comparison of Shock-Wave Oscillation Spectral Distribution to Analytical Prediction	56
44	Typical Base Flow	58
45	Comparison of Spectral Wake Theory with Test Results	61
46	Fluctuating Pressure Distribution Tunnel Condition ($R_{e_\infty} = 2.8 \times 10^6$, $M_\infty = 4$, $R_N = 0.0$)	68
47	Acoustic Intensity Distribution, dB at High α ($\pm 7.2°$)	69
48	Base Acoustic Intensity Distribution (dB) at Various Reynolds Numbers and Mach Numbers ($\alpha = 0°$)	70
49	Normalized Turbulent Flow Spectra for Various Mach Numbers	71
50	Normalized Power Spectral Density Distribution for Transitional Flow $M_\infty = 8$	72
51	Variation of Transition Spectra in Transition Zone ($M_\infty = 4$, $Re_\infty = 1.4 \times 10^6$, $R_N = 0$)	73
52	Comparison of Pressure Spectra in Circumferential Direction (Separated Flow Leeward Sensors), $M_\infty = 8$, $Re_\infty = 2.8 \times 10^6$	74
53	Comparison of Base Flow Pressure Spectra for Various α (Base Center), $M_\infty = 4$, $Re_\infty = 2.2 \times 10^6$	75
54	Broad Band Correlation Functions for Various Flow Conditions	77
55	Comparison Between Turbulent and Transitional Broad Band Convection Velocity	78
56	Comparison of Overall Acoustic Magnitude Prediction Methods to Experimental Data	80
57	Root Mean Square Pressure Fluctuation Vs Mach Number for Attached Turbulent Flow	81
58	Normalized Power Spectral Density Distribution for Turbulent Flow $M_\infty = 4.0$	83
59	Normalized Power Spectral Density Distribution for Turbulent Flow $M_\infty = 8.0$	84
60	Normalized Power Spectral Density Distribution for Turbulent Flow $M_\infty = 10.0$	85
61	Comparison of Present Normalized Power Spectral Density to that of Other Experimenters	87
62	Root Mean Square Pressure Fluctuations vs. Free Stream Mach Number - Transitional Flow	91
63	Comparison of Transitional and Full Turbulent RMS Pressure Fluctuations vs. Mach Number	91
64	Transitional Acoustic Magnitude Vs. Local Mach Number	92
65	Normalized Power Spectral Density Distribution for Transitional Flow $M_\infty = 4$	94

LIST OF ILLUSTRATIONS (Continued)

Figure	Title	Page
66	Normalized Power Spectral Density Distribution for Transitional Flow $M_\infty = 8$	95
67	Normalized Power Spectral Density Distribution for Transitional Flow $M_\infty = 10$	96
68	Transitional Flow Spectral Distribution Obtained in Wind Tunnel Experiments ($M_\infty = 4$)	97
69	Typical $M_\infty = 4$ Normalized Spectra for Fully Turbulent and Transitional Flow	97
70	Functional Relationship of Transitional and Fully Turbulent Characteristic Length Parameters	100
71	Overall Acoustic Intensity for Base Flow (Prediction vs Test)	102
72	Normalized Base Acoustic Spectra ($M_\infty = 4$)	104
73	Normalized Base Acoustic Spectra ($M_\infty = 4$)	104
74	Normalized Base Acoustic Spectra ($M_\infty = 8$)	105

LIST OF TABLES

Table	Title	Page
I	Summary of Nominal Test Conditions	63
II	Summary of Free Stream Conditions	64
III	Local Flow Properties ($\alpha = 0°$)	65
IV	Acoustic Gage Locations	66
V	Acoustic Intensity for Turbulent Flow	67
VI	Peak Acoustic Intensity in Transitional Flow	67
VII	Prediction vs. Test Acoustic Intensity (Turbulent Flow)	82
VIII	List of Applicable Transition Cases	89

SYMBOLS

C_f	=	Skin friction coefficient
C_p	=	Static pressure coefficient
d	=	Base diameter
f	=	Frequency cycles per second
h	=	Step height
h_r	=	Recovery enthalpy
h_w	=	Wall enthalpy
L	=	Scale of base turbulence
M	=	Mach number
P	=	Static pressure
P_r	=	Prandtl Number
$P_{rms}, \bar{P}$	=	Root mean square acoustic pressure
q	=	Dynamic pressure
$\dot{q}$	=	Heat transfer
R_e	=	Reynolds number p. r ft.
R_{e_s}	=	Local wetted length Reynolds number
R_n	=	Nose radius
$R_{(\xi, \eta, \tau)}$	=	Broad-band space time correlation
$R_{pp}(\xi, \eta, \omega)$	=	Narrow band space time correlation coefficient
r	=	Base radius
r_e	=	Defined in equation 4
r_i	=	Recovery factor
S	=	Apparent wake cone surface length

SYMBOLS (Continued)

$(S-X_s)$	=	Distance from shock wave to sensor
t	=	Time
T	=	Temperature
T_w	=	Temperature of wall
U	=	Velocity
$\overline{U}$	=	Velocity at edge of laminar flow region sublayer
$u(f)$	=	Convection velocity - narrow band
U_c, U_{cb}	=	Convection velocity, broad band convection velocity
V_T	=	Effective transport velocity
X_s	=	Longitudinal distance measured upstream from shoulder of cone frustum
α	=	Angle of attack
$\bar{\gamma}$	=	Ratio of specific heats
γ	=	Coherence function
δ	=	Boundary layer thickness
δ^*	=	Boundary layer displacement thickness
η	=	Lateral separation distance between two points (normal to flow)
θ	=	Boundary Layer Momentum thickness
θ_c	=	Cone half angle
μ	=	Coefficient of viscosity
ξ	=	Longitudinal separation distance between two points (in direction of flow)
ρ	=	Density
ω	=	Frequency - radians per second

SUBSCRIPTS

b	=	Base
e	=	Quantity evaluated at boundary layer edge.
o	=	Stagnation conditions
∞	=	Quantity evaluated at free stream
s	=	Quantity evaluated at a wetted length s
t	=	Quantity evaluated at end of transition

SECTION I

INTRODUCTION

During re-entry into the earth's atmosphere, vehicles are subjected to intense fluctuating aerodynamic pressures. As a result, significant vibration response can occur, affecting the performance of components within the vehicle. In order to accurately assess this problem, it is necessary to define the nature of the acoustic environment for various aerodynamic flows with vehicles during re-entry. This has become more important as mission requirements have resulted in higher velocities at relatively lower altitudes.

The purpose of the program undertaken in the present study was to measure the aeroacoustic environment on the surface of a smooth, conical body and use the results to upgrade current analytical formulations. The experiments were conducted at Mach 4, 8, and 10 for several values of free stream Reynolds number, angle of attack and three bluntness ratios.

For the various tunnel conditions and model attitudes, fluctuating pressure measurements were made in fully turbulent flow and at the base of the test vehicle. Two other areas investigated were pressure fluctuation in the transition region where flow changes from laminar to turbulent flow and separated flow resulting from angles of attack equal to the cone half angle of the test vehicle. A sufficient amount of acoustic sensors were located on the vehicle to define fluctuating pressure levels acting along the vehicle.

SECTION II

CONCLUSIONS AND RECOMMENDATIONS

The following formulae are recommended to describe the acoustic magnitude, spectra and cross spectra and cross spectra coefficients for various flow conditions:

1. ATTACHED TURBULENT BOUNDARY LAYER

Magnitude

$$\frac{P_{rms}}{q_e} = \frac{0.007}{1 + r_e \left(\frac{\bar{\gamma} - 1}{2}\right) M_e^2} \qquad \text{(Tol. } \pm 2 \text{ dB)} \tag{3}$$

where $r_e = (1 - \bar{U}/U_e)(r_1 + \bar{U}/U_e)$ (4)

or

$$\frac{P_{rms}}{q_e} = \frac{0.006}{1 + .14 M_e^2}, \; M < 5 \qquad \text{(Tol. } \pm 2 \text{ dB)} \tag{6}$$

$$\frac{P_{rms}}{q_e} = \frac{0.002}{1 + 0.02 M_e^2}, \; M > 5 \qquad \text{(Tol. } \pm 2 \text{ dB)} \tag{44}$$

Spectra

$$\phi(\omega) = \frac{2\delta^*}{\pi U_c} P_{rms}^2 \frac{1}{1 + \left(\frac{\omega\delta^*}{U_c}\right)^2} \tag{11}$$

Cross Spectra coefficients

$$A_\eta(\eta, \omega) = \exp\left(-0.72|\eta|\frac{\omega}{U_e}\right)\left[0.3 + 0.7 \exp\left(\frac{-0.5|\eta|}{\delta^*}\right)\right] \tag{20}$$

$$A_\xi(\xi, \omega) = \exp\left(-0.1\left|\frac{\xi}{U_e}\right|\omega\right)\exp\left(-0.034\frac{|\xi|}{\delta^*}\right) \tag{21}$$

(The above coefficients are expressions for the cross spectra Eqs. 16, 17).

2. TRANSITIONAL BOUNDARY LAYER FLOW

Magnitude

$$\frac{P_{rms}}{q_e} = \frac{0.0041}{1 + 0.013\, M_e^{\,2}} \qquad \text{(Tol. } \pm 2 \text{ dB)} \tag{46}$$

Spectra

$$\phi\,(f) = \frac{4\left(\frac{\delta_t}{U_e}\right) P_{rms}^2}{1 + \left[\, 2\pi f\, \delta_t \,/_{U_e}\, \right]^2} \tag{56}$$

Cross Spectra coefficients

$$A_\eta\,(\eta,\ \omega) = \exp\left(-0.72 \left|\eta\right| \frac{\omega}{U_c}\right) \left[0.3 + 0.7 \exp\left(\frac{-0.5\left|\eta\right|}{\delta^*}\right)\right] \tag{20}$$

$$A_\xi\,(\xi,\ \omega) = \exp\left(-0.1\, \frac{\left|\xi\right|}{U_c}\ \omega\right) \exp\left(-0.034\ \frac{\left|\xi\right|}{\delta^*}\right) \tag{21}$$

3. SEPARATED FLOW (1)

(Expansion Induced Separated Flow)

Magnitude

$$\frac{P_{rms}}{q_\infty} = \frac{0.045}{1 + M_e^2} \qquad \text{(Tol. } \pm 2 \text{ dB)} \tag{27}$$

Spectra

$$\phi\ (f) = \frac{5.9\,\delta\ /U_e\, P_{rms}^2}{\left\{ 1 + \left(\frac{\delta\ \ f}{0.17\ U_e}\right)^{0.83} \right\}^{2.15}} \tag{29}$$

Cross Spectra Coefficients

$$A_\eta\left(\eta, \frac{f\delta}{U_e}\right) = \exp(-.75\eta), \frac{f\delta}{U_e} < 6 \times 10^{-3}$$

$$= \exp\left[-0.75\left(\frac{f\delta}{6 \times 10^{-3}\, U_e}\right)\eta^{0.3}\right], \frac{f\delta}{U_e} \geq 6 \times 10^{-3} \tag{36}$$

$$A_\xi\left(\xi, \frac{f\delta}{U_e}\right) = \exp(0.75\xi), \frac{f\delta}{U_e} < 6 \times 10^{-3}$$

$$= \exp\left[-0.75\left(\frac{f\delta}{6 \times 10^{-3}}\right)\xi\right], 6 \times 10^{-3} \leq \frac{f\delta}{U_e} \leq 6 \times 10^{-2} \tag{35}$$

$$= \exp(-1.5\xi), \frac{f\delta}{U_e} > 6 \times 10^{-2}$$

4. BASE FLOW

Magnitude

$$\frac{p_{rms\,b}}{p_b} = \frac{0.01\, M_b^2}{1 + 0.04\, M_b^2} \quad \text{(Tol. } \pm 2 \text{ dB)} \tag{58}$$

Spectra

$$\phi(f) = \frac{2d\, p^2_{rms\,b}}{U_b\left[1 + \left(\frac{d\pi f}{U_b}\right)^2\right]} \tag{60}$$

Cross Spectra Function

$$R(r) = p^2_{rmsb}\, e^{\frac{\pi U_b}{d} r} \tag{61}$$

No significant angle of attack effects were observed (pressure spectra or acoustic magnitude) on pressure fluctuation measurements made in fully developed turbulent flow, however, the transition region on the test vehicle changed location as predicted.

The increase in the RMS sound pressure level (≈10 dB) near the end of transition evident in the data is similar to the increase in the velocity profile exponents, n, measured by Martellucci*. This trend suggests that the velocity profile exponent as a parameter in defining a single equation for the variation of acoustic intensity in the transition region as well as fully developed turbulent flow.

An equation has been developed defining the peak acoustic magnitude in transional flow based on data obtained for free stream Mach numbers of 4, 8 and 10. This Equation 46 is similar to that defined for turbulent flow (3 or 6) differing only in the coefficient of local Mach number. An assumption that these two equations are both applicable at low Mach numbers implies convergence of Prms/qe for transitional and fully turbulent aerodynamic conditions as M_e approaches 0. Quantitative effects of transition at low Mach numbers should be the subject of further investigations.

The effects of separated flow (attained by placing the model at an angle of attack equal to its half cone angle) on pressure fluctuations on the vehicle were significant. Of significance were the high fluctuating pressures on the windward side of the vehicle which remain high downstream from the transition region, and the low pressure levels on the leeward side of the vehicle in the separated flow region which result in an ≈ 15 dB circumferential variation in fluctuating pressures over a large portion of the vehicle. This will result in excitation of the higher shell harmonics, "hoop modes", thereby inducing responses in the vehicle which should be considered in design analysis.

Base pressure fluctuation measurements were higher than expected. Appropriate adjustments were made to analytical expressions which were initially verified using subsonic data.

*Martellucci, A., "Effects of Mass Transfer on Hypersonic Turbulent Boundary Layer Properties," AIAA Journal, Vol. 10, No. 2, February 1972, pp. 181-187.

SECTION III

PRIOR EXPERIMENTAL DATA REVIEW

1. ATTACHED TURBULENT BOUNDARY LAYER FLOW

a. Acoustic Magnitude

The overall acoustic magnitude of pressure fluctuations in attached turbulent flow from various experimenters is presented in Figure 1. This summary is a representative cross-section of conditions under which acoustic intensity measurements were made (flight, tunnel wall, tunnel-model). Data were not included if flow conditions were suspect, such as Lewis and Banner's X-15 data which probably contains effects of shocks off the fin leading edge, and/or fuselage buffeting. Most experimenters have found that the acoustic magnitude (Prms) is best presented as normalized by the free stream dynamic pressure (q_∞).

For application to flight vehicles the local dynamic pressure (q_e) is a more reasonable choice than q_∞, since it is more definitive of local conditions. Data were therefore plotted in Figure 1 as a function of local properties (M_e & q_e). No adjustment was required to previously published tunnel results since the local free-stream properties are equal.

b. Acoustic Power Spectral Density

Figures 2 and 3[1] contain normalized experimental spectra for subsonic and supersonic flow. As discussed by Lowson[2] the frequency spectra of attached turbulent boundary layer flow scale on a Strouhal number basis. Choice of the proper typical length and velocity is difficult. In general, the free stream velocity (U_∞) is chosen as the velocity parameter and either boundary layer thickness (δ) or boundary layer displacement thickness (δ^*) as the typical length parameter. In this study the local velocity and boundary layer displacement thickness were used to normalize data from various experimenters.

A reasonable collapse of the data is obtained by using these parameters and a definite trend in the data is apparent. No significant difference between subsonic and supersonic flow is evident. Figure 4 presents the same high Mach number data normalized to the boundary layer thickness, (δ). A similar spread of data is evident. The trend in the magnitude of the spectra to increase at Strouhal numbers below 3×10^{-2} is believed to be due to effects of tunnel noise. At high Strouhal numbers (>1) a decrease in spectral values of approximately 20 dB/decade is apparent.

c. Cross Correlation Functions

Spatial correlation properties of a fluctuating pressure field can be obtained by several approaches. White[1] presents two forms of narrow band correlation which yield essentially the same results. Correlation functions may be obtained by direct averaging and normalization of narrow band components resulting in data of the form shown in Figures 5 and 6. Figure 7 illustrates narrow band correlation coefficients obtained using

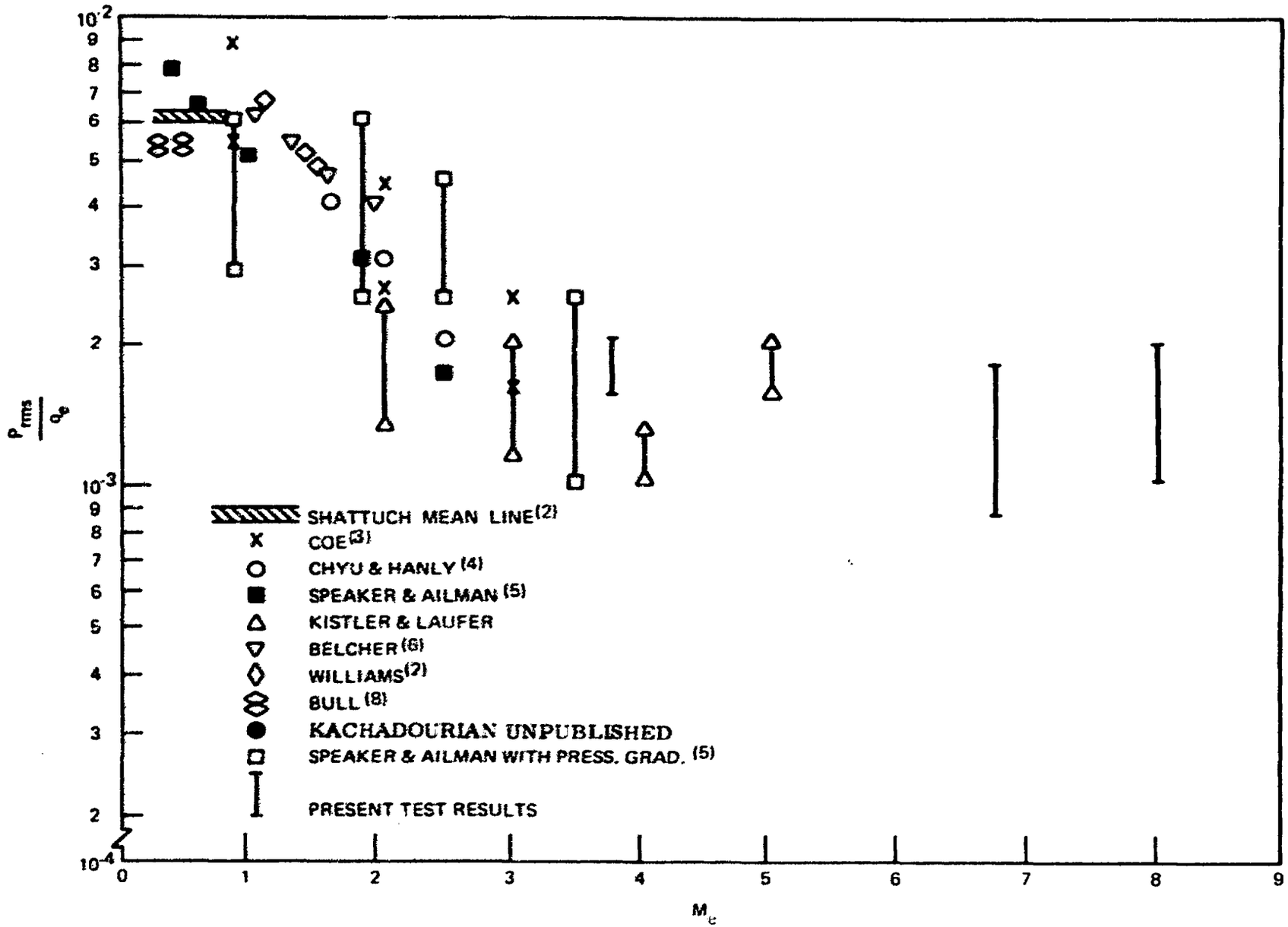

Figure 1. Root Mean Square Pressure Fluctuation Vs. Mach Number for Attached Turbulent Flow

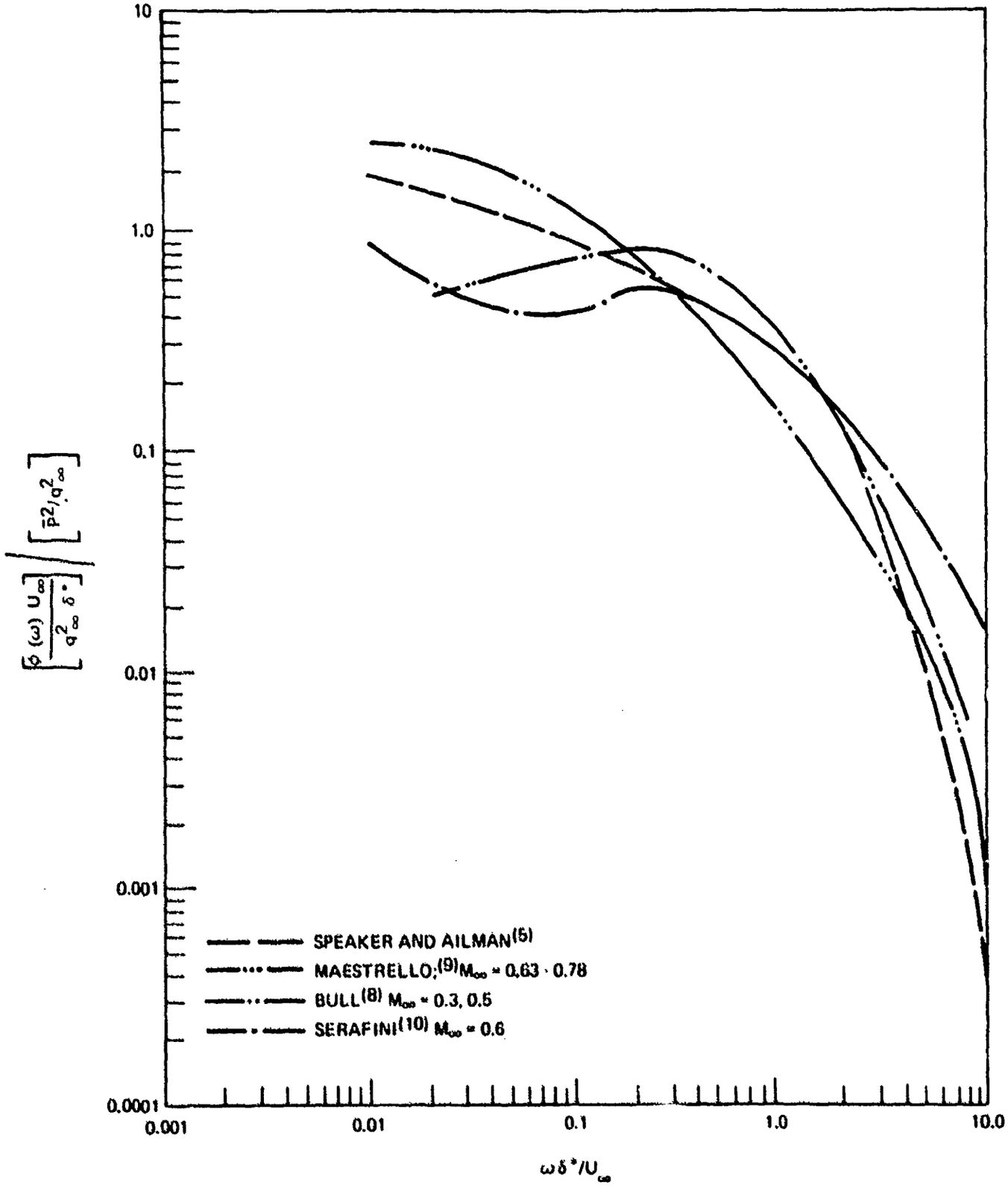

Figure 2. Normalized Power Spectra of Pressure Fluctuation for $M_\infty < 1$

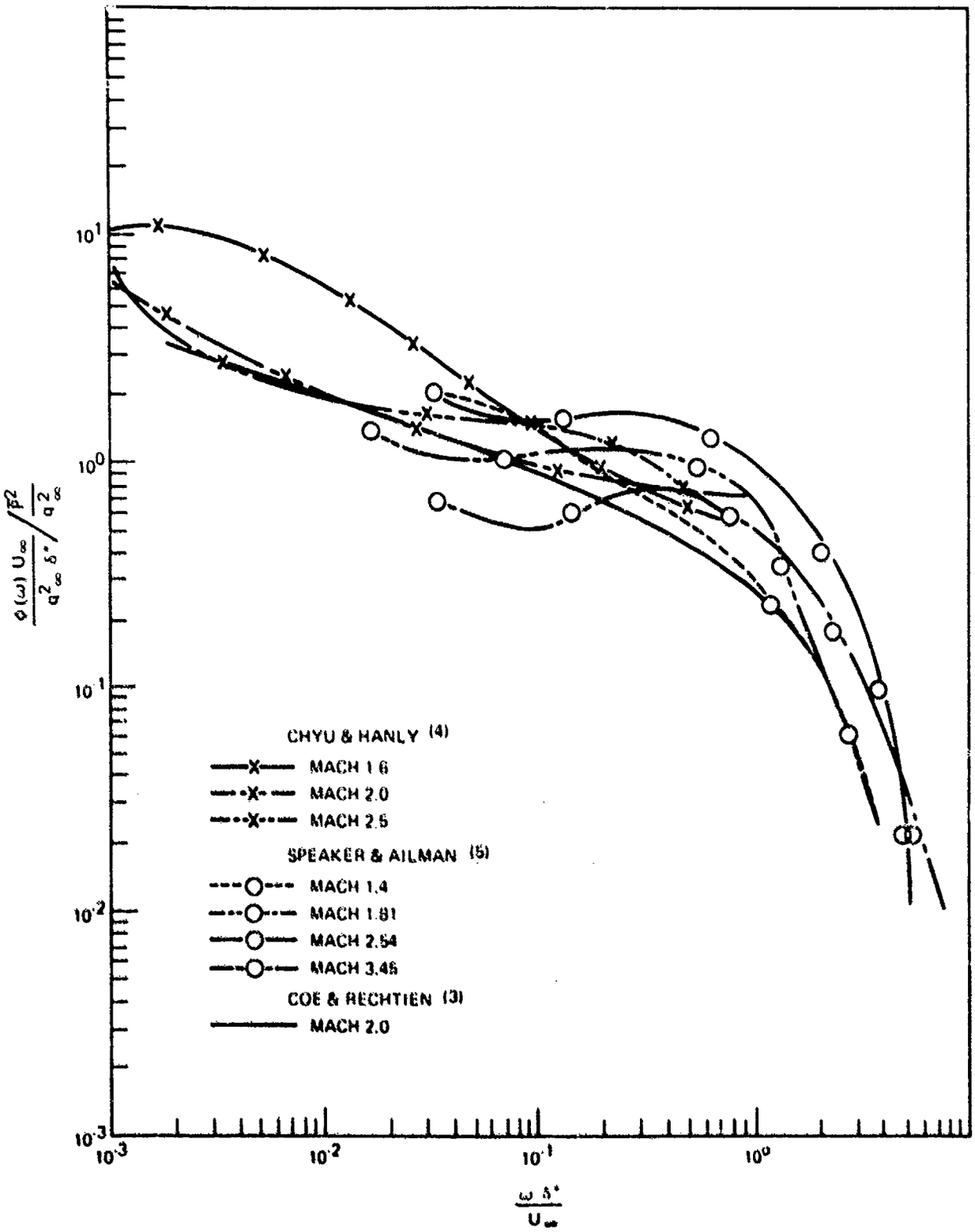

Figure 3. Normalized Power Spectra of Pressure Fluctuation for $M_\infty > 1$ Using δ^* as Normalizing Parameter

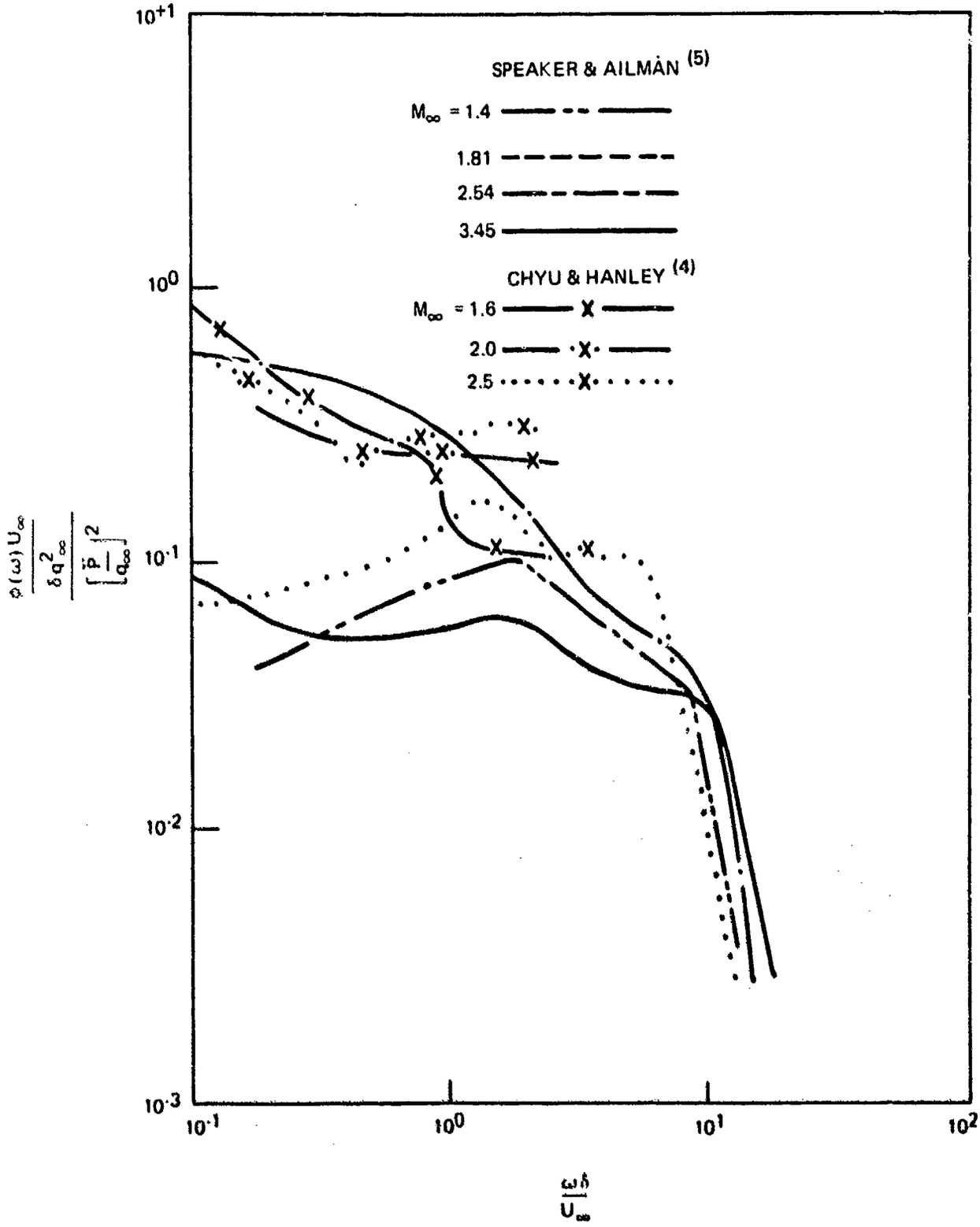

Figure 4. Normalized Power Spectra of Pressure Fluctuation for $M_\infty > 1$ Using δ as Normalizing Parameter

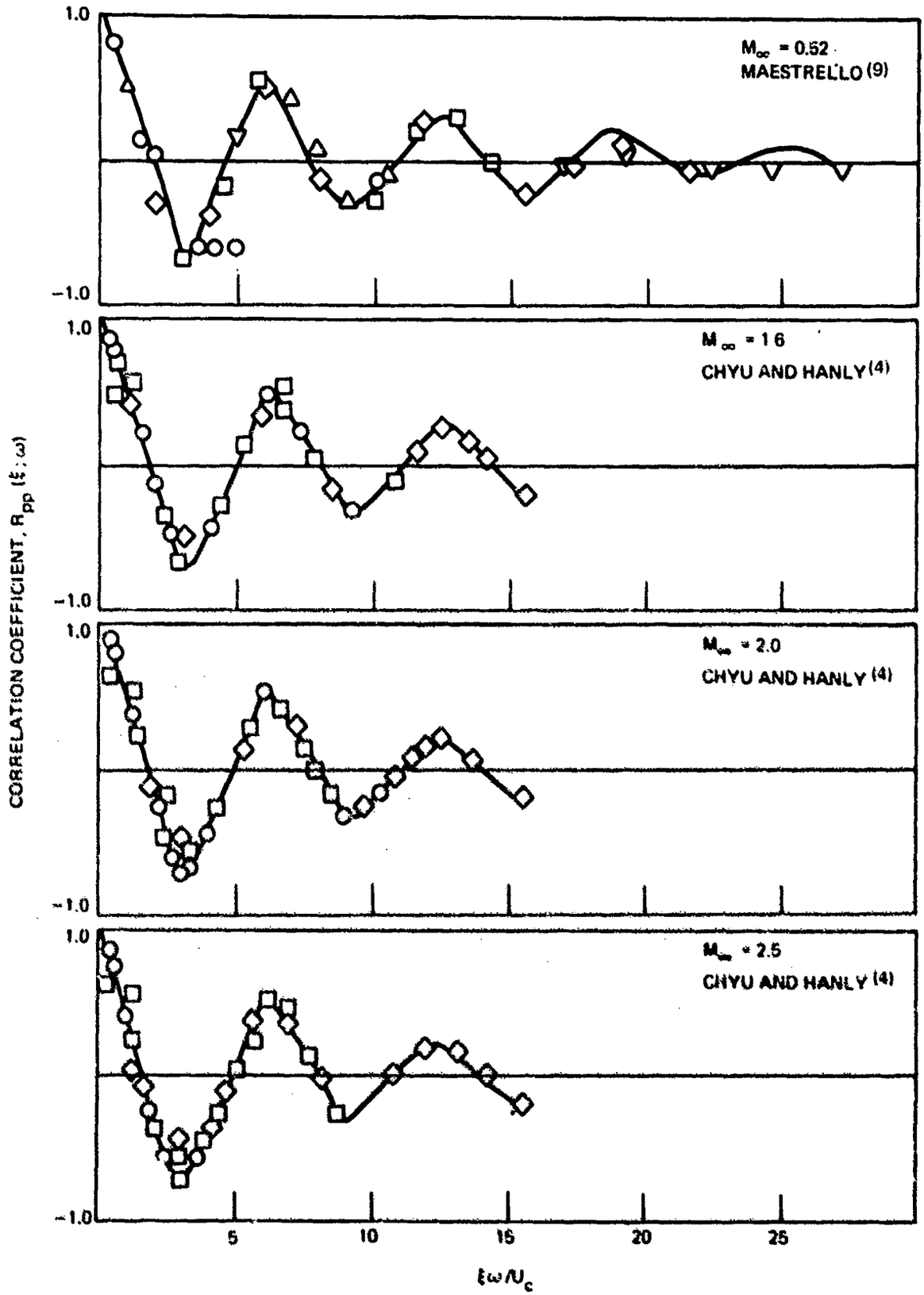

Figure 5. Narrow Band Longitudinal Space Correlation Coefficient for Attached Turbulent Flow

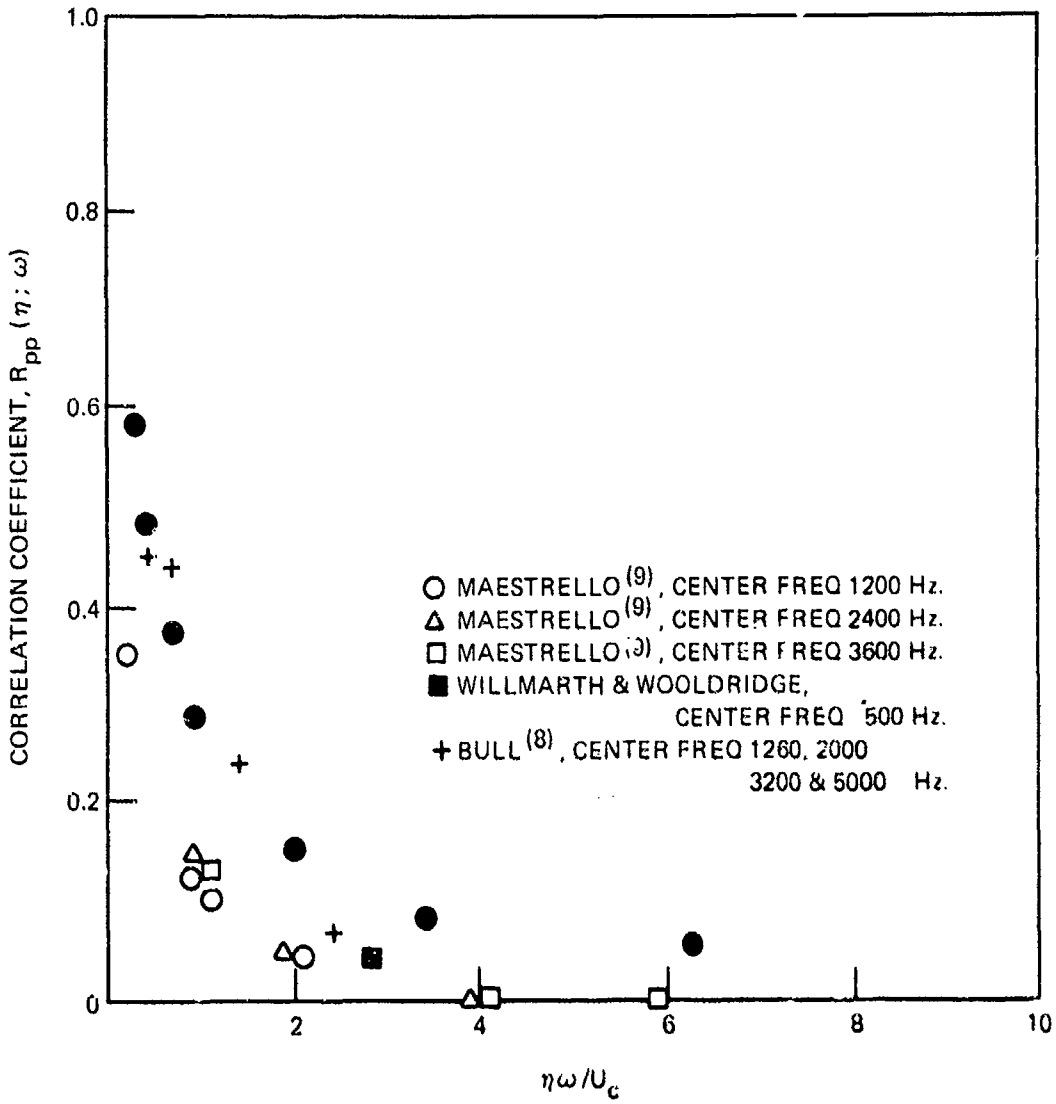

Figure 6. Narrow Band Lateral Space Correlation Coefficient for Attached Turbulent Flow(11)

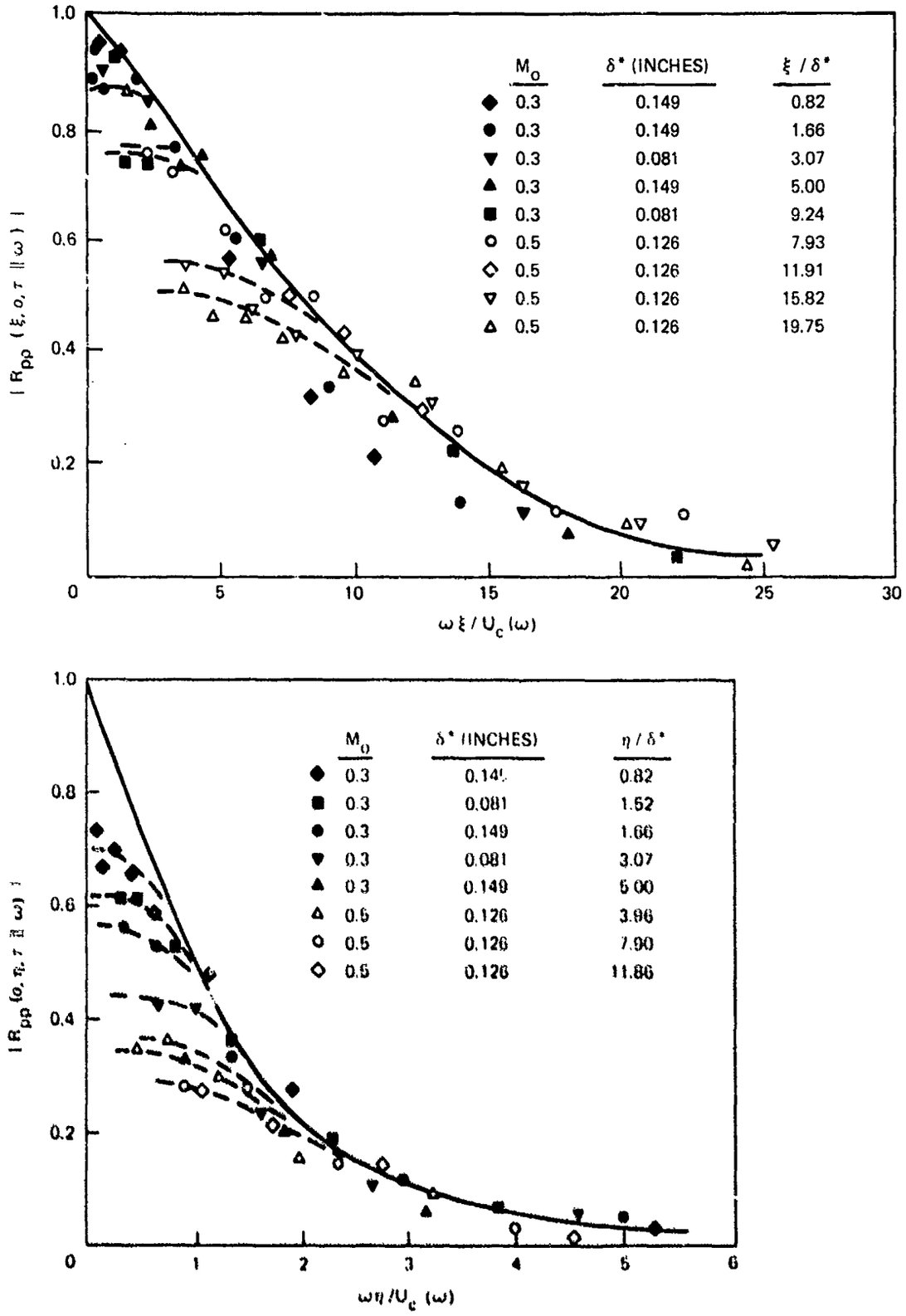

Figure 7. Narrow Band Space-Time Correlation Coefficients for Attached Turbulent Flow[11]

an alternate approach which essentially adjusts the delay times of the space-time correlation functions to a maxima. Bull[8] presents his findings in this form where he brings out the fact that at high frequencies values of ξ/δ^* tend to lie on a common curve; however at low frequencies there is significant spread in the data, indicating that the correlation coefficients tend to be independent of frequency in this region. Therefore, expressions defining cross correlation coefficients require further adjustment at the low frequencies. This can be accounted for by utilizing an exponential function based on a normalized separation distance. Figure 8 presents asymptotic values of narrow band axial and lateral pressure coefficients ($\omega = 0$) as presented by Bull.[8]

The broad band space-time correlations between two pressure time histories are useful in defining behavior of the flow field. Figures 9 and 10 (lateral curves represent correlation peaks at $\tau = 0$) are typical results obtained by various investigators. Results show the typical decrease of peaks with increasing separation distance, characteristic of decay in the turbulent eddy magnitude with distance from the reference point. Also evident at all Mach numbers was the sharp peaks present for small separation distances. As the separation distance increases these sharp peaks become broader and flatter. This effect also occurs in the lateral or cross stream direction. Bull[8] relates this behavior of the space-time correlation curves to the presence of a broad spectrum of frequencies at small separations. At larger separations the spectrum of correlation producing components is narrow and dominated by low frequency components.

d. Convection Velocity

Bull[8] defines broad band convection velocity as the weighted mean convection velocity of a pressure source in the boundary layer which contributes to the correlation. Convection velocity is determined by dividing the separation distance between two sensors by the time between peaks of the respective space-time correlation functions. Figure 11 is a summary of broad band convection velocity as a function of separation distance from various experimenters. Edge velocity and boundary layer displacement thickness are used as normalizing parameters. The variation of velocity with increasing spatial distance from 0.5 U_e to 0.85 U_e is attributed to outward dispersion of turbulent eddies originating in the region of transition between the viscous sublayer and inner part of the fully turbulent region of the constant stress layer.

Narrow band convection velocities, which define the frequency-velocity relationship associated with turbulent eddies progressing with the flow, from various investigations are presented in Figure 12. At frequencies below 5 kHz, the convection velocity approaches unity which indicates that the low frequency components of pressure fluctuations are associated with turbulent eddies in the outer region of the boundary layer. High frequency components of the pressure fluctuations, because of their low convection velocity, are the result of turbulent eddies near the wall.

In comparing Figures 11 and 12 it becomes apparent that the broad-band convection velocity is a good representation of the narrow band convection velocities at Strouhal numbers less than two.

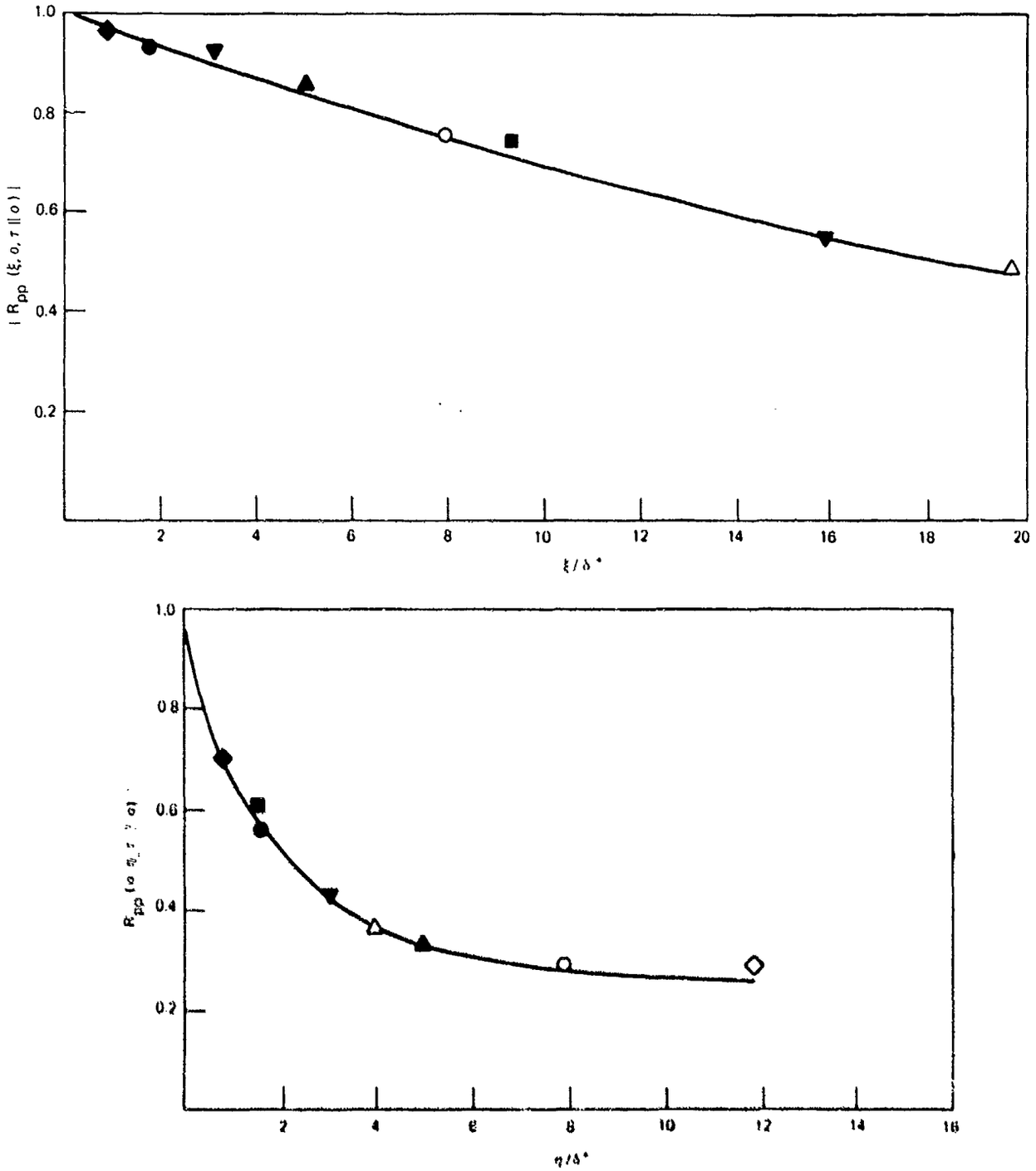

Figure 8. Asymptotic Values of Narrow Band Pressure Coefficients for Attached Turbulent Flow

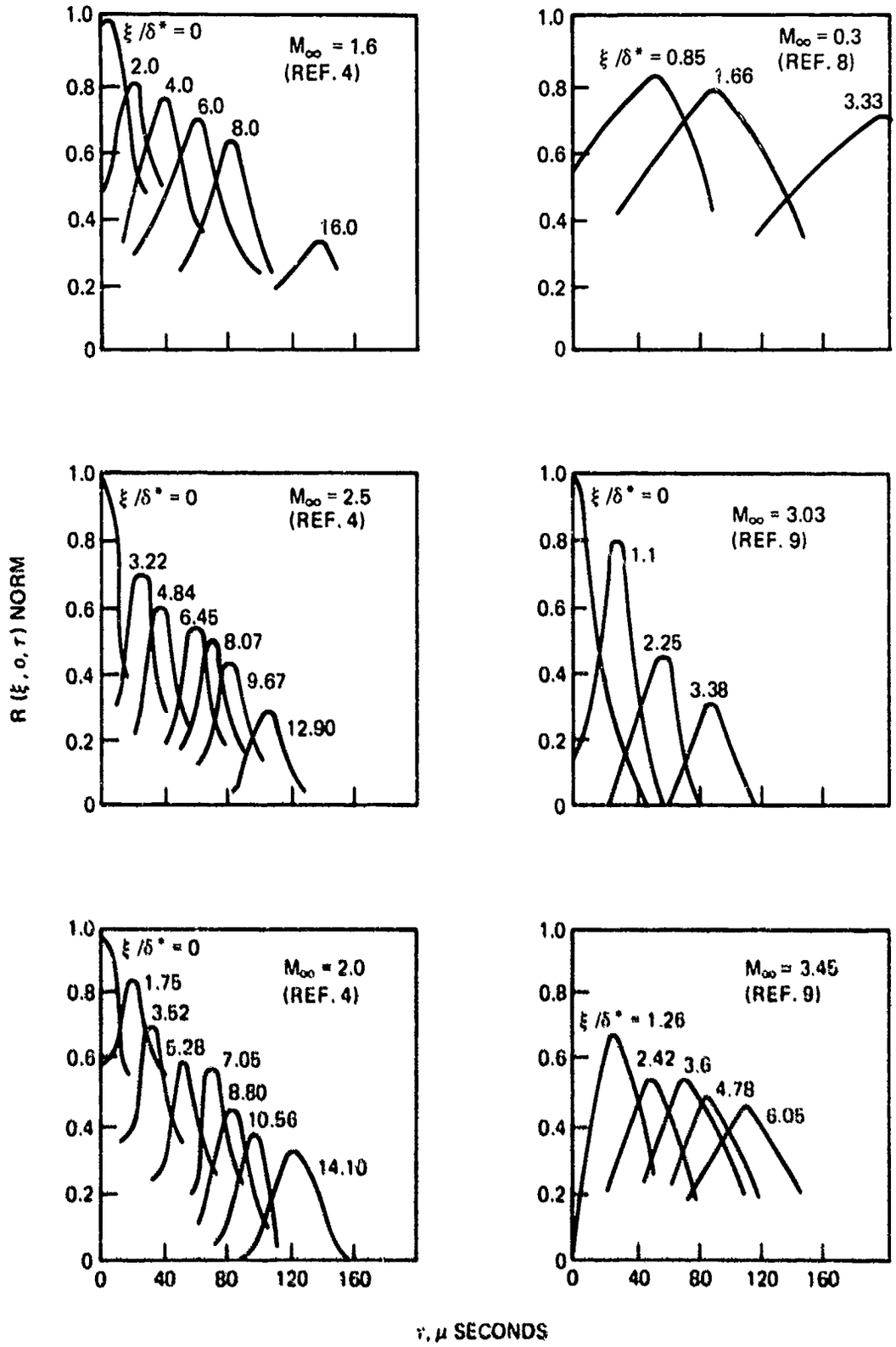

Figure 9. Longitudinal Broad Band Space Time Correlation for Attached Turbulent Flow

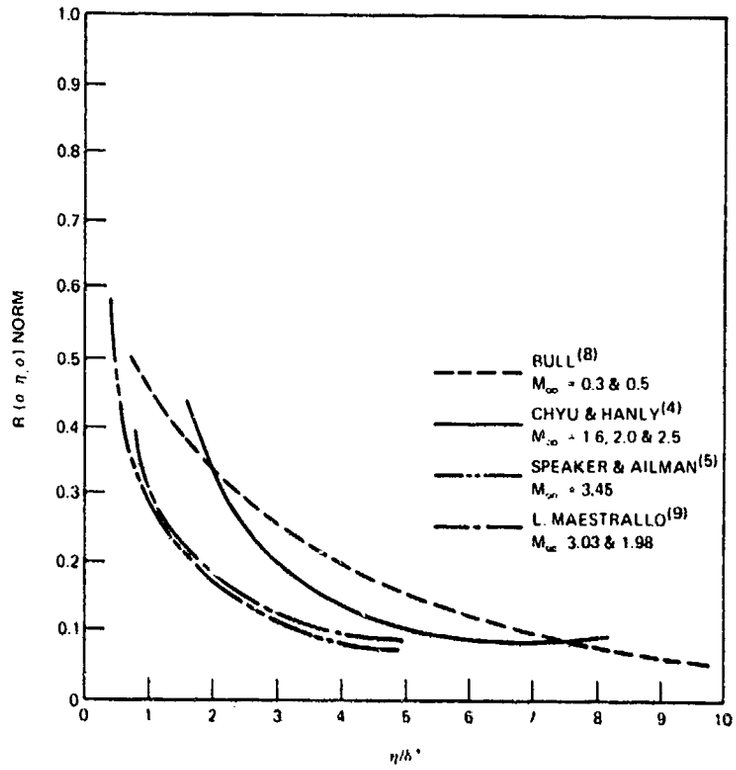

Figure 10. Lateral Broad Band Space-Time Correlation for Attached Turbulent Flow

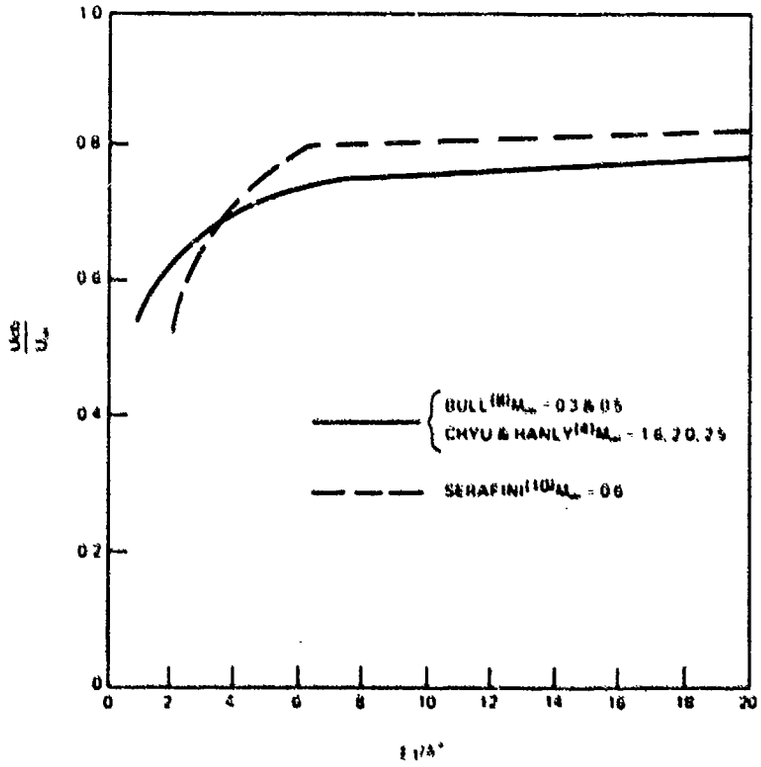

Figure 11. Variation of Broad Band Convection Velocity With Separation Distance

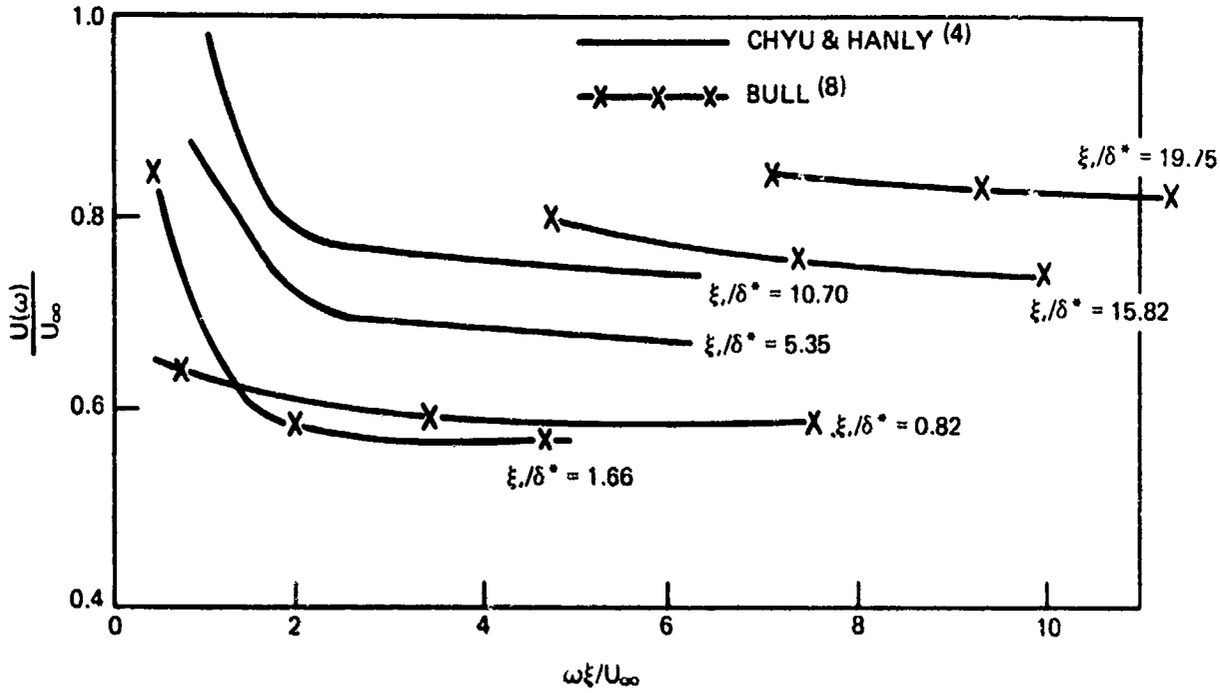

Figure 12. Variation of Narrow Band Convection Velocity With Frequency for Various Separation Distances

2. TRANSITIONAL BOUNDARY LAYER FLOW

Limited experimental data describing acoustic intensity and spectral distribution of transitional flow is available. No data were found defining correlation functions or convection velocities. This flow regime is of considerable interest because vibration data measured on high ballistic coefficient re-entry vehicles were shown to be more severe during transitional flow.

a. Acoustic Magnitude

Pate and Brown[12] measured the acoustic magnitude in transitional flow on a 5 degree conical vehicle at Mach 3 and 4. Tests were conducted at AEDC (Tunnel A facility) where the stagnation pressure was varied, thereby shifting the location of the transition region along the test vehicle. Using this approach, pressure fluctuations associated with laminar, transition and fully turbulent flow were measured using a single sensor. Figure 13 gives the rms pressure fluctuations for the frequency range from 0 to 25 kHz. Similar tests were also performed with a 5 degree cone-cylinder by Saunders and Johnson[13] where acoustic measurements in transitional flow were obtained. These results are also shown in Figure 13. The increase in fluctuating pressure in the transition region is clearly evident at both Mach numbers for all tests.

Figure 14 presents the available acoustic magnitude measured during transition. Included in this figure data point obtained during re-entry flight of a high ballistic

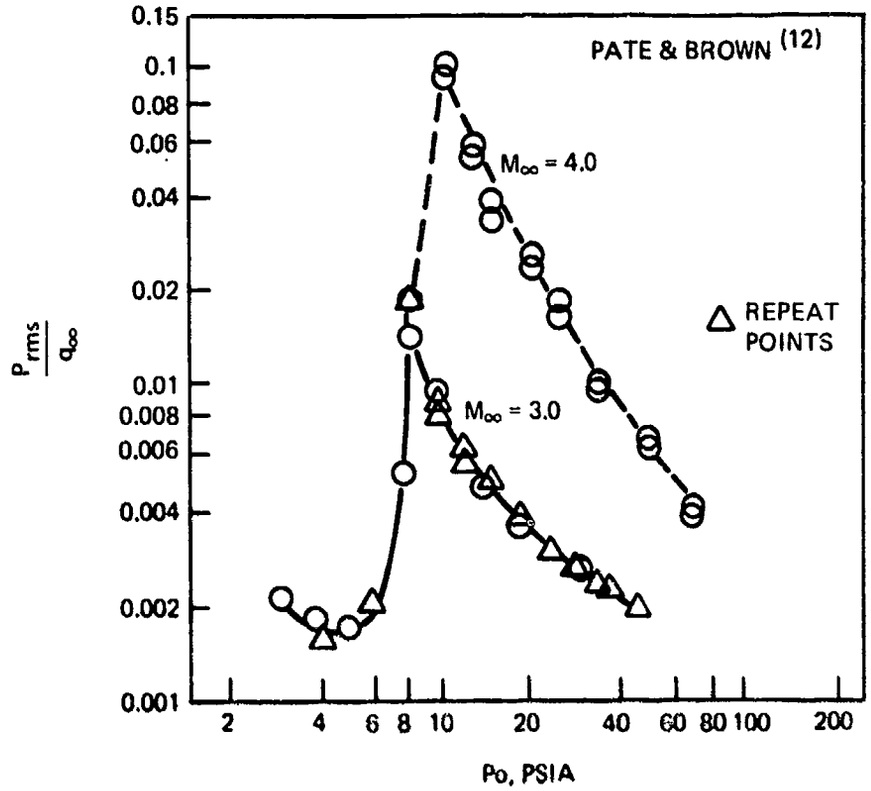

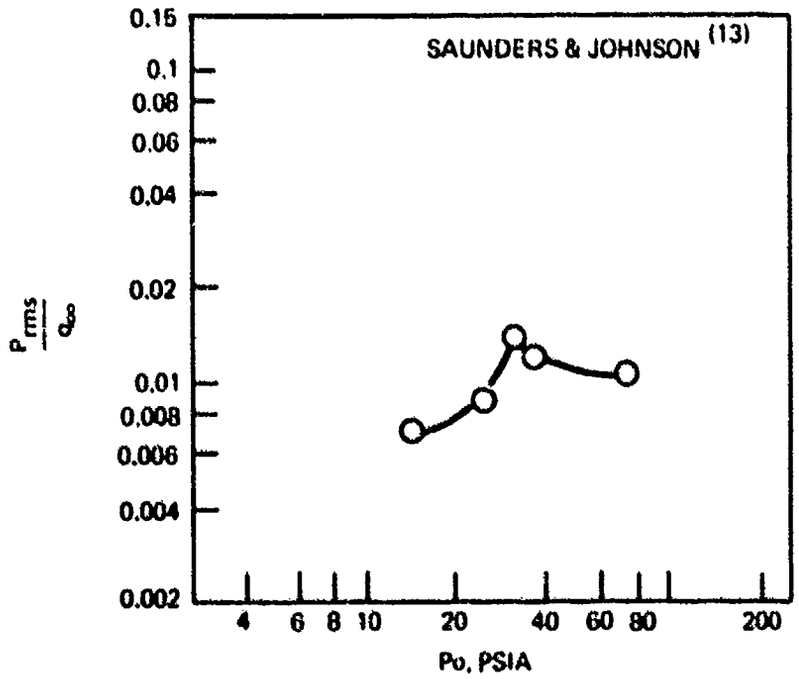

Figure 13. Root Mean Square Pressure Fluctuations Peak Value Represents Transitional Flow

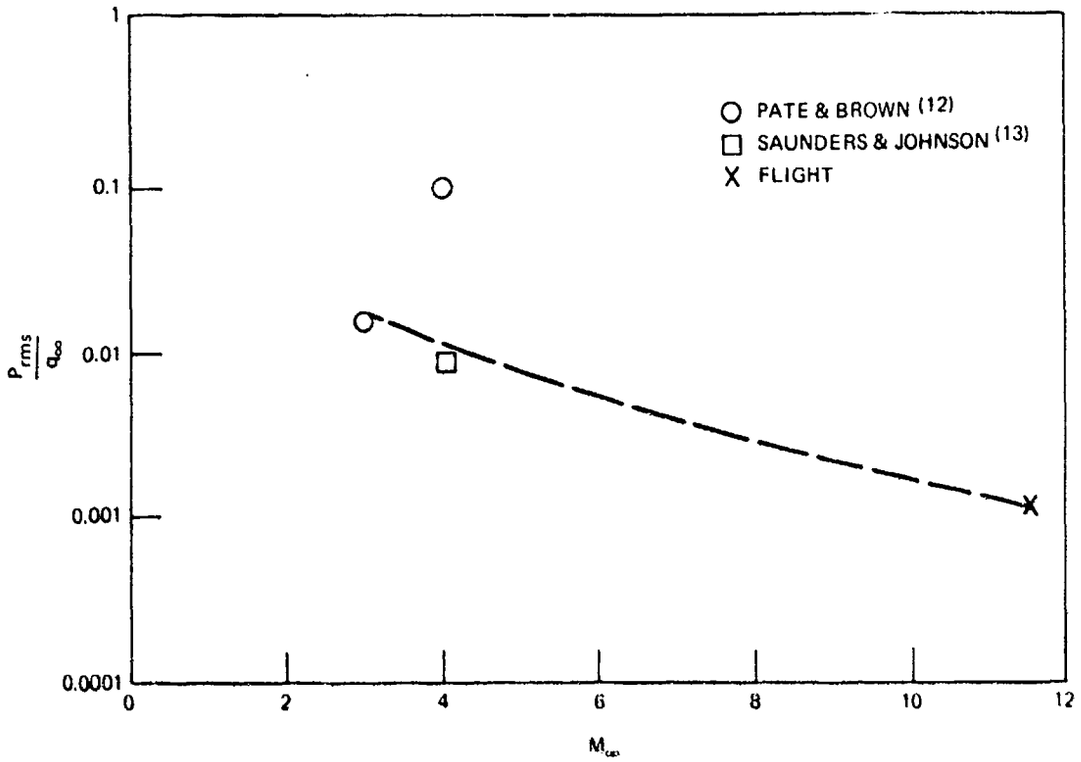

Figure 14. Root Mean Square Pressure Fluctuations Vs. Free Stream Mach Number

coefficient re-entry vehicle. Telemetry data for this flight were limited to 4 kHz; however, the data point shown in Figure 14 was obtained by extrapolating the available data using Houbolt's distribution(14) for fully turbulent flow. The normalized rms pressure out to 4 kHz had a value of $P_{rms}/q = 0.00018$.

b. Acoustic Power Spectral Density

The spectral distribution in transitional flow are shown in Figure 15 for measurements made in wind tunnel experiments. Results show a considerable amount of energy in the low frequency range. Figure 16 is a comparison of spectra obtained during transition and fully turbulent (M_e >10) flow from flight test data(15). The characteristic high levels at low frequencies are also evident in the spectra, although not as severe as was shown in wind tunnel experiments. Though no firm conclusions can be drawn because of the limited amount of data, it appears that a considerable amount of the low frequency spectral data may be attributed to tunnel noise and electrical effects. Shown in Figure 17 are typical acceleration spectral densities measured on a internally mounted component during a re-entry vehicle flight (M_e >10). Comparing measurements made during transitional and fully turbulent flow, the transition period is seen to be more severe by approximately 3 dB at peak and 6 dB throughout the remainder of the spectra. This is lower than observations made on external environments where fully developed turbulent and transitional flow differ by about 10 dB.

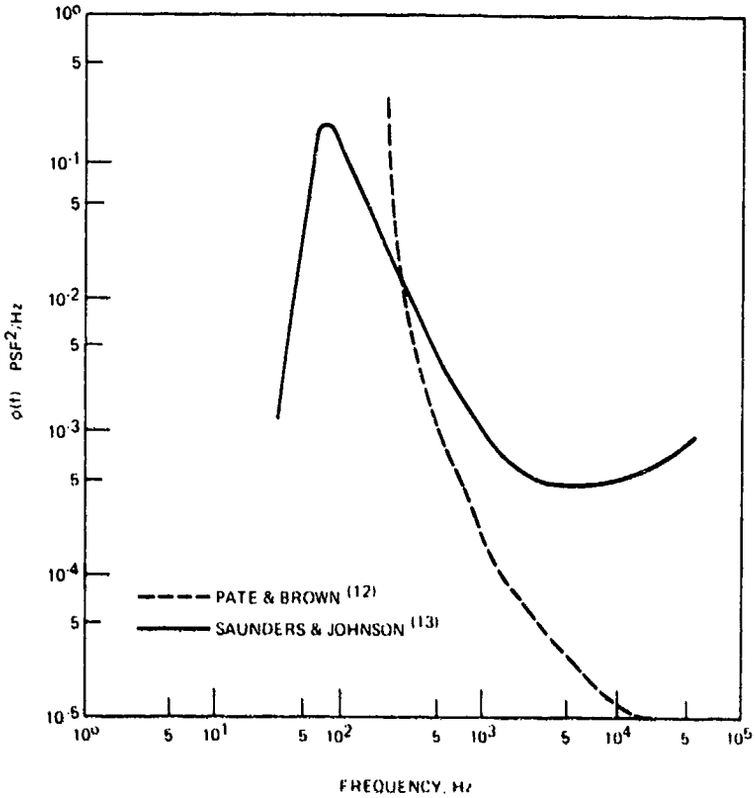

Figure 15. Transitional Flow Spectral Distribution Obtained in Wind Tunnel Experiments

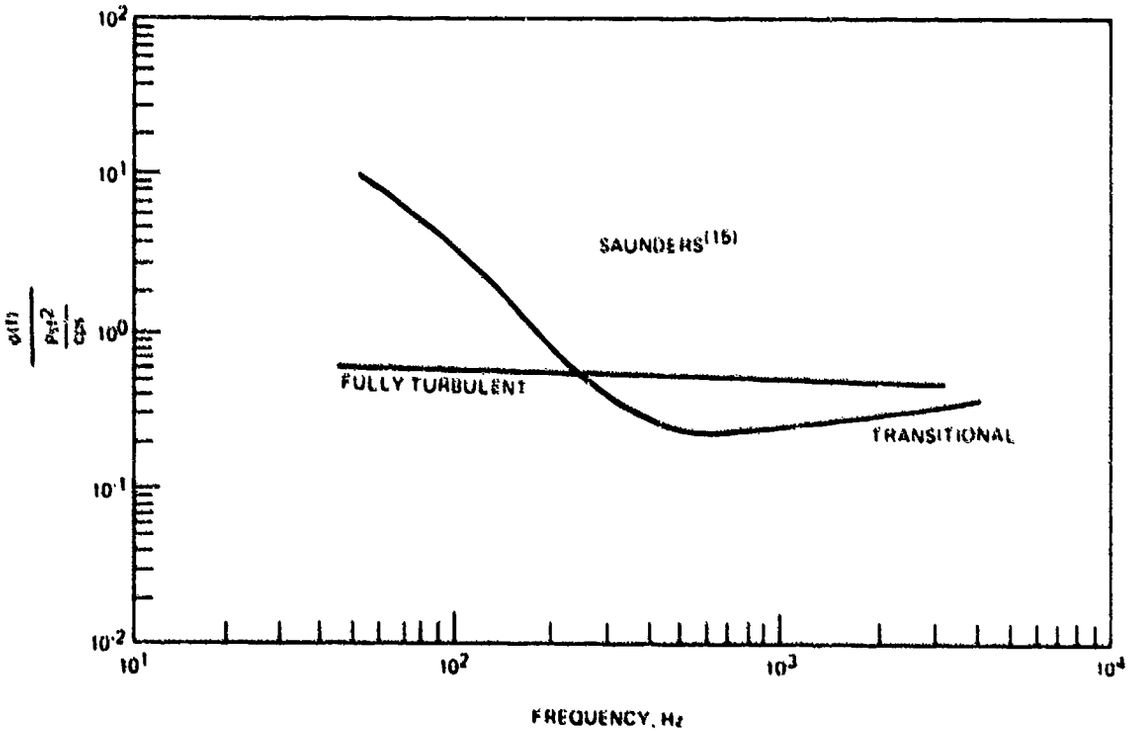

Figure 16. Comparison of Transition and Turbulent Flow Pressure Spectra Measured in Flight

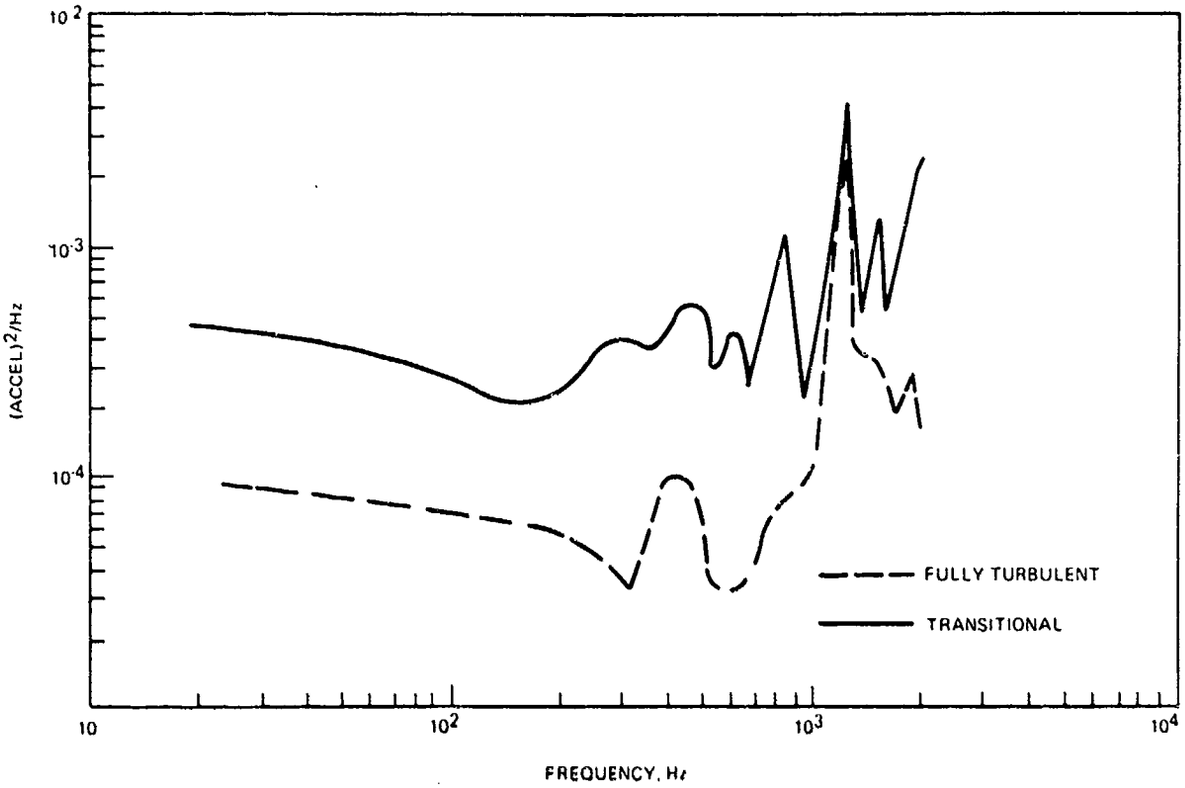

Figure 17. Comparison of Acceleration Spectra Measured in Transitional and Fully Turbulent Flow

3. SEPARATED FLOW

a. Acoustic Magnitude

A review of separated flow data given by Robertson in Reference 1 divides the separated flow into various categories, several of which are:

(1) expansion induced separated flow

(2) separated flow upstream of compression corner

(3) flare induced separation

(4) shock wave interaction

The following is a brief summary of data presented in the above reference. Figure 18 represents the overall acoustic magnitude normalized by the free stream dynamic pressure as a function of local Mach number for various separated flow environments downstream from expansion corners. Such expansion induced separated flow is representative of regions aft of cone-cylinder junctions, rearward facing steps and in the near wake of boattail configurations. Tolerance brackets shown in the data represent variations due to nonhomogeneous flow within the region of constant static pressure rather than scatter in the measurements.

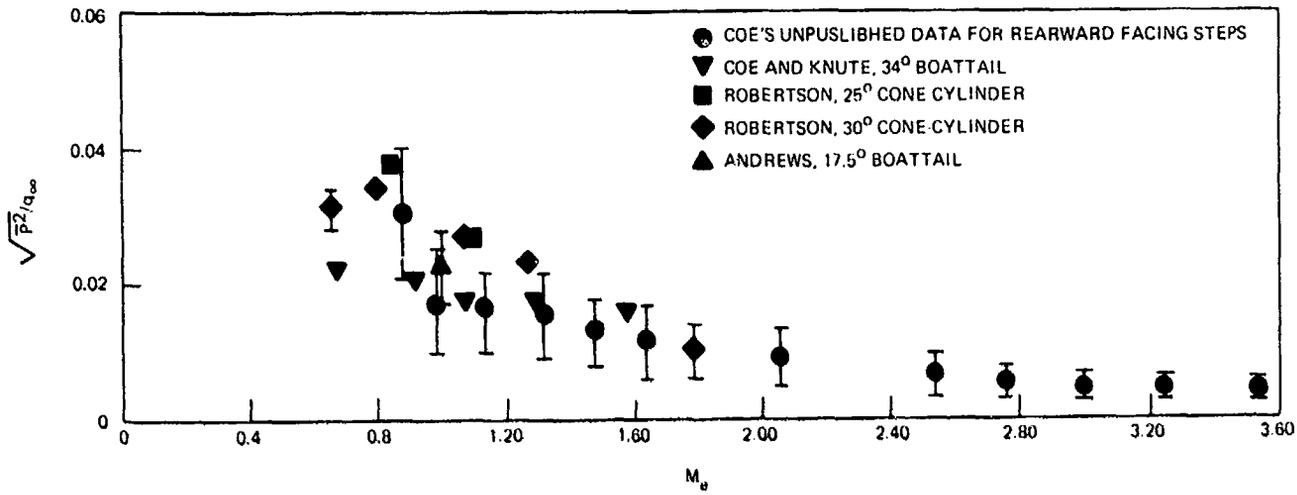

Figure 18. Overall Acoustic Magnitude Vs. Local Mach Number for Expansion Induced Separated Flow(1)

Data representative of flare induced separation and separated flow upstream of compression corners is given in Figure 19. No analytical expressions have been developed for this type of flow since insufficient data in regards to local flow conditions is available. In general the overall pressure level appears to increase slightly with increasing Mach number. This may be due to the improper choice of ordinate variable.

The oscillation of a shock wave produces intense fluctuating pressures for the region in close proximity to the shock wave. Included in Figure 20 as examples of shock-wave oscillation and reattachment data are measurements by Chyu and Hanly.(4) Speaker and Allman(5) have also defined overall intensity levels for the separated flow reattachment as well as shock interaction. These also appear in Figure 20.

b. Acoustic Power Spectral Density

A summary of available data for separated flow power spectra obtained in the homogeneous region of compression is given in Figures 21 and 22. Rechtein(16) performed a study (at Mach 2) where various characteristic lengths were used in normalizing the frequency parameter along with the mean local velocity. Characteristic lengths such as calculated displacement thickness in the separated flow region, calculated displacement thickness associated with the zero velocity streamline, and distances of the measurement behind the shock wave were used. Of these parameters, the distance of the measurement behind the shock was the most appropriate length parameter for frequency scaling. This

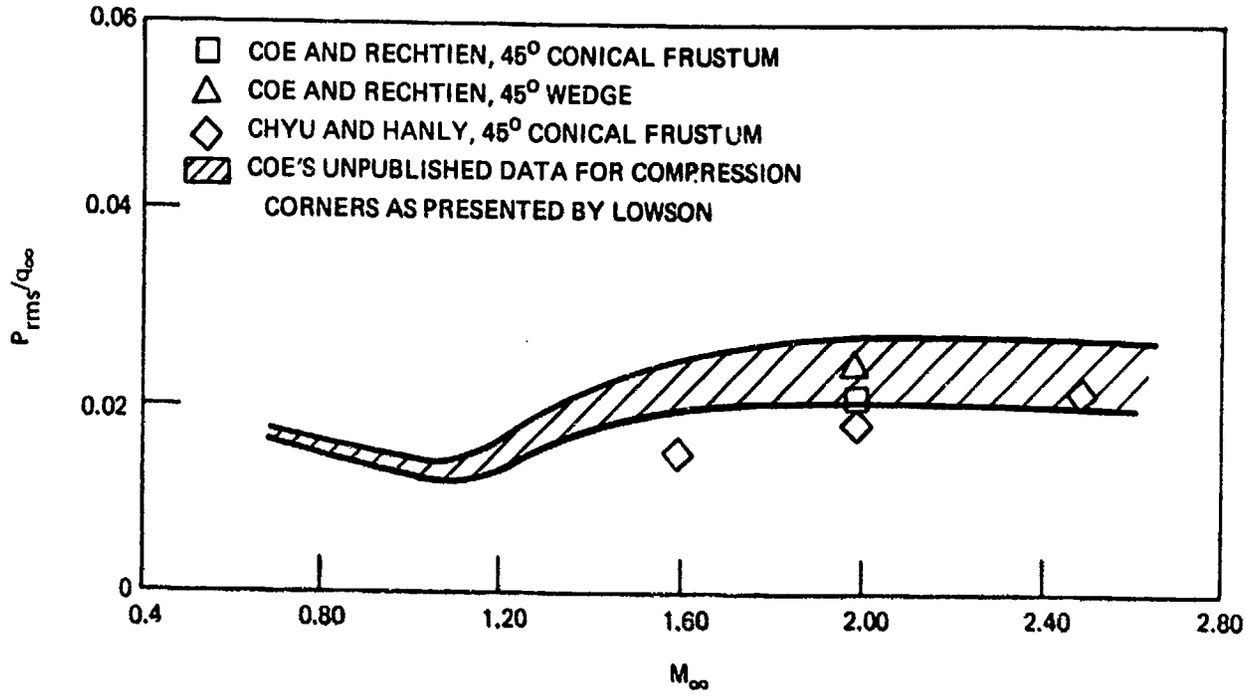

Figure 19. Overall Acoustic Magnitude Vs. Free Stream Mach Number for Separated Flow Upstream of Compression Corners(1)

length parameter was also shown to be most appropriate in the normalization of the amplitude scales of the power spectral densities. Other parameters used to normalize the spectra amplitude in conjunction with the length parameter were local static pressure, free stream dynamic pressure and the square of the Mach number. Of these, the free stream dynamic pressure was found to collapse the data best. Figure 23 compares this normalization technique to that used by Chyu and Hanly, who employed the boundary layer displacement technique in the attached flow region prior to the shock front, free stream dynamic pressure and velocity as normalization parameters. Both normalizing techniques appear to collapse the data well with slightly better collapse of data using attached boundary layer displacement thickness. Figure 24 is a comparison of spectral data for expansion induced separated flow and compression induced flow obtained by Speaker and Ailman(5) at $M_\infty = 3.45$. Though the curves are several orders of magnitude apart, their shapes are similar. The difference in spectral level is probably due to normalizing parameters.

Robertson(1) presents spectral characteristics of shock-wave oscillation for both two and three-dimensional protuberances (given in Figure 25). The spectrum shows a significant amount of energy in the low frequency range and a steep roll-off of approximately 8 dB/octave for a Strouhal frequency range of 1×10^{-2} to 2×10^{-1}. Speaker and Ailman have also conducted experiments examining the spectral distribution in the vicinity of a two-dimensional shock wave impinging upon the turbulent boundary layer, as well as in the region of flow reattachment, with similar results.

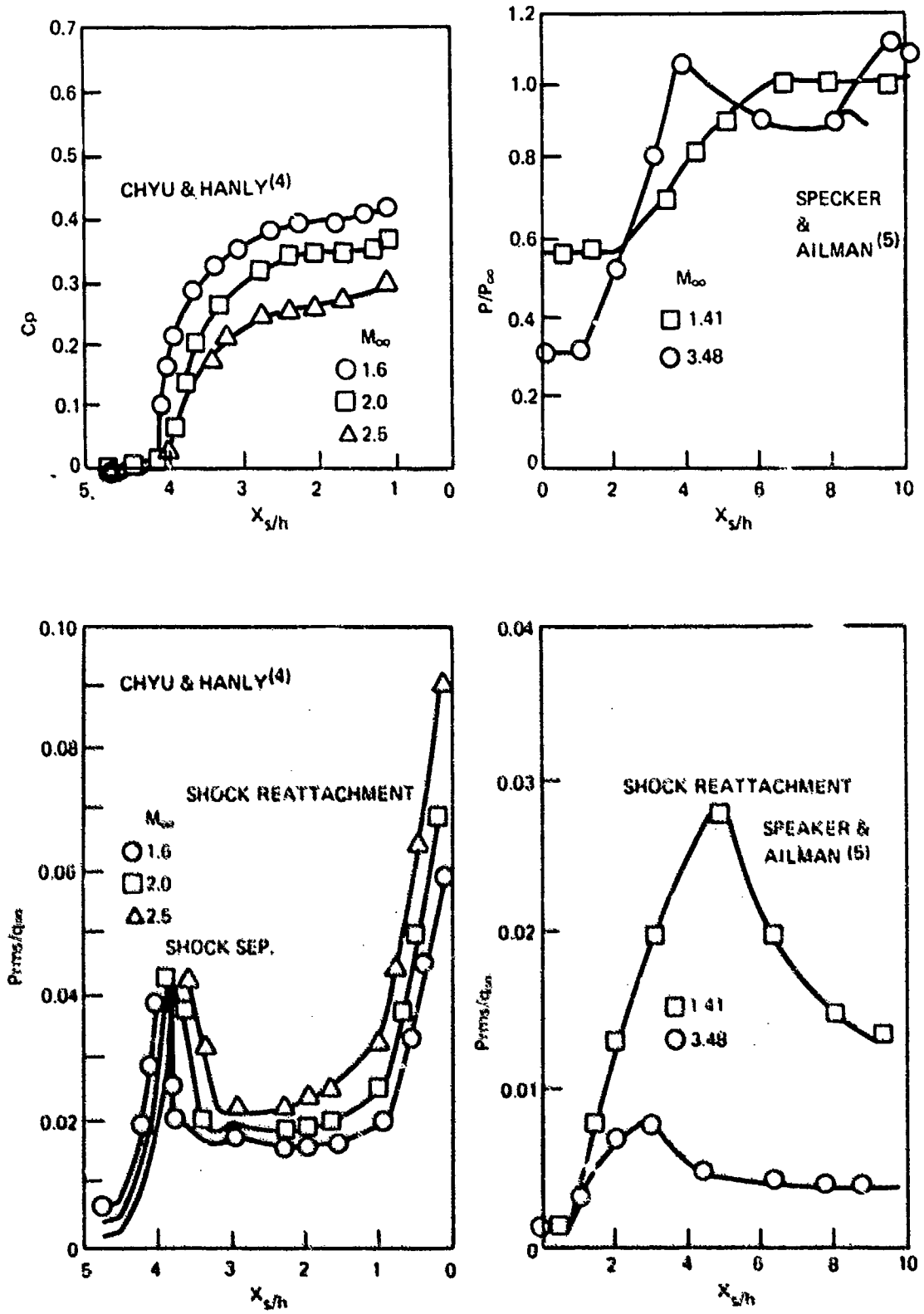

Figure 20. Acoustic Magnitude Distribution Representing Shock Separation and Reattachment

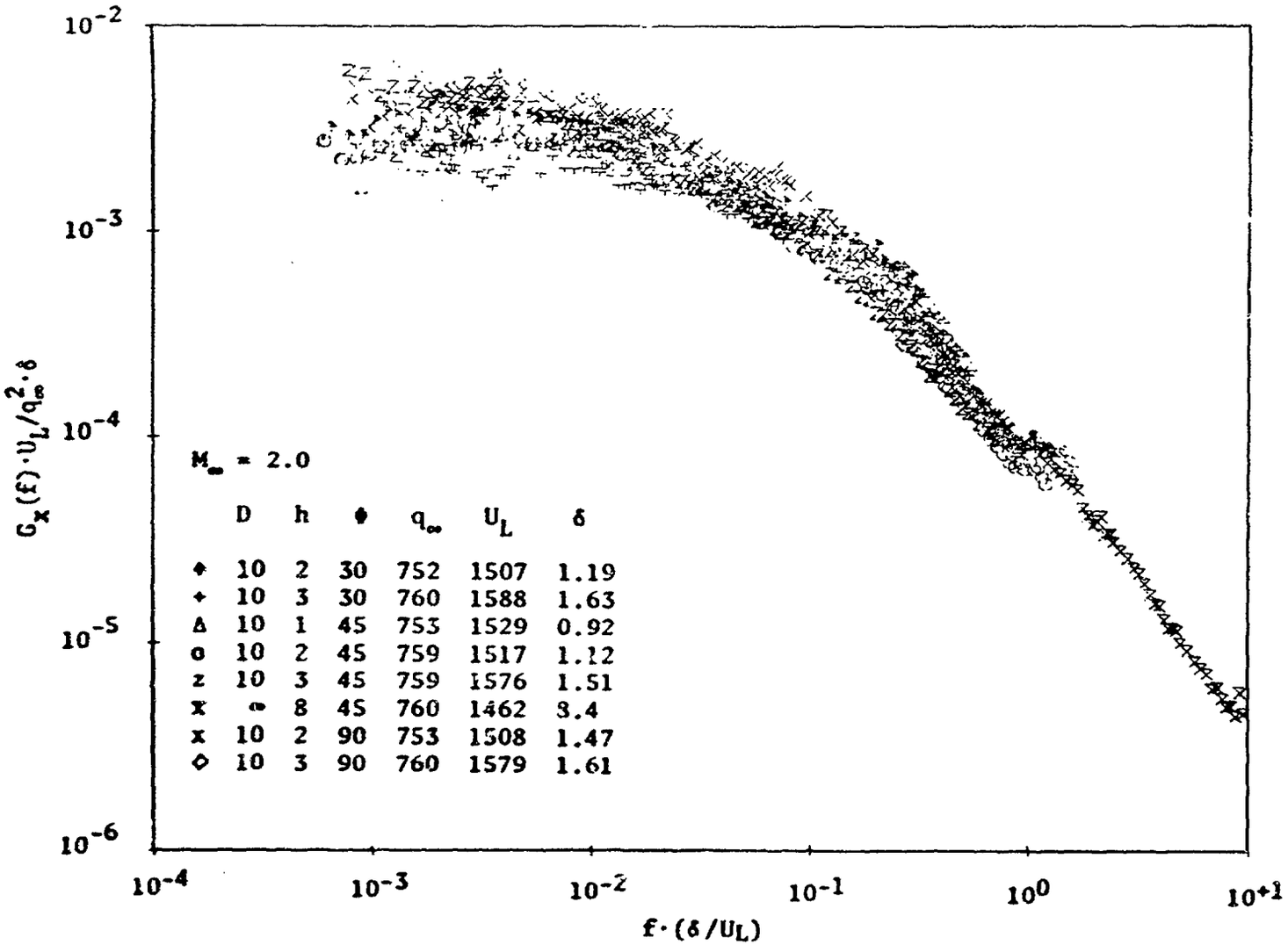

Figure 21. Normalized (Using δ) Pressure Spectra Representative of Separated Flow (Prel. Data Taken from Ref. 16 With Permission From NASA Ames)

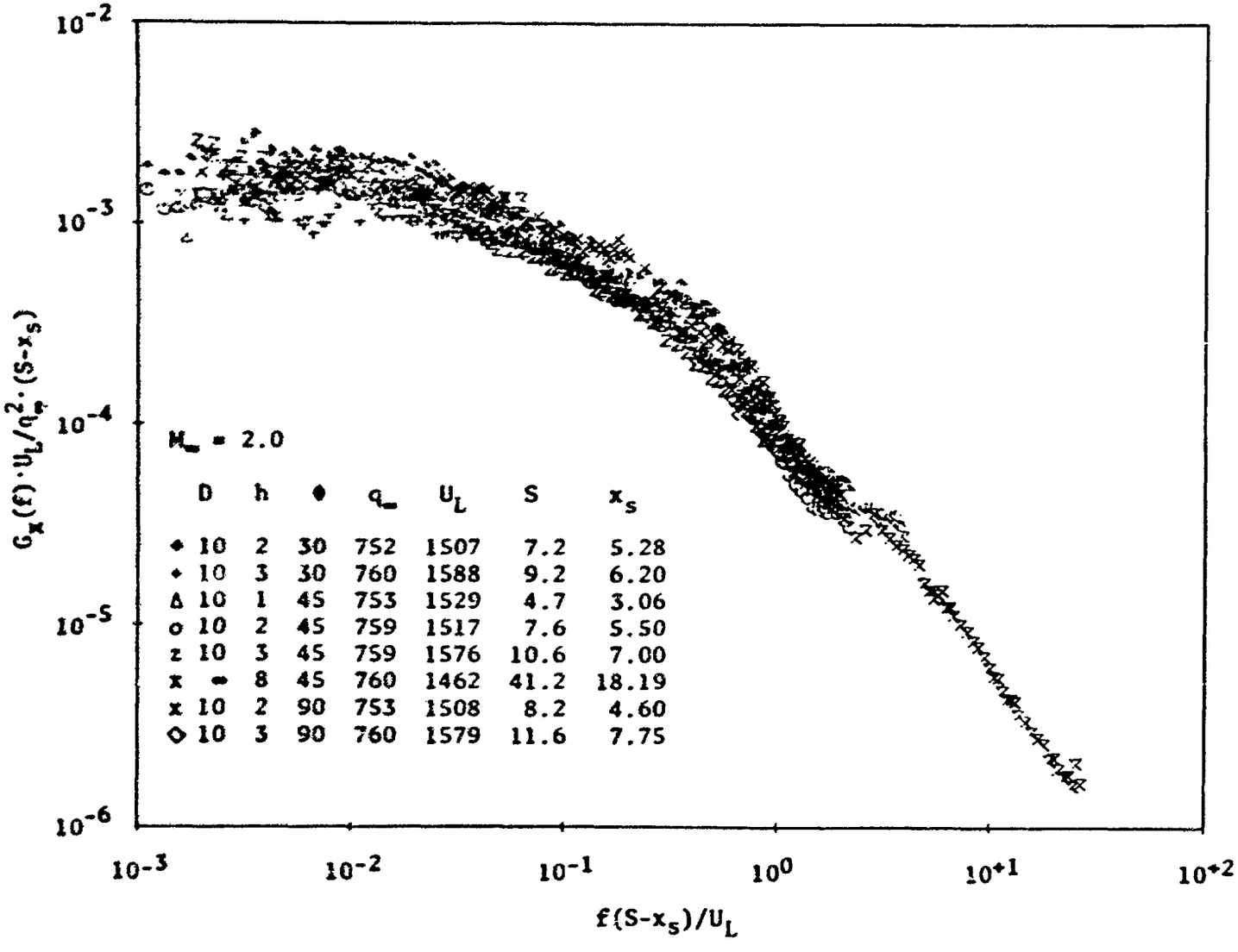

Figure 22. Normalized (Using $S-X_S$) Pressure Spectra Representative of Separated Flow (Preliminary Data Taken From Ref. 16 With Permission From NASA Ames)

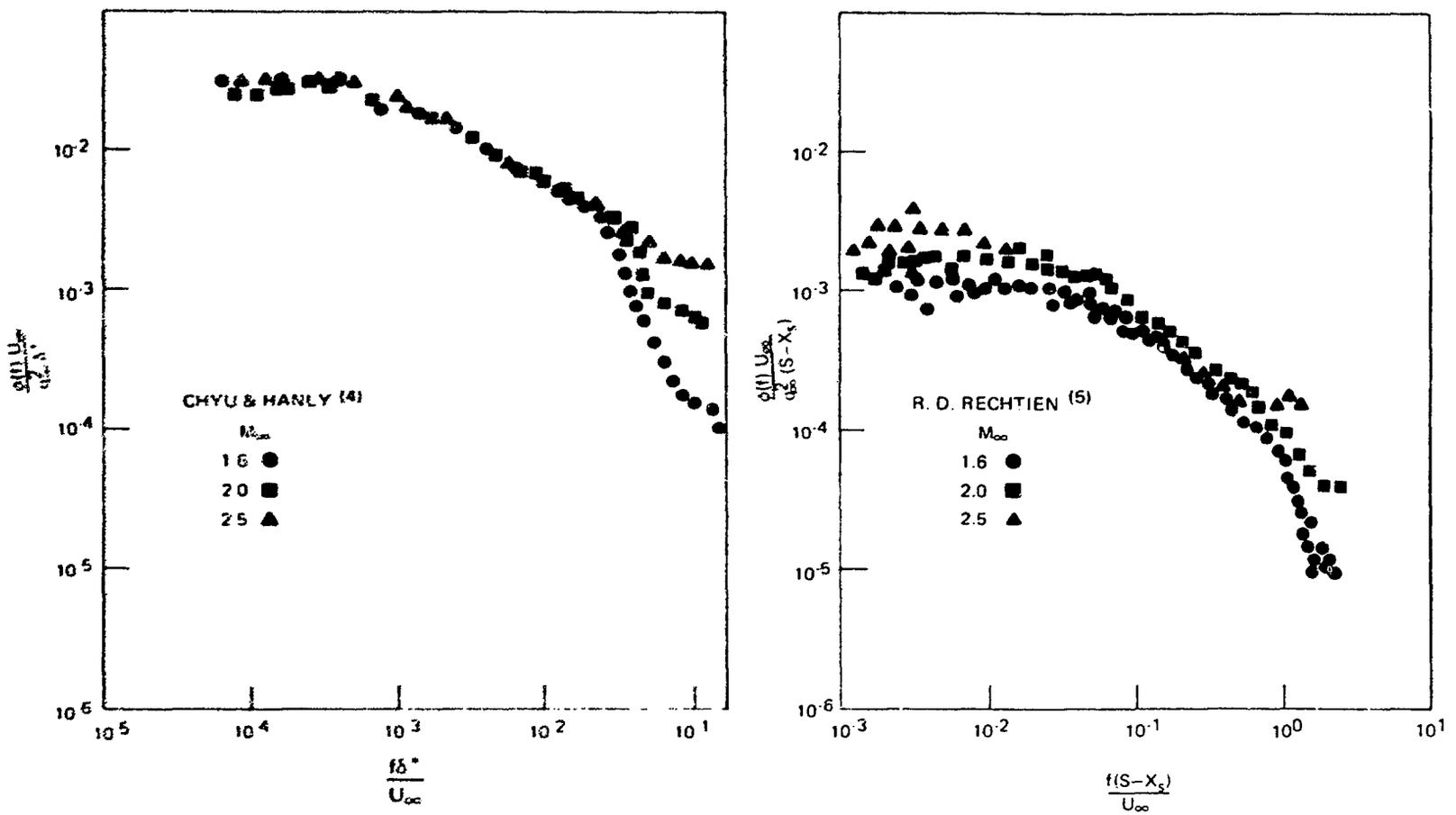

Figure 23. Comparison of Normalization Technique for Separated Flow Spectra

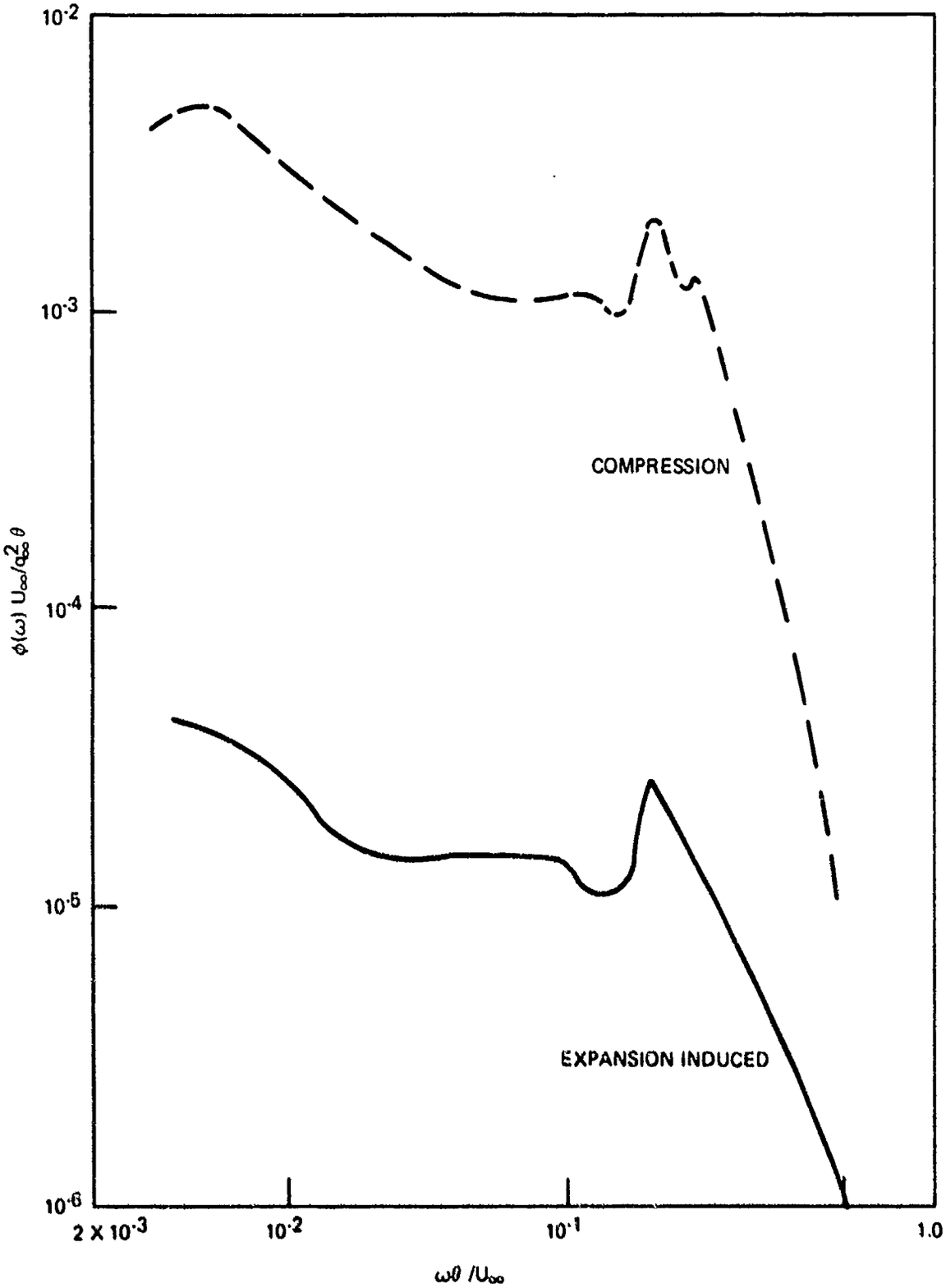

Figure 24. Comparison of Expansion and Compression Induced Separated Flow Spectra(5)

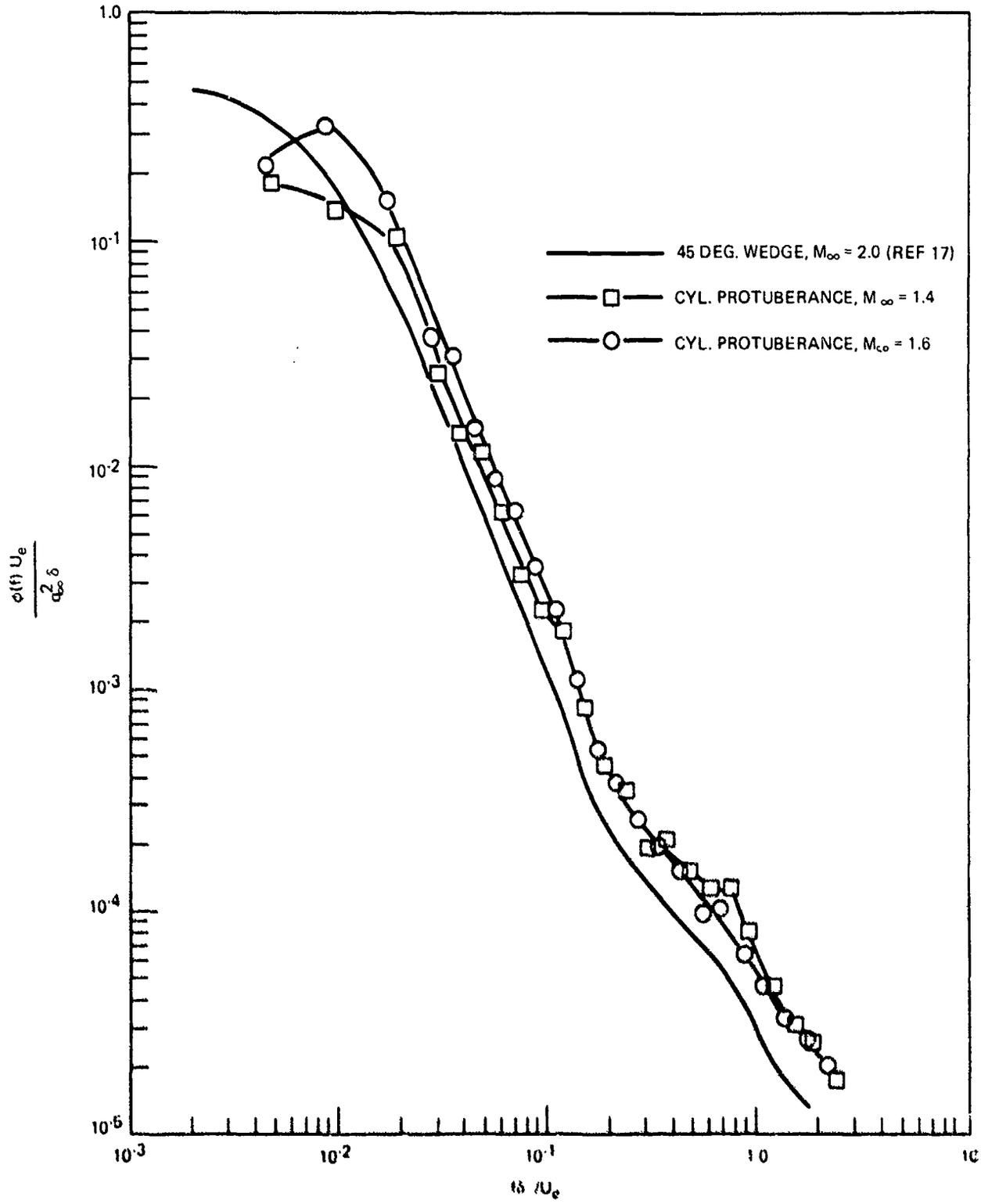

Figure 25. Comparison of Power Spectra for Shock-Wave Oscillation Induced by Two and Three Dimensional Protuberances(1)

c. Cross Correlation Functions

Normalized narrow band longitudinal cross spectra for separated flow are presented in Figure 26 for the Mach No. range of 1.6 to 2.5[4]. These cross spectra are similar to those obtained for fully turbulent flow and are represented as damped sinusoids. The rate of decay is approximately 50% greater in separated flow when compared to full turbulent flow and a slight increase in the rate of decay was observed as the Mach number was decreased. These effects become more pronounced in the coherence functions shown in Figure 27.

Broad band space correlation functions for the above experiment are presented in Figure 28. Similar to that observed from narrow band analysis was the fact that correlation in the attached flow was significantly higher than that in the separated flow.

Shown in Figure 29[1] is the degree of correlation which exists between the region under a detached shock wave and adjacent regions of attached and separated flow. Weak correlation is noted for adjacent regions with strong correlation existing within the shock region.

d. Convection Velocity

For separated flow, the narrow band convection velocity varies from 0.2 U_0 (at low wave numbers) to approximately unity at high wave numbers, thus convective velocities derived from broad band analyses (cross correlation functions) are not representative of all frequency components making up the pressure field as was the case for attached turbulent flow. Figure 30[4] presents typical separated flow (compression corner induced separation) narrow band convection velocities for various separation distances at Mach 2. Figure 30 compares the narrow band convection velocities for separated and attached flow. Detailed studies of the narrow band convection velocity in separated flow were conducted by Rechtien.[16] Typical results of his studies are presented in Figure 31 where the frequency scale (normalized by distance from separation point and local velocity, Figure 32 unnormalized) has been divided into three regions in order to describe the mechanisms attributed to the pressure field in separated flow. Low frequency components of the pressure field below Strouhal numbers of 0.15 are a result of slow recirculating fluid in the region underlying the high speed separated shear flow. (Significant scatter in data is attributed to small phase angles used to calculate convection velocities at low Strouhal numbers.) For Strouhal numbers between 0.15 and 1.1 measured fluctuations are due to convected patterns in the outer regions of the separated boundary layer. Above a Strouhal number of 1.1, pressure fluctuations are due to eddy Mach wave radiation originating in a limited region immediately behind the flow separation shock wave.

4. BASE FLOW

As was the case for transitional flow, only limited data were available defining the pressure spectra and overall magnitude for base flow. No data defining correlation functions or convection velocities were found.

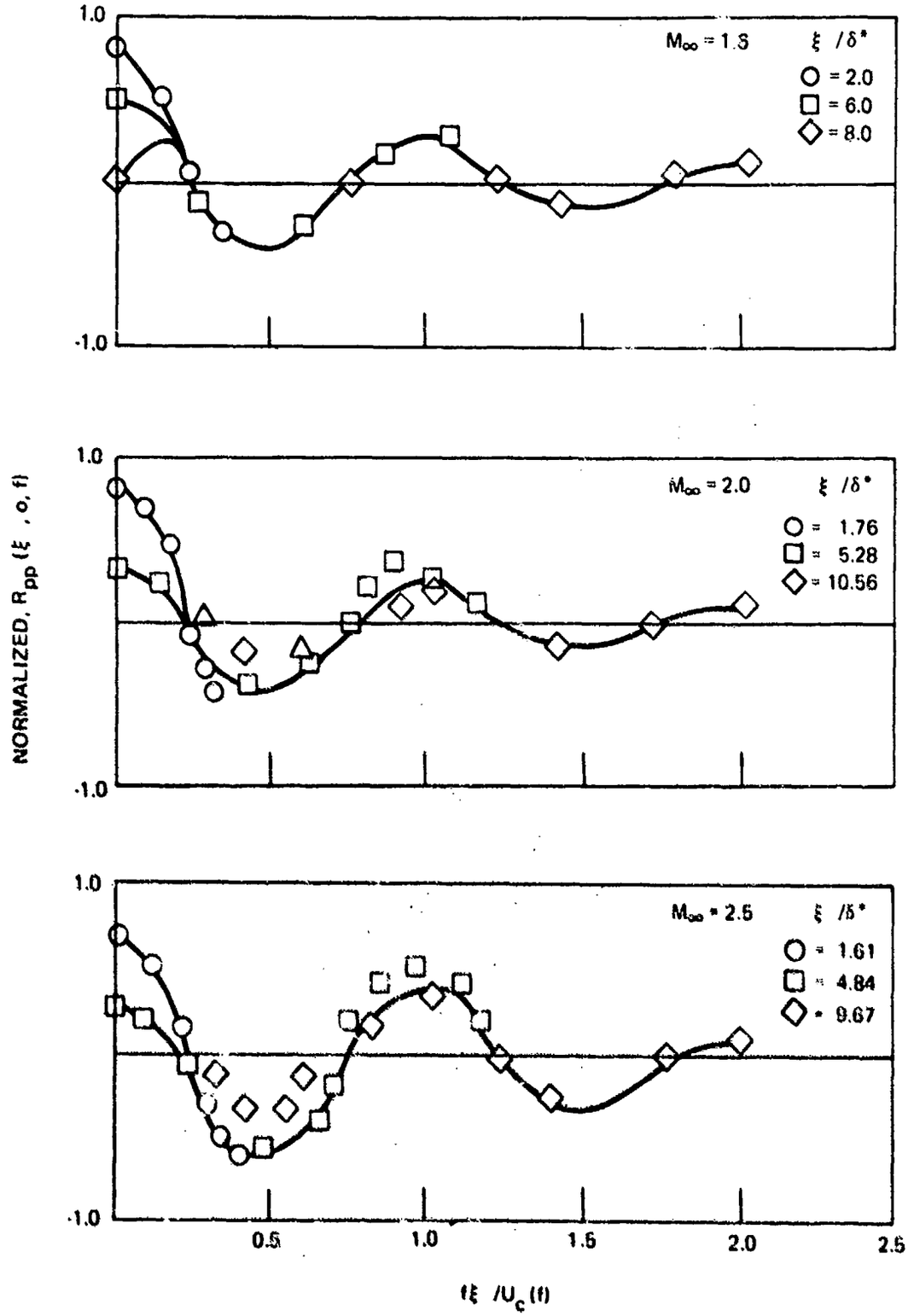

Figure 26. Normalized Narrow Band Longitudinal Cross Spectra for Separated Flow(4)

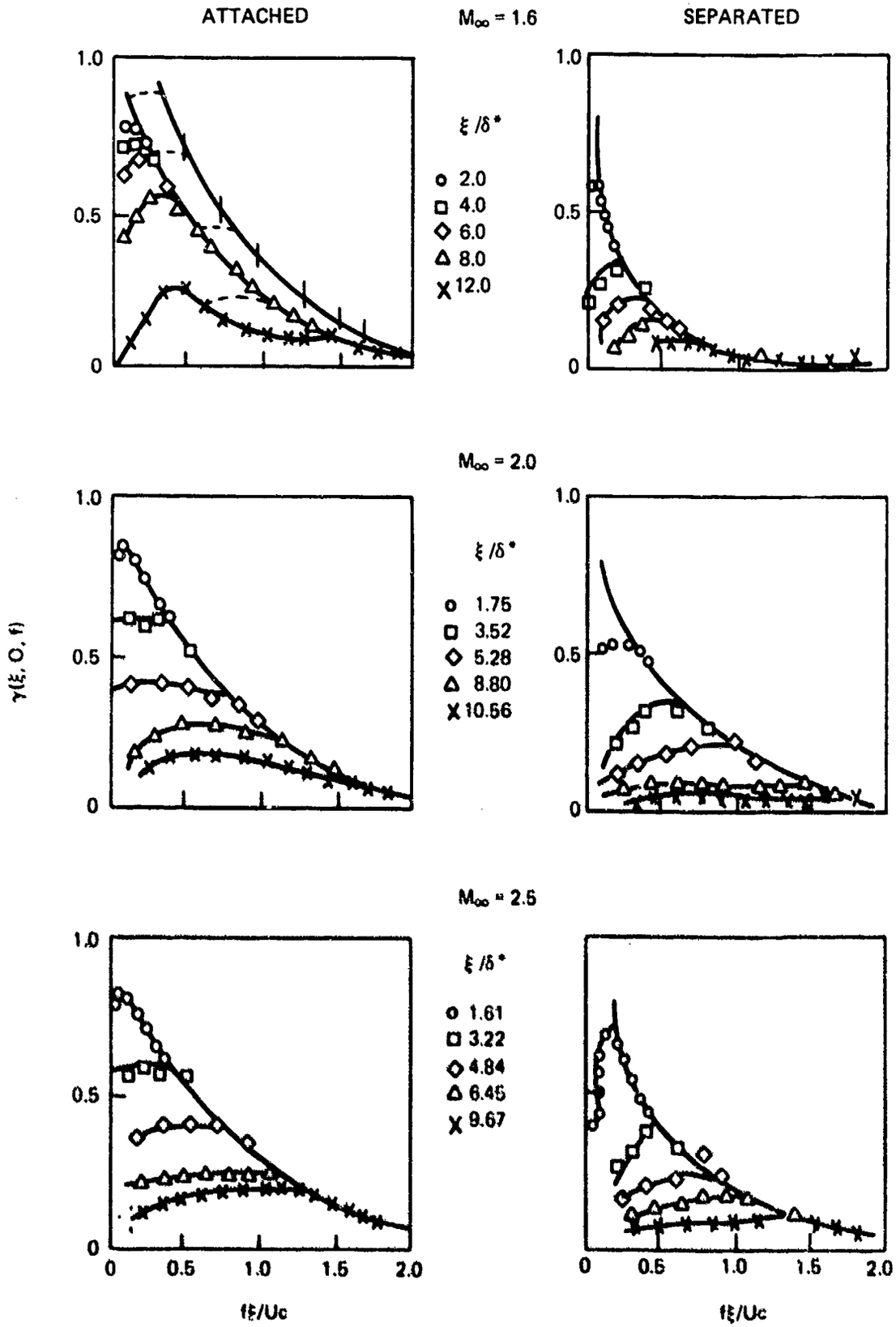

Figure 27. Coherence Function for Attached and Separated Flow(4)

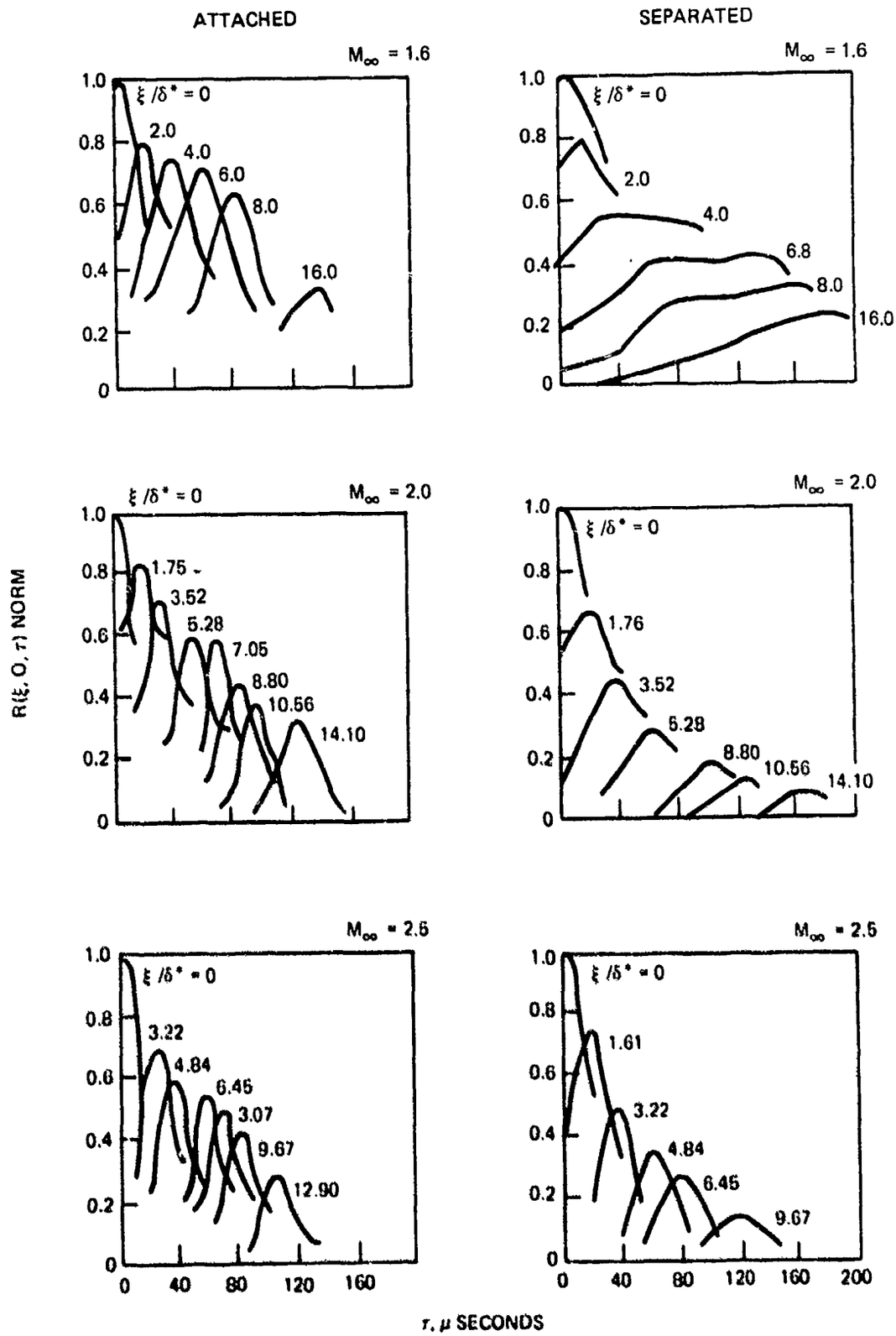

Figure 28. Broad Band Space Correlation Function for Attached and Separated Flow(4)

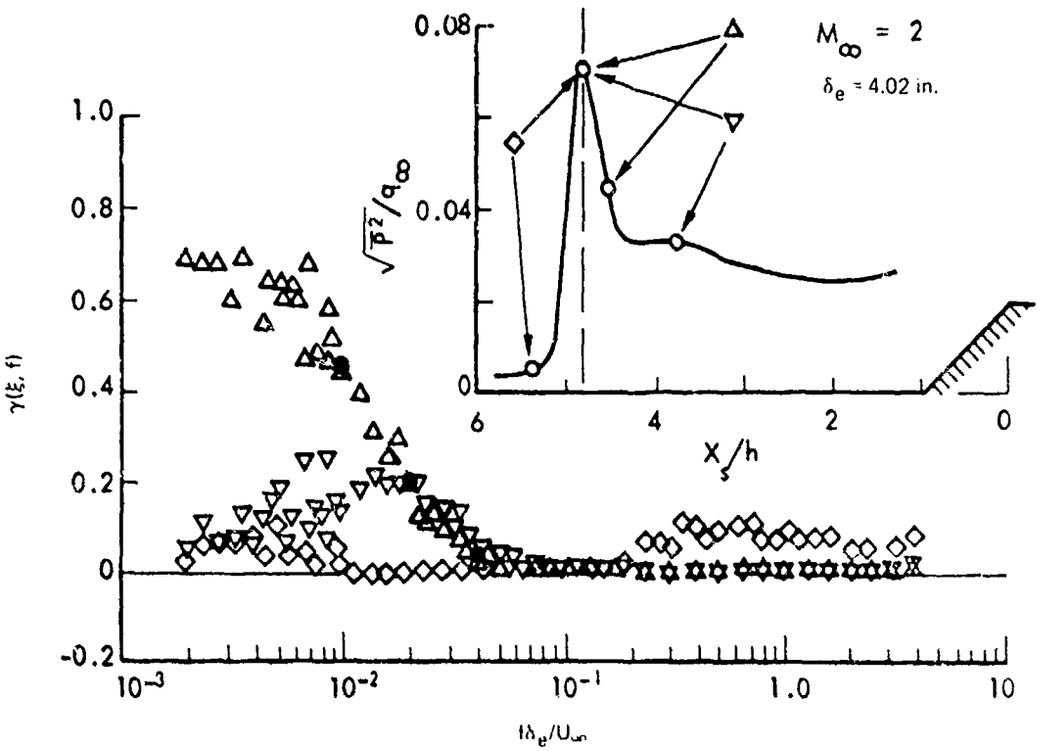

Figure 29. Correlation of Pressure Fluctuations Between Shock Wave and Adjacent Attached and Separated(1) Flow

a. Base Flow Acoustic Magnitude and Spectra

Eldred(18) published experimental results at subsonic flow (V = 68 to 352 fps) of random pressure fluctuations for base flow. Contained in the table insert of Figure 33 are normalized overall pressure levels for two locations on a circular base at several Mach numbers. The apparent trend for the normalized overall intensity is to increase as one moves away from the center of the plate.

Also shown in Figure 33 is the typical spectral distribution measured during these tests. Data was scaled to a Strouhal number using the base diameter as the characteristic length and free stream velocity as the associated velocity. As expected, a significant amount of energy is associated in the low frequency region.

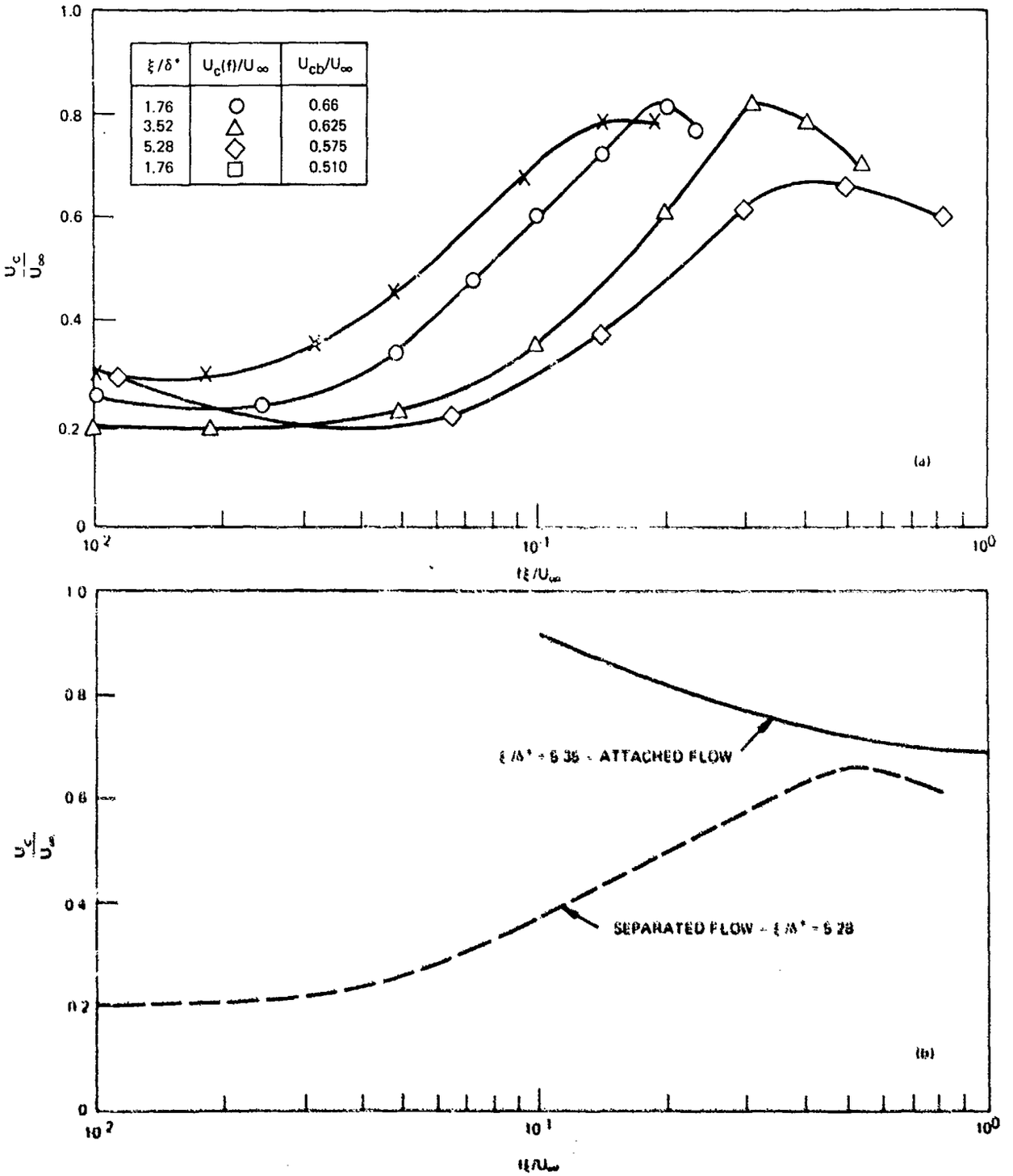

Figure 30. Narrow Band Convection Velocities in Separated Flow Vs. Strouhal Number[4]

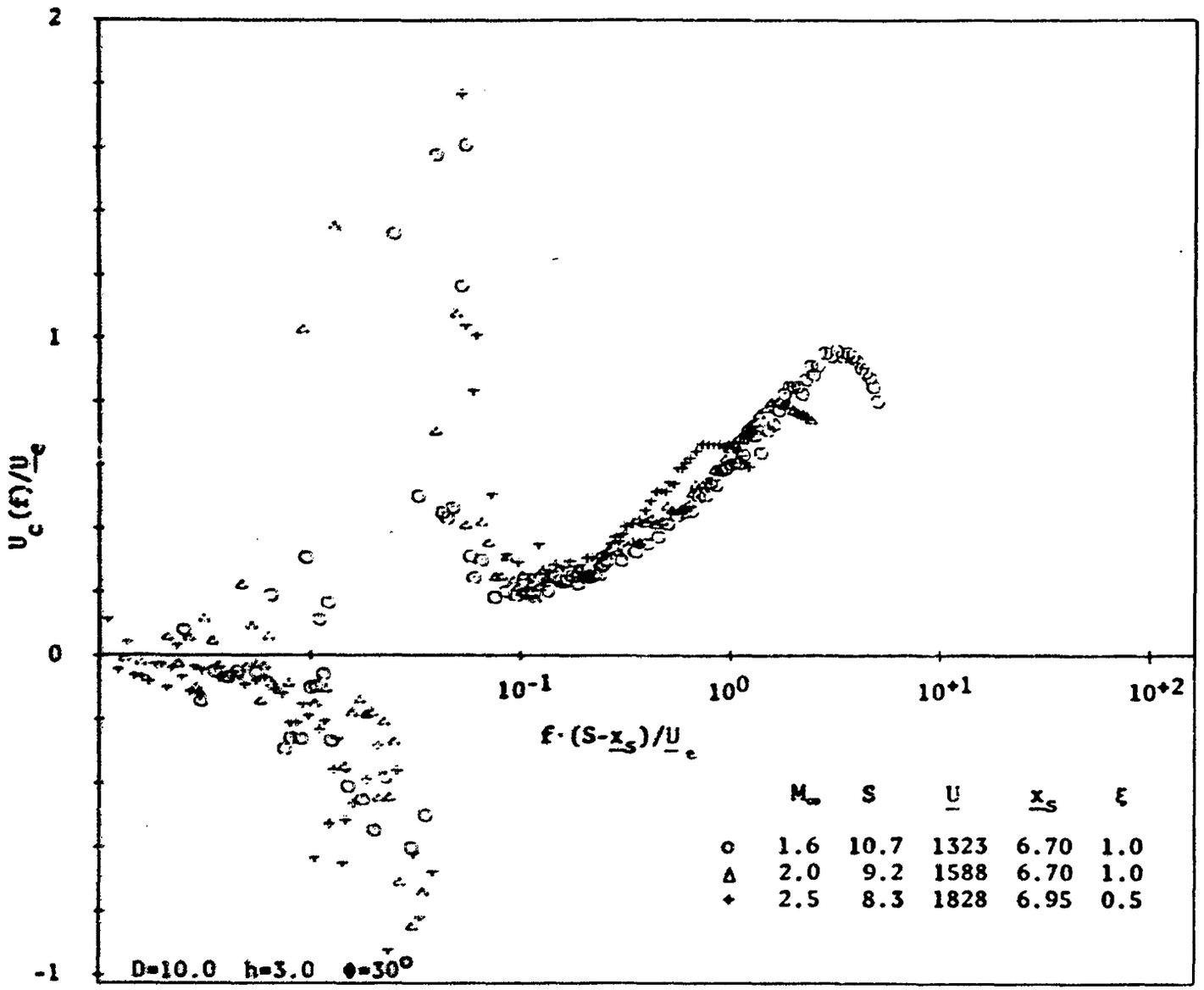

Figure 31. Narrow Band Convection Velocities Using Separation Distance as Normal (Preliminary Data Taken from Ref. 16 With Permission from NASA Ames)

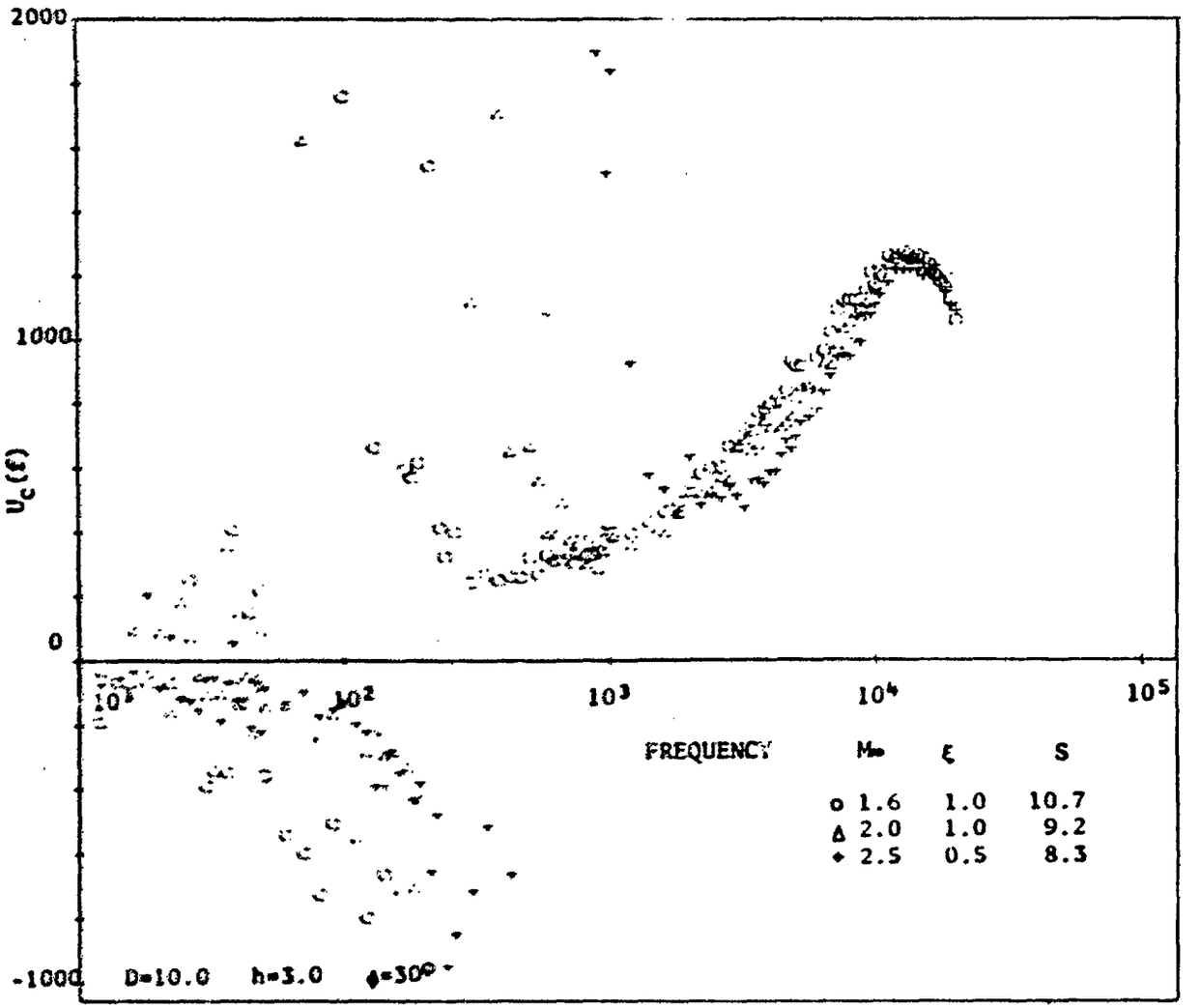

Figure 32. Typical Unnormalized Narrow Band Convection Velocity for Separated Flow (Preliminary Data Taken from Ref. 16 With Permission From NASA Ames)

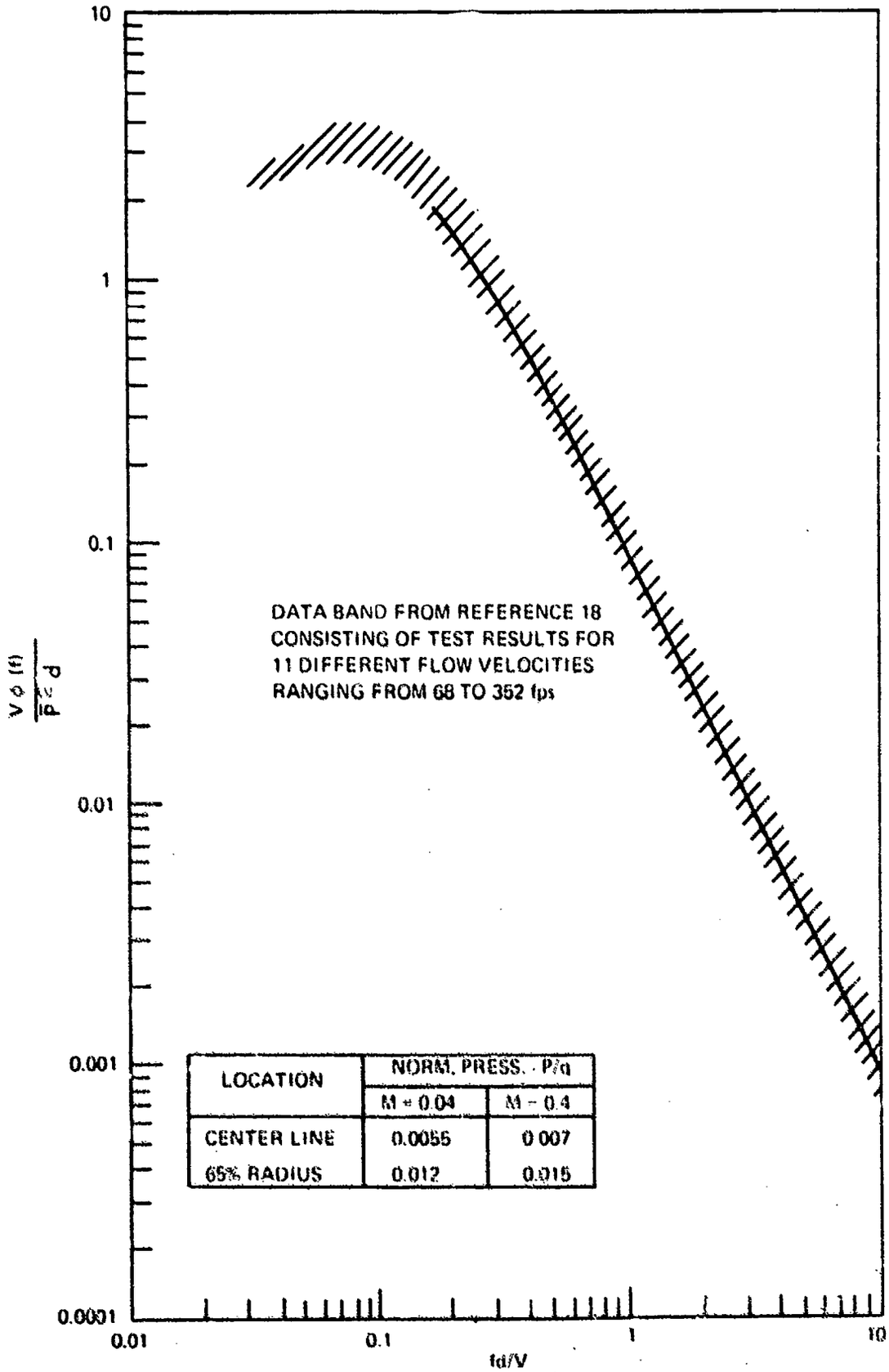

Figure 33. Typical Spectral Distribution in Base Flow (Subsonic)

SECTION IV

PRIOR PREDICTION METHODS REVIEW

This section briefly discusses existing mathematical models of aero-acoustic environments for various type flows expected during the re-entry phase of high ballistic coefficient vehicles. Extensive analytical and experimental studies have been performed by several investigators for defining acoustic properties during turbulent flow. Limited prediction techniques have been published for separated and base flow. No mathematical models for transitional flow were found to exist in the literature.

1. ATTACHED TURBULENT BOUNDARY LAYER FLOW

a. Acoustic Magnitude

It is not the intent of this study to summarize the historical background of pressure fluctuations in turbulent flow, since that subject has been the source of theoretical and experimental investigations for many years. What will be reviewed are present methods used in defining aero-acoustic environments during turbulent flow. Houbolt[14] performed a study assuming that eddy velocity is proportional to free-stream velocity and the local mean density in the region of maximum noise generation was the significant variable governing noise production. Using Euler's equation for flow and Crocco's equation for the temperature velocity relation, the rms pressure levels (Equations 1 & 2) as a function of Mach number and dynamic pressure (or free stream pressure P) is defined as:

$$P_{rms} = \frac{0.007}{1 + 0.012\,M^2}\,q \tag{1}$$

or

$$P_{rms} = \frac{0.0049\,M^2}{1 + 0.012\,M^2}\,p \tag{2}$$

Houbolt in unpublished work has further refined his above expression to include temperature, gas density and a recovery factor to obtain:

$$P_{rms} = \frac{0.007q}{1 + r_e\left(\frac{\gamma - 1}{2}\right) M^2} \tag{3}$$

where

$$r_e = (1 - \bar{U}/U_e)\,(r_1 + \bar{U}/U_e) \tag{4}$$

$$T_w/T_e = 1 + r_1 \left(\frac{\bar{\gamma} - 1}{2}\right) M^2 \tag{5}$$

Similar studies performed by Lowson [2] assuming an adiabatic wall, constant static pressure through the boundary layer, and Crocco's relation resulted in the following equations for the overall fluctuating pressure intensity:

$$P_{rms} = \frac{0.006}{1 + 0.14\,M^2}\,q \tag{6}$$

$$P_{rms} = \frac{0.0042\,M^2}{1 + 0.14\,M^2}\,p \tag{7}$$

Ailman [19] developed an expression for the pressure intensity based on a review of test results for the Mach number range from 0.6 to 5. This expression, given in Equation 8, must be used with some reservations at Mach numbers greater than five.

Figure 34 gives the pressure intensity normalized by dynamic pressure as a function of Mach number for the various investigators discussed. Of the various prediction techniques, Lowson's equation, because of its simplicity and good agreement with experimental data was found to be most representative.

$$P_{rms} = 3 \times 10^{-4}\left[5 + (M_\infty - 4)^2\right] q_\infty \tag{8}$$

b. Acoustic Power Spectral Density

Bull and Willis' [21] semi-empirical approach defined the spectral relation in turbulent flow as:

$$\phi(\omega) = \frac{q_\infty^2\,\delta^*}{U_\infty}\left[5.32\,e^{-\omega_o^2} - 1.25\,e^{-10\,\omega_o^2}\right] \times 10^{-5} \tag{9}$$

where

$$\omega_o = \frac{\omega\,\delta^*}{1.125\,U_\infty}$$

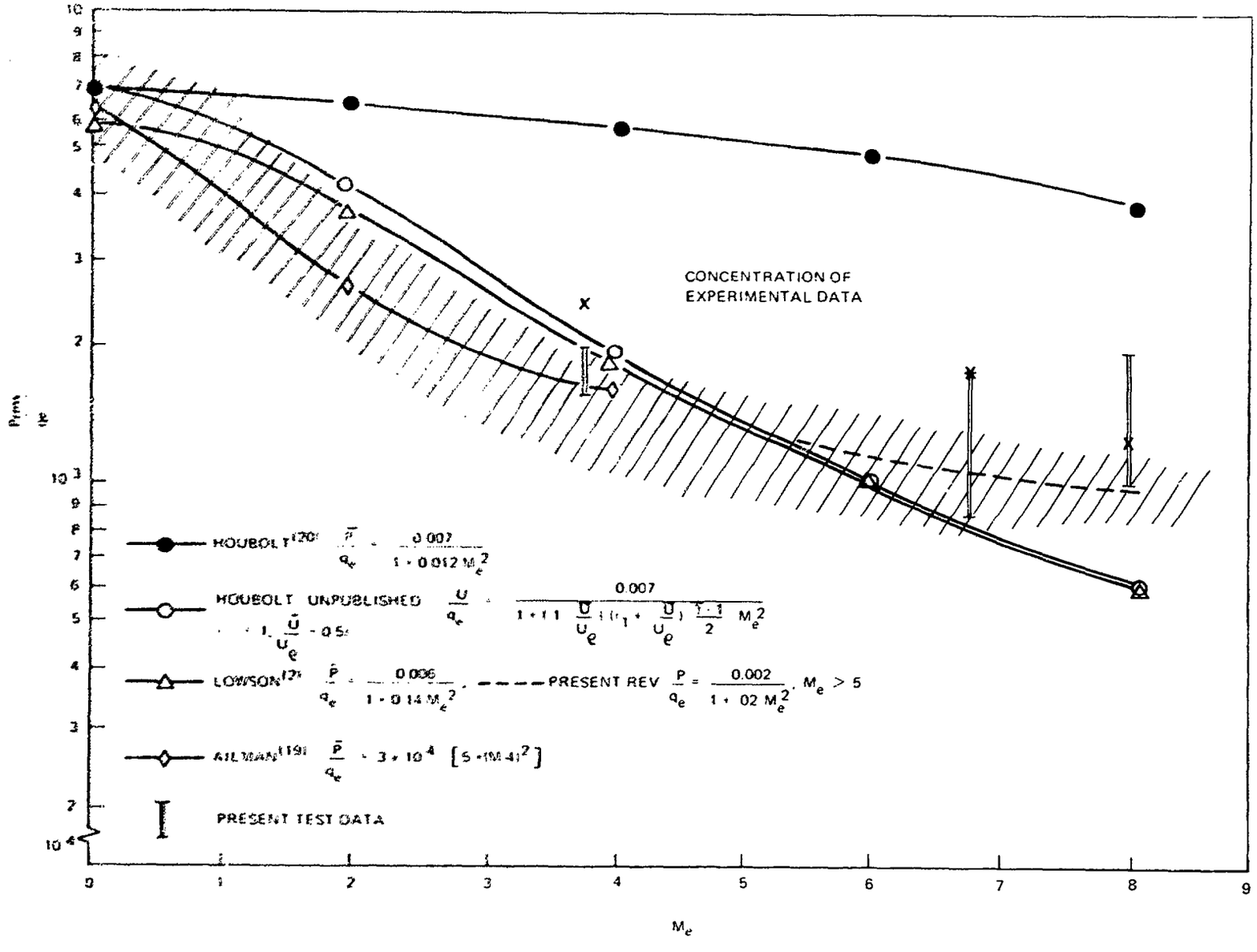

Figure 34. Comparison of Overall Acoustic Magnitude Prediction Methods to Experimental Data

Later, Bull[22] using miniature pressure-sensing elements in subsonic wind tunnel tests and auto-correlation functions developed the following:

$$\phi(\omega) = \frac{q_\infty^2 \delta^*}{U_\infty} \left[3.7\, e^{-2\omega_0} + 0.8\, e^{-0.47\,\omega_0} - 3.4\, e^{-8.\,\omega_0} \right] \times 10^{-5} \tag{10}$$

where

$$\omega_0 = \omega \delta^* / U_\infty$$

Using experimental data and engineering logic, Houbolt[14, 20] derived a spectral relation for turbulent flow as:

$$\phi(\omega) = \frac{2\delta^*}{\pi U_c} P_{rms}^2 \frac{1}{1 + \left(\frac{\omega \delta^*}{U_c}\right)^2} \tag{11}$$

Lowson[2] using subsonic and supersonic data developed an empirical Equation (12) which introduced the boundary layer thickness as a representative length parameter. This is given by the following:

$$\phi(\omega) = \frac{P_{rms}^2}{\omega_0 \left\{ 1 + (\omega/\omega_0)^2 \right\}^{3/2}} \tag{12}$$

$$\omega_0 = 8\, U/\delta$$

Robertson[1] using recent measurements at supersonic speeds developed Equation 12:

$$\phi(\omega) = \frac{\delta^* P_{rms}^2}{U_\infty} \frac{1}{\frac{\omega_0 \delta^*}{U_\infty} \left\{ 1 + (\omega/\omega_0)^{.9} \right\}^{2.0}} \tag{13}$$

where

$$\omega_0 = 0.5\, U_\infty / \delta^*$$

This Equation 13 does give the best fit to experimental data as shown in Figure 35; however, Houbolt's Equation 11 is recommended for general use because of its simplicity. Since no one characteristic length (δ or δ^*) gives better collapse of the data, Lowson's Equation is also recommended for use if boundary layer thickness is known. Figure 36 compares Lowson's Equation with typical spread in test data.

c. Cross-Correlation Functions

Cross-correlation and cross-spectrum functions pertinent to the aero-acoustic environment are related through their Fourier transforms as follows:

$$\phi(\xi, \eta, \omega) = \int_{-\infty}^{\infty} R(\xi, \eta, t)\, e^{i\omega t}\, dt \tag{14}$$

and

$$R(\xi, \eta, t) = 1/2\pi \int_{-\infty}^{\infty} \phi(\xi, \eta, \omega)\, e^{-i\omega t}\, d\omega \tag{14a}$$

The cross-spectrum can also be expressed in terms of the co-spectral density and quad spectral density:

$$\phi(\xi, \eta, \omega) = \phi_R(\xi, \eta, \omega) - j\,\phi_i(\xi, \eta, \omega) \tag{15}$$

where the co-spectral density is used in defining characteristics of the fluctuating pressure field. Lowson[2] and Robertson[1] using data obtained by Bull [8] defined the cross-correlation function for turbulent flow assuming that the cross-power spectral density is a function only of the separation distances. These functions are of the form:

$$\phi_R(\xi, o, \omega) = A_\xi(\xi, \omega) \cos \frac{\omega \xi}{U_c} \left[\phi_{\xi_1}(\omega)\, \phi_{\xi_2}(\omega)\right]^{1/2} \tag{16}$$

$$\phi_R(o, \eta, \omega) = A_\eta(\eta, \omega) \left[\phi_{\eta_1}(\omega)\, \phi_{\eta_2}(\omega)\right]^{1/2} \tag{17}$$

From Bull's data the following expressions for the correlation coefficients are given as:

$$A_\eta(\eta, \omega) = \exp\left(-0.72\,|\eta|\,\frac{\omega}{U_c}\right) \exp\left(\frac{-2.0\,|\eta|}{\delta}\right) \tag{18}$$

$$A_\xi(\xi, \omega) = \exp\left(-0.1\,\frac{|\xi|\,\omega}{U_c}\right) \exp\left(\frac{-0.27\,|\xi|}{\delta}\right) \tag{19}$$

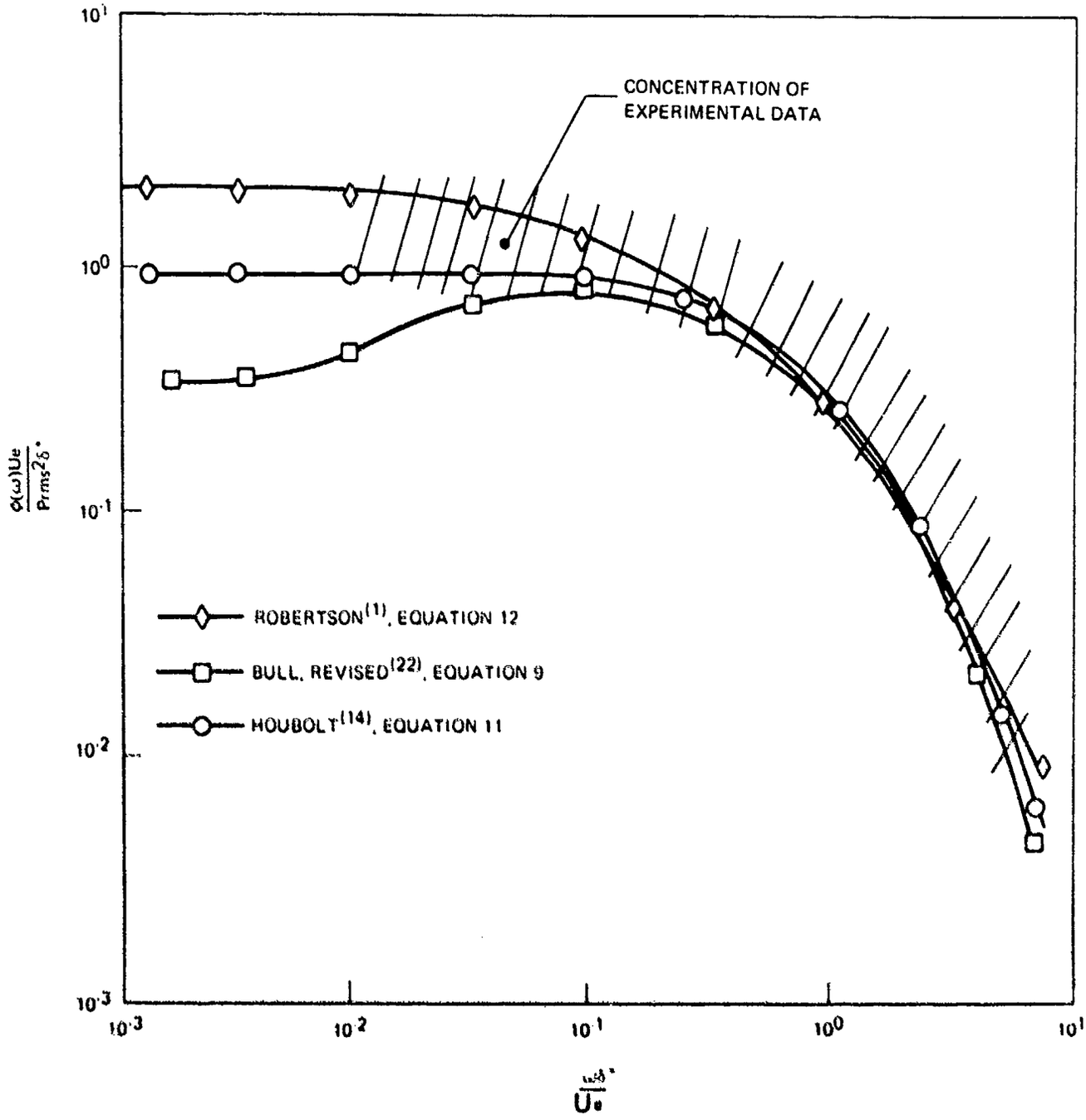

Figure 35. Comparison of Normalized Power Spectra Prediction Methods to Experimental Data

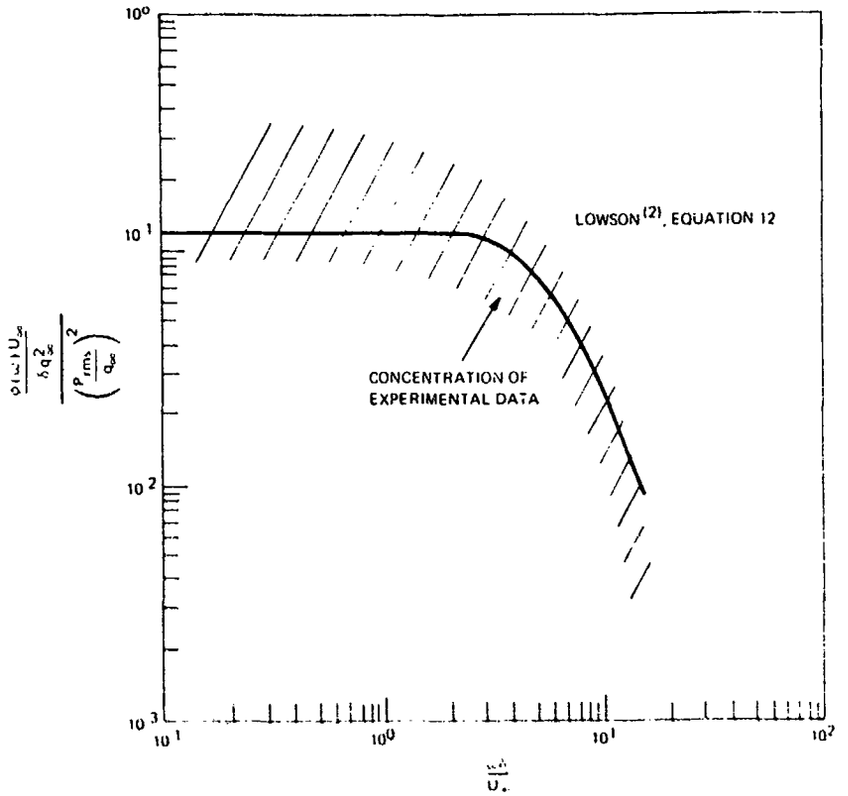

Figure 36. Comparison of Lowson's Normalized Power Spectra (Using δ) to Experimental Data

These correlation coefficients may also be expressed in terms of boundary layer displacement thickness as:

$$A_\eta(\eta, \omega) = \exp\left(\frac{-0.72\,|\eta|\,\omega}{U_c}\right)\left[0.3 + 0.7\exp\left(\frac{-0.5\,|\eta|}{\delta^*}\right)\right] \tag{20}$$

(Figure 38) (Figure 39)

$$A_\xi(\xi, \omega) = \exp\left(\frac{-0.1\,|\xi|\,\omega}{U_c}\right)\exp\left(\frac{-0.034\,|\xi|}{\delta^*}\right) \tag{21}$$

(Figure 37) (Figure 39)

Lowson[2] suggests that when using the separable form of the correlation coefficient in response analysis, the correlation area is underestimated by a factor of $\pi/2$ and should be adjusted accordingly. This factor stems from the fact that the coefficients will remain constant along straight lines on the surfaces, forming a diamond pattern surrounding the origin which physically is unreasonable. An elliptical form would be more realistic. Therefore a ratio of areas is required, leading to a $\pi/2$ factor. Correlation functions defined by Crocker[23] and White [11] are of similar forms to those previously discussed

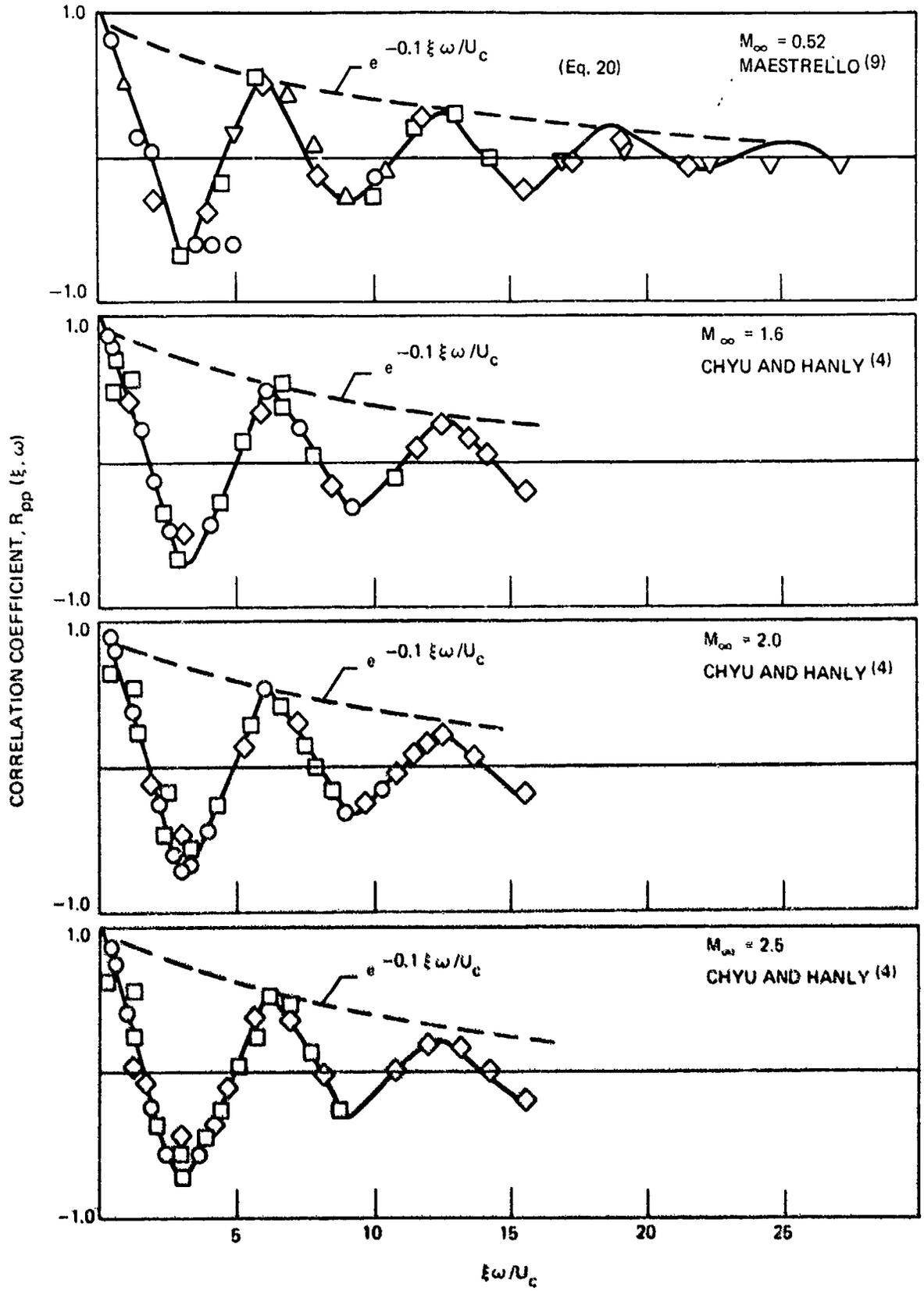

Figure 37. Comparison of Frequency Dependent Narrow Band Long Space Correlation Coefficient with Analytical Expression

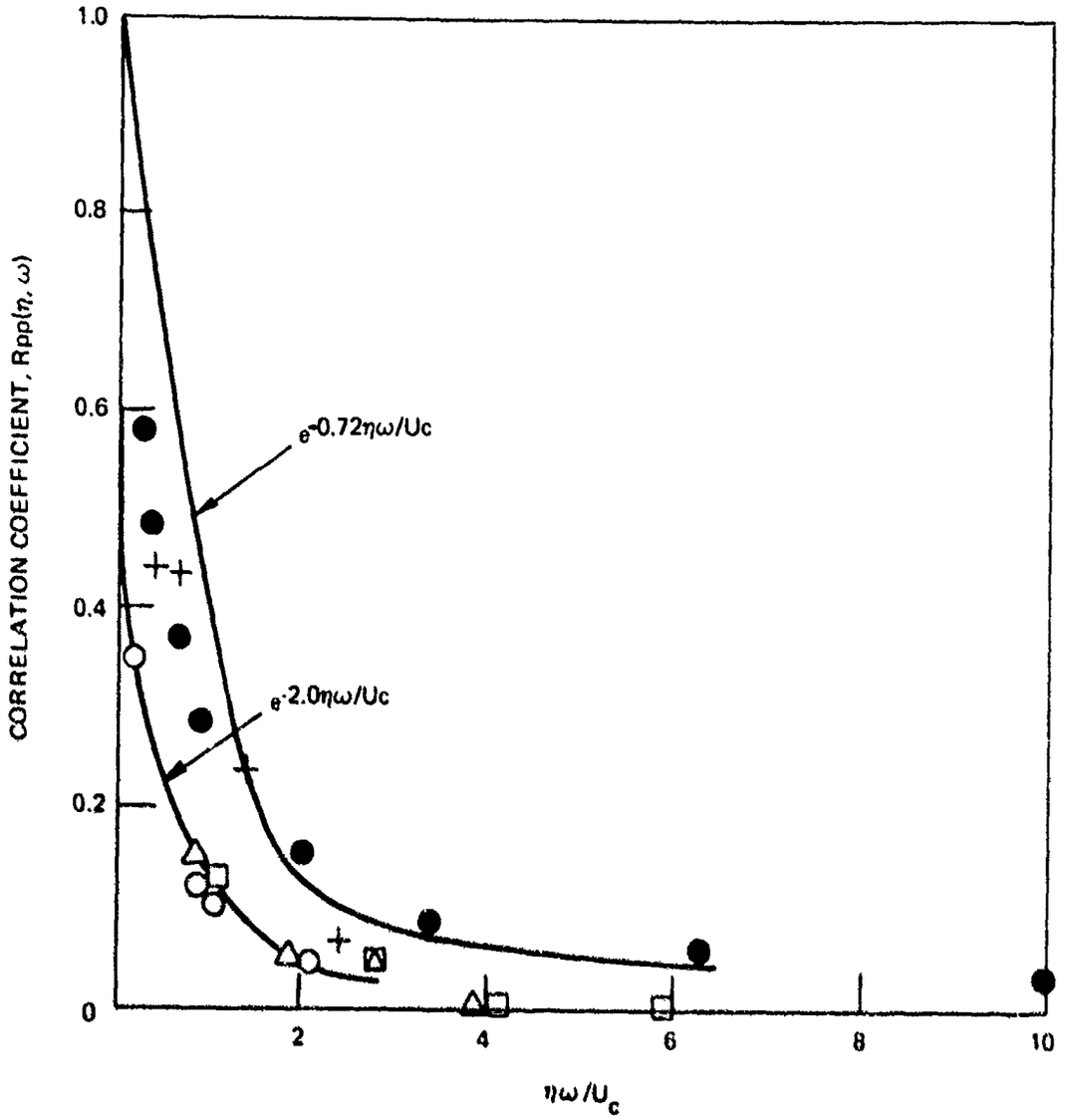

○ MAESTRELLO[9], CENTER FREQ 1200 Hz.
△ MAESTRELLO[9], CENTER FREQ 2400 Hz.
□ MAESTRELLO[9], CENTER FREQ 3600 Hz.
■ WILLMARTH & WOOLDRIDGE, CENTER FREQ 500 Hz
+ BULL[8], CENTER FREQ 1260, 2000, 3200 & 5000 Hz.

Figure 38. Comparison of Frequency Dependent Narrow Band Lat. Space Correlation Coefficient With Analytical Expression

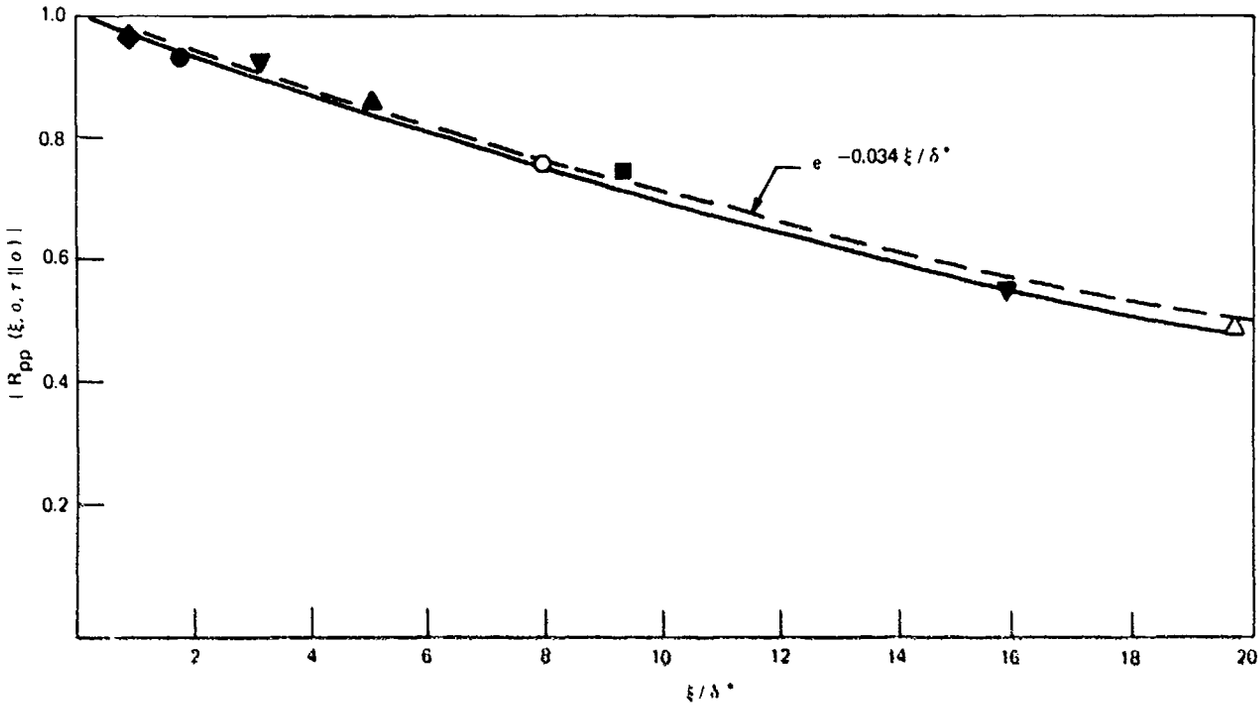

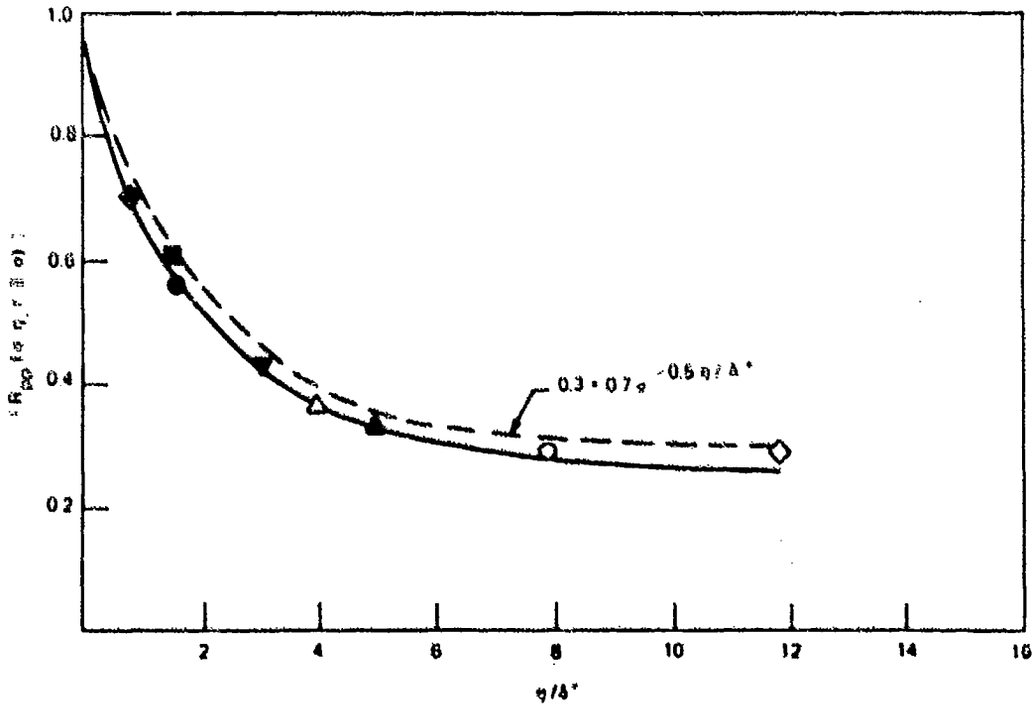

Figure 39. Comparison of Spatial Dependent Long. and Lat. Correlation with Analytical Expressions

except the coefficient of 0.72 in Equation 18 is specified as 2.0. Subsequent published data suggests that a coefficient of 0.72 is more reasonable (Figure 38). Maestrello[9] suggests the cross-correlation coefficient to be:

$$A(\xi, \eta, \omega) = e^{\left[\frac{-|\xi|}{\alpha_1 \delta} \quad \frac{-|\eta|}{\alpha_2 \delta} \quad \frac{-i\omega\xi}{U_c}\right]} \tag{22}$$

where

$$\alpha_1 = \frac{50}{C_f R_\theta}, \quad \alpha_2 = 0.26$$

Using Maestrello's data at Me = 0.6 results in the following expression for

$$e^{-1.7\frac{|\xi|}{\delta}} e^{-3.9\frac{|\eta|}{\delta}} e^{-i\omega\xi/U_c}$$

which suggests a significantly higher decay rate than that defined by Bull (Equations 18, 19).

Houbolt (Equation 23) defined a similar general expression for the cross-correlation function as Maestrello, however specific longitudinal exponential values were not presented.

$$A(\xi, \eta, \omega) = e^{\left[-C\eta/\delta^* - a\xi/\delta^* - i\omega\xi/U_c\right]} \tag{23}$$

where C = 1, a - to be defined, varies with Mach No.

Neither Houbolt nor Maestrello defined exponent decay terms as functions of ω/U_c. This approach appears acceptable in the practical design of high beta vehicles, due to the low frequency range of interest ($f \leq 2$khz) and high convective velocities, causing the exponential term ($e^{-\omega\xi/U_c}$) to approach unity.

d. Convection Velocity

Using experimental data, Lowson[2] defines the convection velocity normalized to the free stream velocity as:

$$U_c/U_\infty = 0.075 + 0.3 \exp\left(\frac{-0.11\delta\omega}{U_\infty}\right) - 0.25 \exp(-1.2\,\xi/\delta) \tag{24}$$

where the broad band convection velocity corresponds to $\frac{\omega\delta}{U_\infty} = 8$

resulting in

$$\frac{U_{cb}}{U_\infty} = 0.8 - 0.25 \exp(-1.2\,\xi/\delta) \tag{25}$$

A corresponding equation for the broad band convection velocity as a function of boundary layer displacement thickness would be

$$\frac{U_{cb}}{U_\infty} = 0.8 - 0.5 \exp(-0.4\, \xi/\delta^*) \tag{26}$$

2. SEPARATED FLOW

A comprehensive treatment of separated flow and oscillating shocks in terms of prediction methods is given by Robertson[1]. This section briefly summarizes those results.

a. Acoustic Magnitude

For expansion induced separated flow, Equation 27 is recommended:

$$P_{rms} = \frac{0.045}{1 + M_e^2}\, q_\infty \tag{27}$$

The expression given by Equation 27 is compared with experimental data in Figure 40. This expression is similar in form with that proposed for attached turbulent flow. At this time no general expression is available for defining fluctuating pressure levels in the region upstream of compression corners, since insufficient experimental data is available. The data as shown in Figure 19 appear to increase with free stream Mach number. It would seem reasonable that local flow conditions would play an important part in defining an expression for the overall fluctuating pressure.

At the point of flow separation, the flow intermittently fluctuates between a separated flow and attached flow condition. This represents an alternating unbalance between the large pressure rise through the shock wave, exceeding that required for separated flow. Hence, extremely large fluctuating pressures can result from this condition. Data is limited for this environment and no empirical equation has been uncovered in the literature. Using limited data of Reference[1] an expression for fluctuating pressures at the point of separation is proposed as:

$$P_{rms} = \frac{0.14}{1 + 0.5\, M_\infty^2}\, q_\infty \tag{28}$$

Figure 41 compares available data with Equation 28. Chyu and Hanly[4] present fluctuating pressure data normalized by the free stream dynamic pressure at the point of shock reattachment. These levels are significantly higher than at the point of separation. However, insufficient data is available to derive a representative expression for fluctuating pressure in the region of shock wave reattachment.

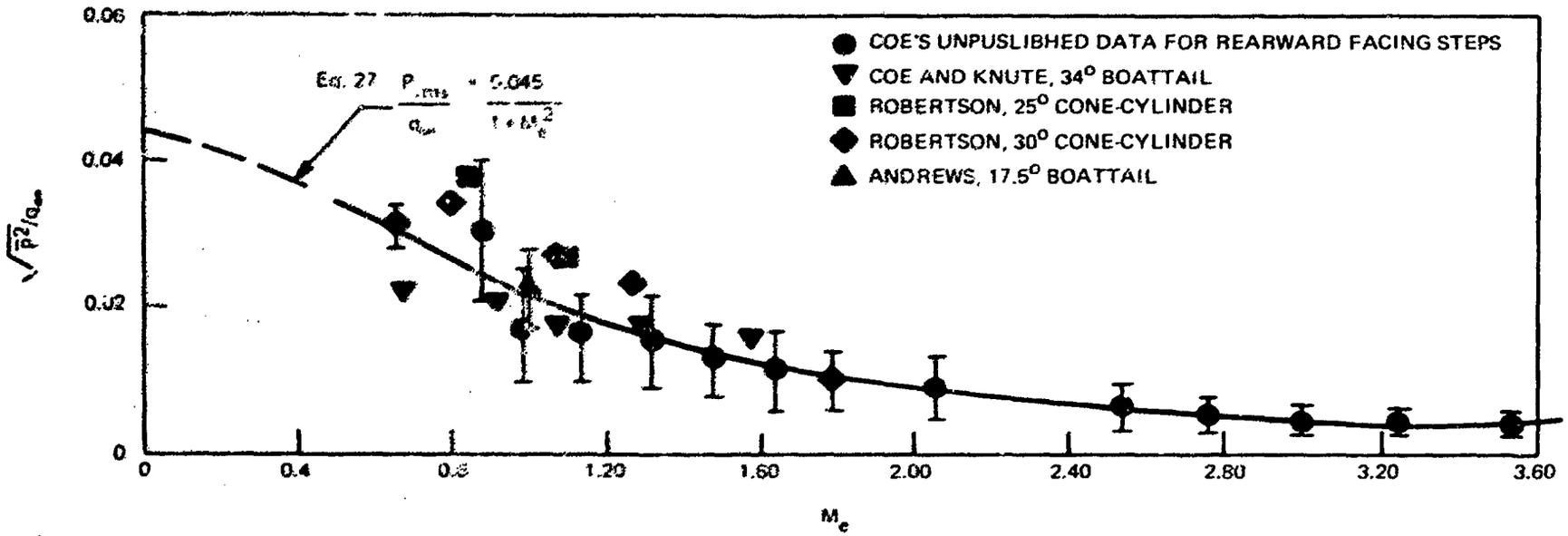

Figure 40. Comparison of Overall Acoustic Intensity for Separated Flow With Analytical Predictions

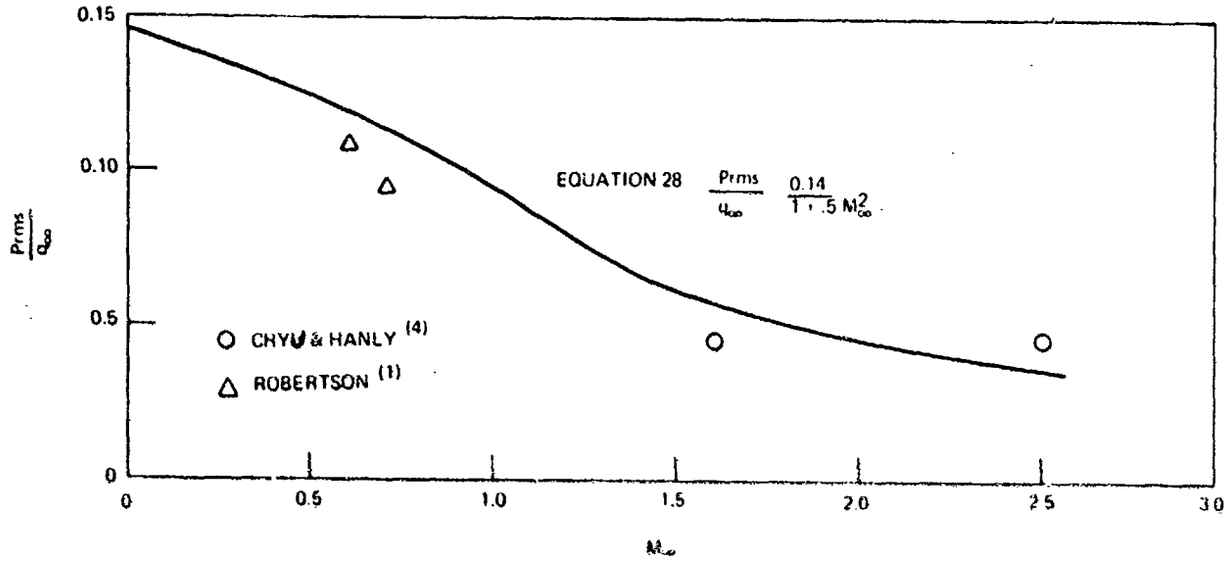

Figure 41. Comparison of Overall Acoustic Magnitude at the point of flow Separation With Analytical Predictions

b. Acoustic Power Spectral Density

Using data obtained by Rechtien[11] for the homogeneous region of compression corners, Robertson defined the normalized power spectra as:

$$\frac{\phi(f) U_e}{q_\infty^2 \, \delta} = \frac{P_{rms}^2 / q_\infty^2}{\frac{f_o \delta}{U_e} \left\{ 1 + (f/f_o)^{.83} \right\}^{2.15}} \tag{29}$$

$$f_o = 0.17 \, U_e / \delta$$

Equation 29 appears to be a reasonable expression for expansion induced separated flow even though it is derived based on data taken in compression corners, as indicated in Figure 24. Figure 42 compares this expression with typical test data.

Equation 32 defines the power spectral density distribution for shock wave oscillation in homogeneous flow. Robertson derived this expression by combining the spectral distributions for separated flow (Equation 29) and shock wave oscillation, Equation 30, (in the absence of viscous flow) with an experimentally derived weighting function (K_1). Flow parameter used in these expressions are for conditions upstream of the shock wave.

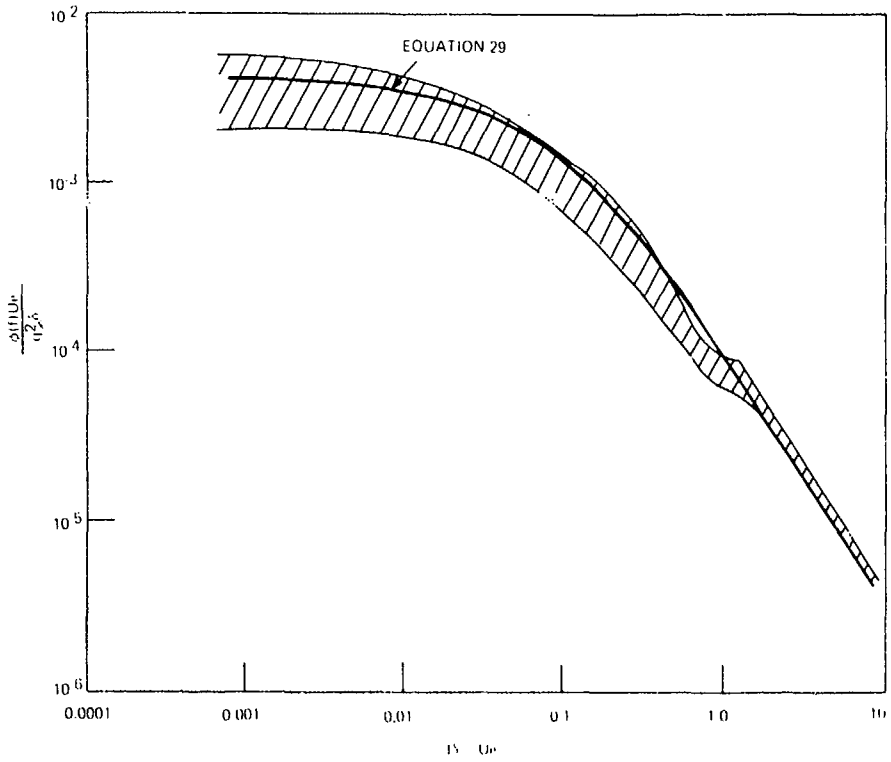

Figure 42. Comparison of Separated Flow Power Spectra With Analytical Expression

$$\left[\frac{\phi(f)\,U_e}{q_\infty^2\,\delta}\right]_{SW}^{I,H} = \frac{\left(P_{rms}^2/q_\infty^2\right)_{SW}^{I,H}}{\left(\frac{f_o\,\delta}{U_e}\right)_{SW}\left\{1+(f/f_o)^{1.55}\right\}^{1.7}} \tag{30}$$

where

$$\left(\frac{\delta\,f_o}{U_e}\right)_{SW} = 1 \times 10^{-3}$$

and

$$\left(\frac{P_{rms}^2}{q_\infty^2}\right)_{SW}^{I,H} = \left[\frac{P_{rms}^2}{q_\infty^2}\right]_{SW}^{H} - K_1\left[\frac{P_{rms}^2}{q_\infty^2}\right]_{S}^{H} \tag{31}$$

$$\left[\frac{P^2_{rms}}{q^2_\infty}\right]^H_{SW}$$ — Overall level of shock oscillation peak corresponding to the mean location of the shock wave.

$$\left[\frac{P^2_{rms}}{q^2_\infty}\right]^H_{S}$$ — Overall level of homogeneous separated flow.

$$\left[\frac{\phi(f)\, U_e}{q^2_\infty\, \delta}\right]^H_{SW} = \frac{\left(\frac{P^2_{rms}}{q^2_\infty}\right)^{I,\,H}_{SW}}{\left(\frac{f_o\,\delta}{U_e}\right)_{SW}\left\{1+\left(\frac{f}{f_o}\right)^{1.55}\right\}^{1.7}} + K_1\left(\frac{f_o\,\delta}{U_e}\right)_S\left\{1+\left(\frac{f}{f_o}\right)^{0.83}\right\}^{2.15} \tag{32}$$

Subscripts: SW - Shock wave

S - Separated flow

Superscripts: I - Absence of viscosity

H - Homogeneous flow

$$K_1 = 0.25\left(\frac{f_o\,\delta}{U_e}\right)_{SW} = 1 \times 10^{-2}$$

A comparison of the predicted spectral distribution for shock wave oscillation is presented in Figure 43.

c. Cross-Correlation Function

Chyu and Hanly[4] data indicate that decay of the normalized cross spectra for separated flow is exponential at high values of $\omega\,\xi/U_e$, similar to that observed for

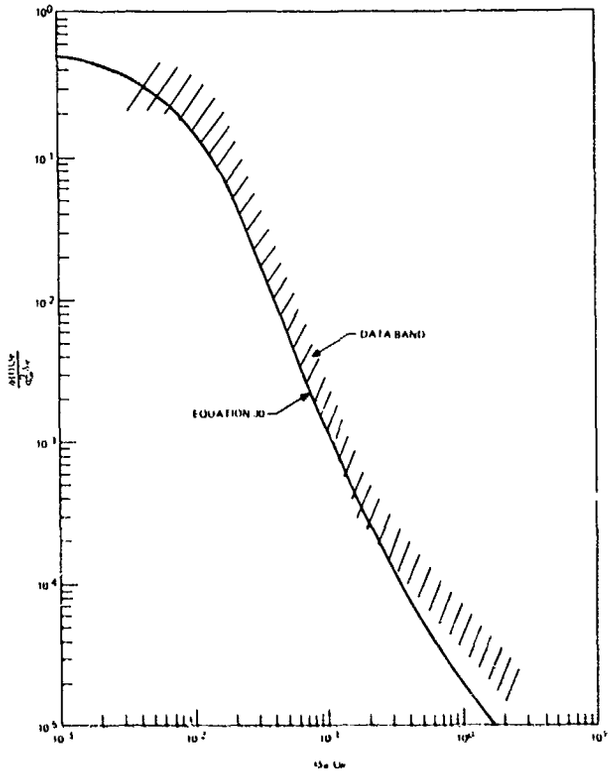

Figure 43. Comparison of Shock-Wave Oscillation Spectral Distribution to Analytical Prediction

attached flow. Thus as a first approximation, the normalized longitudinal co-spectra may be represented by:

$$A(\xi, f) = e^{-a \frac{\omega \xi}{U_e}} \cos \frac{\omega \xi}{U_c} \tag{33}$$

and

$$A(\eta, f) = e^{-b \frac{\omega \eta}{U_e}} \tag{34}$$

However, the associated decay rates were found to vary for each test Mach number (1.6 to 2.5), suggesting that the decay rate may be dependent on Mach number as well as local flow conditions. This suggests that the above functions (Equations 33, 34) should be expressed in the following form:

$$A\left(\xi, \frac{f \delta}{U_e}\right) = e^{(-a_\xi)^{\xi}} \cos \frac{\omega \xi}{U_c} \tag{35}$$

$$A\left(\eta, \frac{f\delta}{U_e}\right) = e^{(-\alpha \quad)\eta} \tag{36}$$

where for longitudinal correlation (ξ)

$$\alpha = 0.75, \quad \frac{f\delta}{U_e} < 6 \times 10^{-3}$$

$$\alpha = 0.75\left[\frac{f\delta/U_e}{6 \times 10^{-3}}\right], \quad 6 \times 10^{-3} \quad \frac{f\delta}{U_e} \leq 6 \times 10^{-2}$$

$$\alpha = 1.5\left[\frac{f\delta/U_e}{6 \times 10^{-3}}\right], \quad \frac{f\delta}{U_e} > 6 \times 10^{-2}$$

for lateral correlation

$$\alpha = 0.75, \quad \frac{f\delta}{U_e} < 6 \times 10^{-3}$$

$$\alpha = 0.75\left[\frac{f\delta/U_e}{6 \times 10^{-3}}\right]^{0.3}, \quad \frac{f\delta}{U_e} \geq 6 \times 10^{-3}$$

Limited data has been published defining the cross-power-spectra of fluctuating pressures beneath oscillating shock waves. Robertson defines the longitudinal co-spectra as:

$$A(\xi, f) = e^{-40 f\delta/U_e} \cos 2\pi \frac{f\delta}{U_e} \tag{37}$$

No data or expressions defining the transverse spatial characteristics of shock induced fluctuating pressures were found in the literature.

3. BASE FLOW

Houbolt's technique[20] was the only method available for predicting base pressure fluctuating characteristics. This method is based upon knowledge of the characteristic of

aerodynamic turbulent flow and the application of engineering logic rather than experimental data. Houbolt's formulation is summarized in the following sections.

a. Acoustic Intensity

The pressure fluctuations in base flow are a function of the strong shear flow along the wake cone and a complex recirculation flow. Houbolt assumed that the mean density at some effective location, for example point A in Figure 44, has governing control on base fluctuating pressures. Assuming that the eddy velocities are proportional to the mean shear flow velocity, a simple form for the rms pressure level is expressed in terms of density and pressure

$$P_{rms_b} = c \frac{\rho}{\rho_b} q_b = c \frac{T_b}{T} q_b,$$

resulting in a general expression for overall sound pressure level.

$$P_{rms_b} = \frac{.7\, c\, M_b^2}{1 + .2\, r\, M_b^2}$$

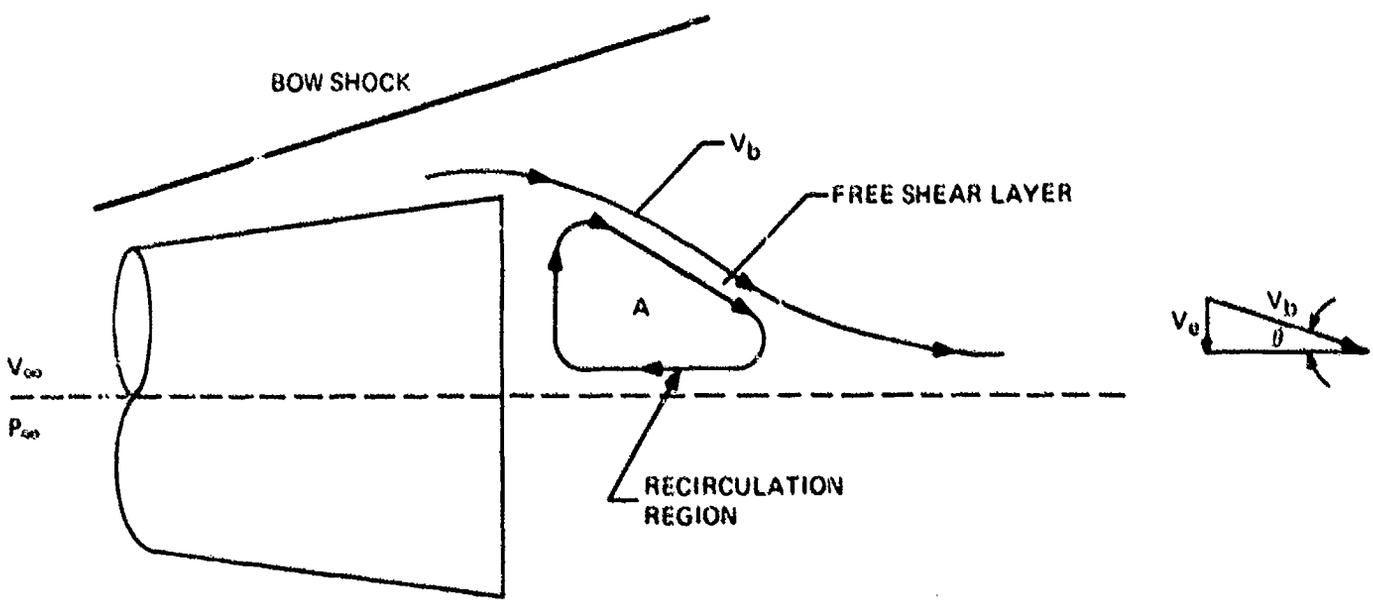

Figure 44. Typical Base Flow

Tentative values have been established for c and r with c chosen to agree with data obtained in Reference 2. A value of 0.9 was chosen for the recovery factor assuming that a strong shear and minimal cooling occurs. The resulting expression for base fluctuations is therefore:

$$P_{rms_b} = \frac{0.01\, M_b^2}{1 + 0.18\, M_b^2}\, P_b \tag{38}$$

b. Acoustic Power Spectral Density

In order to arrive at the base spectral density at a given point a correlation function of the form

$$R(t) = P^2_{rms_b}\, e^{-\frac{V_T}{L} t} \tag{39}$$

is assumed, where V_T is an effective transport velocity and L is the scale of turbulence defined as:

$$L = \int_0^\infty \frac{R(x)}{P^2_{rms_b}}\, dx, \quad (x = V_T\, t) \tag{40}$$

The spectral function consistent with the above defined correlation function is:

$$\phi(\omega) = \frac{2\, P^2_{rms_b}\, L}{\pi\, U_e} \quad \frac{1}{1 + \left(\frac{L\omega}{U_e}\right)^2} \tag{41}$$

Assuming that the scale of turbulence is on the order of the base radius and the transport velocity is related to the transverse component of the flow velocity along the wake boundary the following spectral function results

$$\phi(\omega) = \frac{2\, P^2_{rms_b}\, S}{\pi\, U_b} \quad \frac{1}{1 + \left(\frac{\omega S}{U_b}\right)^2} \tag{42}$$

where S is the apparent wake cone surface length. Figure 45 compares the above expression with experimental data obtained from Reference 7.

c. Cross Correlation

No experimental data or strict derivation of the correlation function was found. Houbolt has assumed the following function:

$$R(t) = P^2_{rms_b} \; e^{-\frac{V_T}{L} t} \tag{43}$$

where

$$L \approx R_b, \; V_T = U_b \sin\theta$$

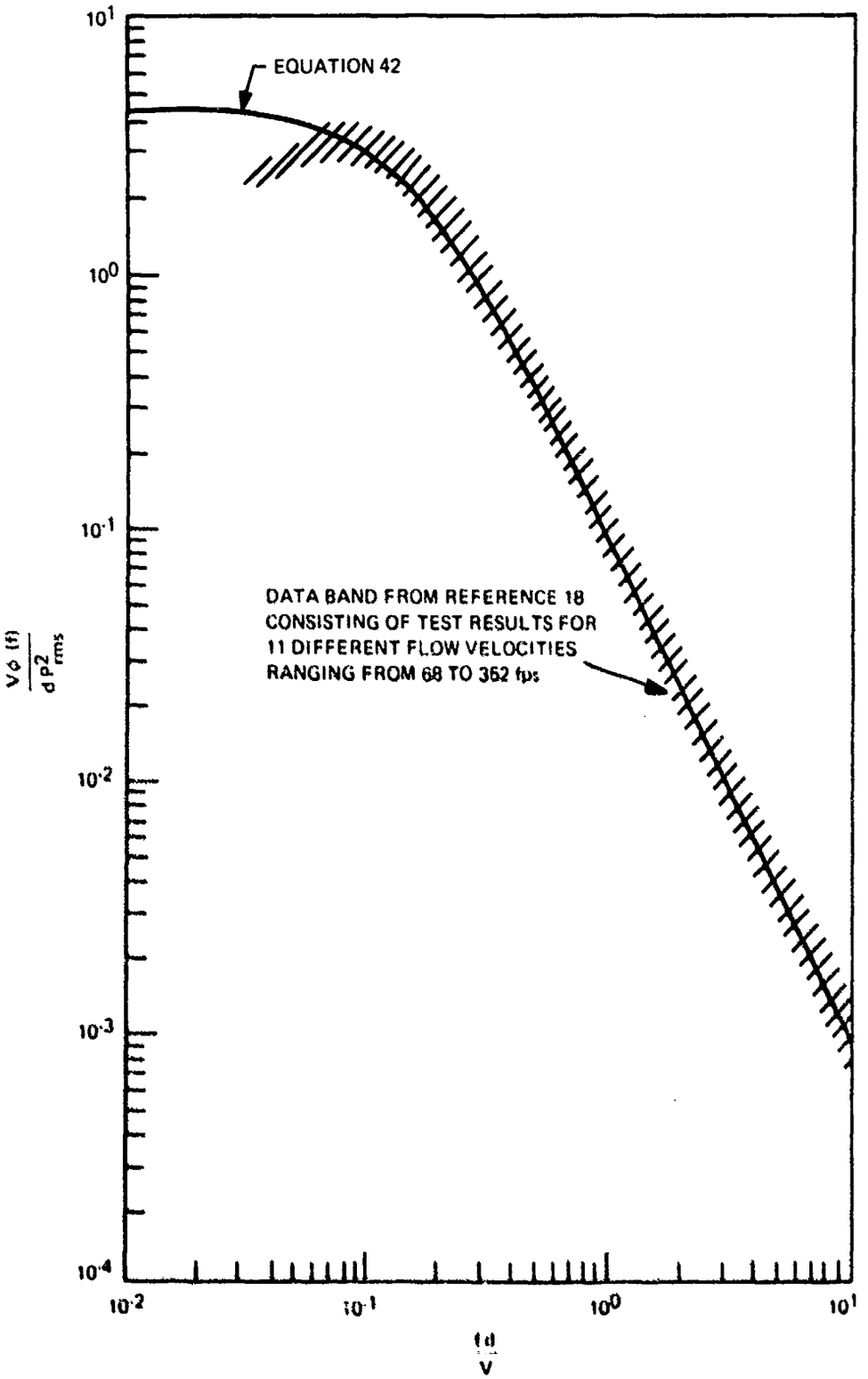

Figure 45. Comparison of Spectral Wake Theory with Test Results

SECTION V

SUMMARY OF TEST RESULTS

This section represents a condensation of Section II (Volume II) of this study. Fluctuating pressure data were obtained for transitional, turbulent, separated and base flow at various angles of attack (α), Mach numbers and nose radii. Several acoustic sensors were located on the surface of the forward section of the test model (0 to 8 inches) in laminar flow to measure tunnel tare noise. This term is used since in addition to tunnel noise, some radiated noise contribution from turbulent flow downstream is also measured by these sensors. For various tunnel conditions especially at the higher Mach numbers, these sensors measured significant fluctuating pressures which tended to mask measurements made in fully developed turbulent flow. However, it was possible to correct the data in order to obtain realistic approximations to the true values. Tunnel conditions, model attitude and configurations for which data was obtained are given in Table I. Tables II and III define the free stream and local aerodynamic properties while Table IV presents a summary of acoustic sensors installed in the test vehicle along with location definition.

1. ACOUSTIC MAGNITUDE

Fluctuating pressures (from 0-20 kHz) during turbulent flow were obtained from the aft array of acoustic sensors for the three test Mach numbers: 4, 8 and 10. These pressures, normalized by the local dynamic pressure are listed in Table V. It was observed that as Reynolds numbers were increased, tunnel tare noise also increased. This is attributed to the inclusion of an additional stage of compression necessary for desired tunnel conditions and the forward advancement of the region of transition along the test vehicle. Actual and corrected pressure data at all Mach numbers are given in Table V, which illustrates the effect of tunnel tare noise. Because of the uncertainty in tunnel tare noise, it is recommended that the levels given in Table V be considered as an upper and lower bound of the true pressure data.

Table VI summarizes the peak normalized fluctuating pressures under transition of flow. The spatial distribution of the acoustic environment for transition is a gradual build-up in fluctuating pressure reaching a maximum value toward the end of the transition zone. Fully turbulent flow is achieved at distances downstream ranging from 10 to 100 boundary layer thicknesses from onset. Typical fluctuating pressure distributions along the vehicle are shown in Figure 46.

Several tests were conducted at $M_\infty = 8.0$ with the test model at an attitude of ± 7.2 degree (vehicle half-cone angle) which exposed the main array of acoustic sensors to both windward and leeward flow resulting in a complete fluctuating pressure map of the vehicle. Figure 47 represents typical fluctuating pressure distributions measured at these high angles of attack. Of significance in these runs are the unexpectedly high fluctuating pressures on the windward side of the vehicle which remain high downstream from the transition region. Co-existent with these high levels are the surprisingly low pressure levels

TABLE I. SUMMARY OF NOMINAL TEST CONDITIONS

Facility	Mach Number	Reynolds Number ($\times 10^{-6}$ Ft^{-1})	Stagnation Pressure (psia)	Stagnation Temperature (°F)	Nose Radius (in.)	Angle of Attack (Degrees)
A	4	1.4	18	140	0	0 ±1 ±2 -4 -7.2 -8.2
		2.2	28		0	0 ±1 ±2 -4 -7.2
		2.8	35.7		0	0 ±1 ±2 -4 -7.2
		2.2	28		0.055	0 ±1 ±2 -4 -7.2
		3.0	38.1		0.110	0 ±1 ±2 -4 -7.2
B	8	1.4*	285	785	0	0 ±1 ±2 ±4 ±7.2
		1.4	285	785	0	0 ±1 ±2 ±7.2
		2.2	475	833	0	0 ±1 ±2 ±4 ±7.2
		2.8	620	853	0	0 ±1 ±2 ±7.2
		2.2	475	833	0.055	0 ±1 ±2 ±4 ±7.2
		3.25	730	865	0.110	0 ±1 ±2 ±7.2
C	10	1.34	1080	1450	0	0, -0.5, ±1, ±2, -4, -7.2
		2.2	1810	1450	0	0, -0.5, ±1, ±2, -4, -7.2
		2.2	1810	1450	0.055	0 ±1 ±2 -4 -7.2
		2.2	1810	1450	0.110	0
		2.2	1810	1450	0	-0.5 (with trip)

*Tunnel doors open, remaining tests in Tunnel B with doors closed.

TABLE II. SUMMARY OF FREE STREAM CONDITIONS

Facility	M_∞	Re_∞ ft ($\times 10^{-6}$)	P_0 (psia)	T_0 (°R)	U_∞ (fps)	q_∞ (fsia)	P_∞ (psia)	T_∞ (°R)	ρ_∞ (Lbm/ft^3)
A	4	1.4	18.2	605	2352	1.348	0.120	144	1.28×10^{-6}
		2.2	28.4	602	2332	2.109	0.187	143	2.0×10^{-6}
		2.8	39.9	597	2332	2.651	0.236	142	2.56×10^{-6}
		3.0	38.3	603	2332	2.832	0.252	143	2.70×10^{-6}
B	8	1.4	286.2	1257	3742	1.351	0.0305	92.2	8.93×10^{-4}
		2.2	473.8	1297	3800	2.212	0.0497	94.7	1.41×10^{-3}
		2.8	620.9	1321	3836	2.866	0.0641	95.9	1.80×10^{-3}
		3.25	728.2	1320	3835	3.342	0.0745	95.7	2.10×10^{-3}
C	10	1.4	1081	1910	4793	1.717	0.0245	95.7	6.92×10^{-4}
		2.2	1811	1911	4804	2.755	0.0383	93.6	1.105×10^{-3}

on the leeward side of the vehicle measured in the separated flow region. The composite distribution results in a 15 to 20 dB circumferential variation in fluctuating pressures over a significant portion of the vehicle surface.

Fluctuating pressure measurements were also made on the base of the test vehicle. Figure 48 presents typical distributions for three Reynolds numbers at Mach 4 and 10. As Reynolds number increased, fluctuating pressures were also observed to increase proportionally.

The effects of bluntness were also investigated and found to have only negligible effect except for moving the transition location on the vehicle surface.

2. POWER SPECTRAL DENSITY

Acoustic spectra for turbulent flow were obtained at Mach 4, 8 and 10. As previously noted, tunnel tare noise was appreciable in relation to turbulent flow data. As Reynolds number or Mach number are increased tunnel tare also increases. Using data from $Re_\infty \approx 1.4 \times 10^6$ affords the maximum separation of noise and true data. Figure 49 gives spectra as obtained from measured data with no consideration to tunnel tare noise.

TABLE III. LOCAL FLOW PROPERTIES ($\alpha = 0°$)

Facility	M_∞	R_{e_∞}/ft (x 10^{-6})	R_N (in.)	M_e	q_e (psia)	P_e/P_∞	Forward Array, x = 22.5 in.					Aft Array, x = 38.0 in.				
							C_f (x 10^3)	Re_δ (x 10^{-6})	δ (in.)	δ^* (in.)	δ (in.) x 10^3	C_f (x 10^3)	Re_δ (x 10^{-6})	δ (in.)	δ^* (in.)	θ (in.) x 10^3
A	4	1.4	0	3.69	1.63	1.55	3.09	3.15	0.130	0.050	6.75	1.85	5.34	0.465	0.179	24.2
		2.2	0	3.69	2.59	1.56	1.98	5.05	0.236	0.091	9.13	1.63	8.20	0.473	0.182	24.6
		2.6	0	3.69	3.25	1.55	1.70	6.01	0.271	0.104	14.1	1.53	10.64	0.472	0.182	24.5
		2.2	0.055	3.70	2.55	1.51	2.00	4.69	0.114	0.043	5.77	1.68	8.31	0.422	0.163	21.8
		2.25	0.110	3.69	3.66	1.51	2.63	6.84	0.098	0.038	5.10	1.57	11.87	0.389	0.151	20.1
B	5	1.4	0	6.71	2.64	2.97	2.13	3.75	0.139	0.061	5.76	1.31	6.67	0.414	0.180	17.4
		2.2	0	6.72	4.39	2.64	1.41	6.26	0.212	0.092	8.99	1.16	10.45	0.419	0.182	17.7
		2.8	0	6.73	5.70	2.63	1.27	7.95	0.240	0.104	10.2	1.09	13.33	0.415	0.180	17.6
		2.2	0.055	6.71	4.27	2.62	1.96	6.02	0.114	0.050	4.76	1.21	10.22	0.378	0.164	16.0
		2.25	0.110	6.77	6.74	2.62	1.46	8.65	0.097	0.042	4.06	1.11	15.41	0.343	0.148	14.5
C	10	1.4	0	9.00	4.17	3.75	1.94	3.42	0.137	0.061	5.61	1.20	6.99	0.385	0.167	16.0
		2.2	0	9.02	7.05	3.74	1.27	7.12	0.193	0.084	8.06	1.04	11.88	0.382	0.167	15.9
		2.2	0.055	9.04	6.79	3.54	1.74	6.65	0.104	0.045	4.30	1.06	11.43	0.345	0.150	14.3

TABLE IV. ACOUSTIC GAGE LOCATIONS

	X Dim. From Point	Ray Location & Gage No.							
		0°	5.97°	10.08°	19.1°	32.25°	90°	180°	270°
Cone Surface	8.00	1							
	8.375						2		
	16.00	3							
	22.50	4		5		6	7	8	9
	23.00	10							
	23.60	11							
	24.60	12							
	25.90	13							
	32.00	14							
	38.00	15	16		17		18	19	
	38.50	20							
	39.10	21							
	40.10	22							
	41.40	23							
	Radius								
Cone Base	0.00	24							
	1.50	25							
	3.00	26					28		
	4.75						29	27	

ARRAY #1

ARRAY #2

TABLE V. ACOUSTIC MAGNITUDE FOR TURBULENT FLOW

Free Stream Mach No.	Local Mach No.	P_{rms}/q_e (0-20 kHz)	
		Actual Data	Corrected Data
4	3.7	1.62×10^{-3}	1.31×10^{-3}
8	6.8	1.1×10^{-3}	0.58×10^{-3}
10	8.1	1.27×10^{-3}	0.67×10^{-3}

TABLE VI. PEAK ACOUSTIC MAGNITUDE IN TRANSITIONAL FLOW

Free Stream Mach No.	Local Mach No.	P_{rms}/q_e (0 to 20 kHz)
4	3.7	2.86×10^{-3} to 3.16×10^{-3}
8	6.8	1.85×10^{-3} to 2.70×10^{-3}
10	8.1	1.67×10^{-3} to 1.96×10^{-3}

Figure 50 represents typical normalized spectra (using local flow properties) for transitional flow. Figure 51 gives the third octave pressure distributions at various points in the transition region. During transition onset and decay it was noted that the high frequency portion of the spectra were initially affected. At the point of peak transition levels across the complete pressure spectrum (0 to 20 kHz) are increased 5 to 15 dB when compared to tunnel tare noise and 5 to 10 dB when compared to turbulent flow.

At angles of attack equal to the half cone angle of the test vehicle, separated flow occurs on the leeward side. Figure 52 represents the pressure spectral distribution obtained at the aft circumferential array at a model attitude of +7.2°. Sensor 15 represents the spectrum in separated flow while sensor 19 is in transitional flow. A 10 to 20 dB variation exists across the spectrum which could result in significant hoop excitation, due to the harmonic distributions of pressure.

Typical base pressure spectra at Mach 4 are shown in Figure 53, measured at the base center for various angles of attack. In general peak levels were measured at zero angle of attack. As Reynolds number increased base spectra was observed to increase proportionally. Data was obtained for various nose radii, however, no effects were observed on base sensors, indicating that the base spectra is unaffected by changes in bluntness.

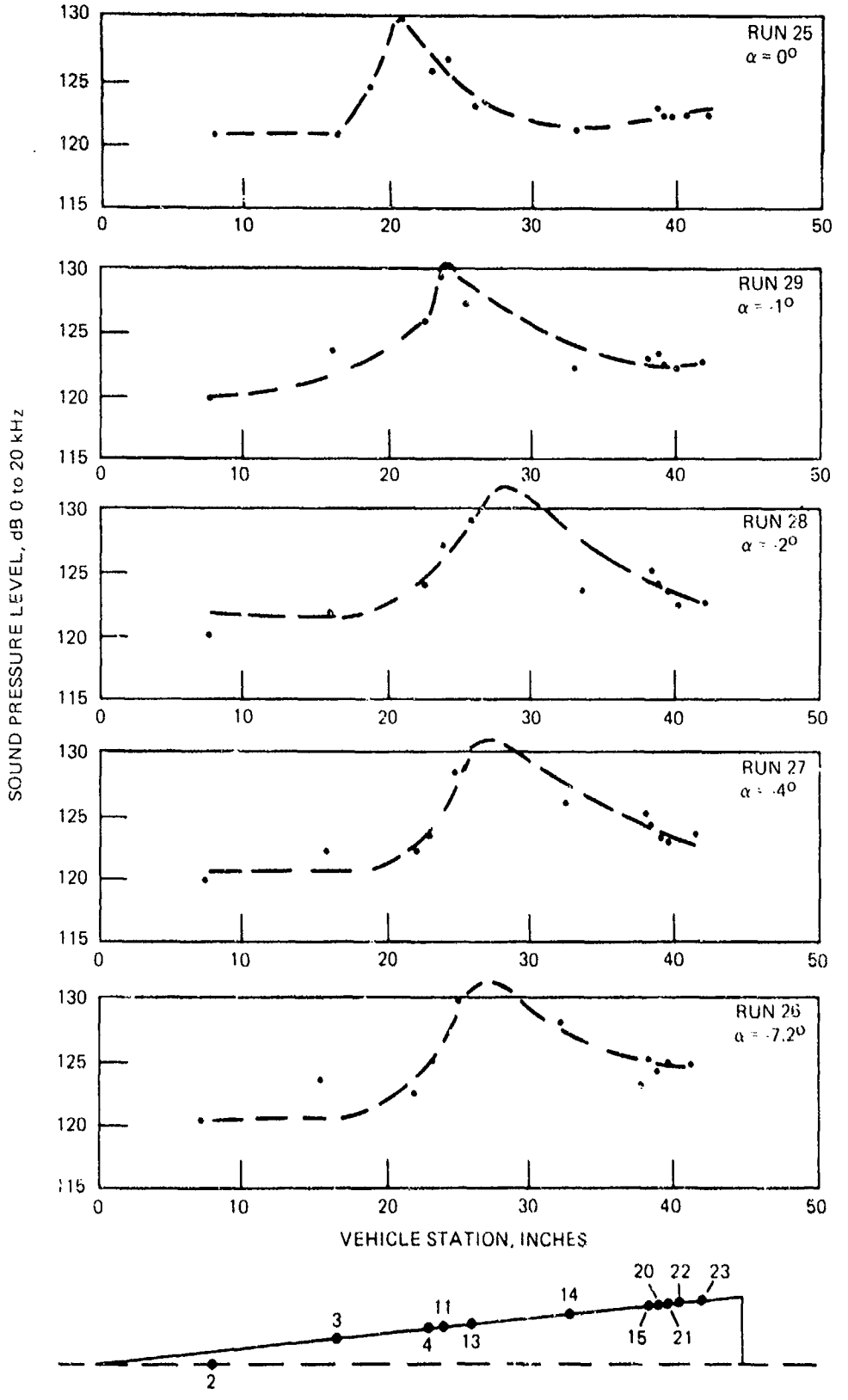

Figure 46. Fluctuating Pressure Distribution Tunnel Condition ($R_{e_\infty} = 2.8 \times 10^6$, $M_\infty = 4$, $R_N = 0.0$)

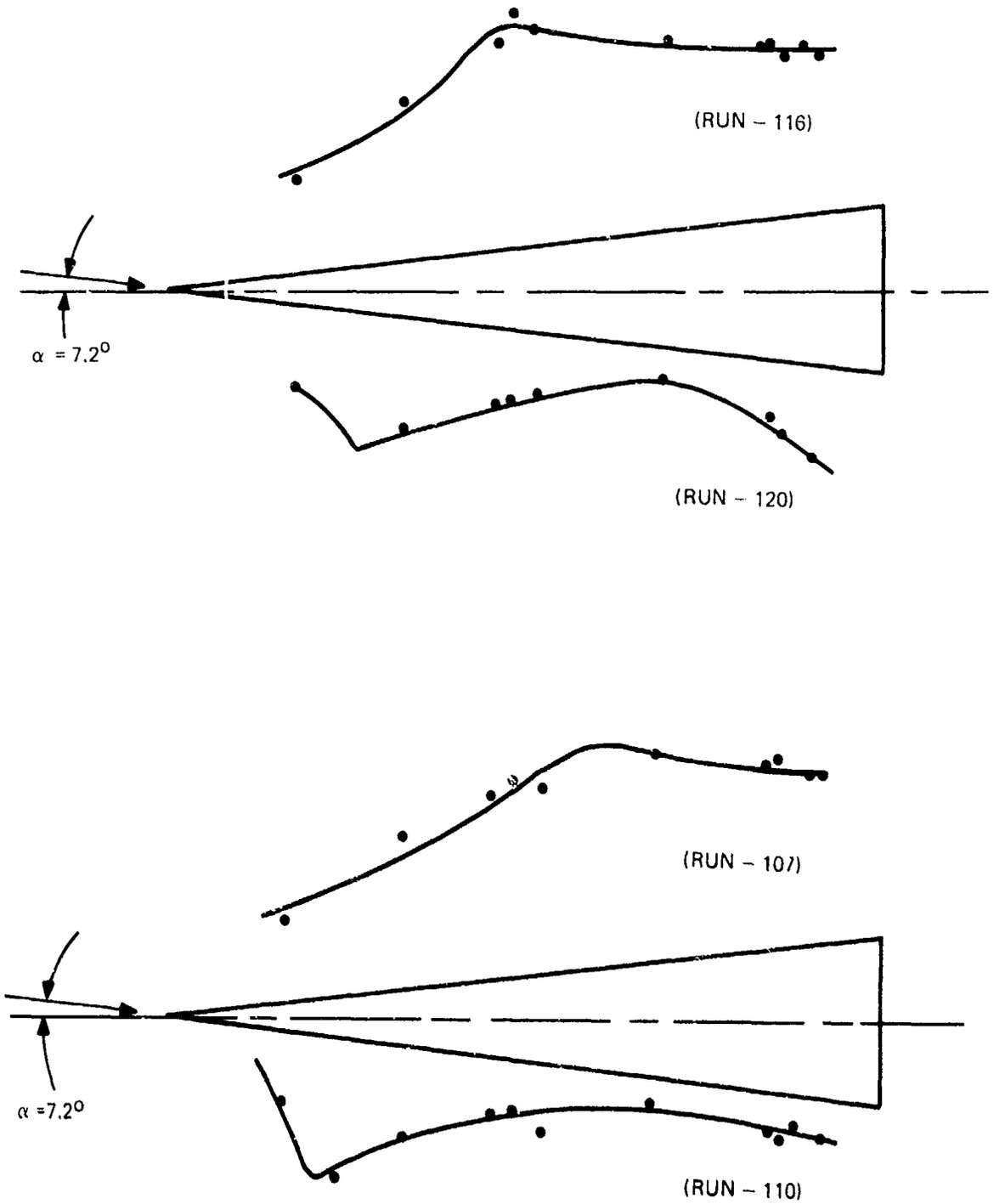

Figure 47. Acoustic Intensity Distribution, dB at High α (±7.2°)

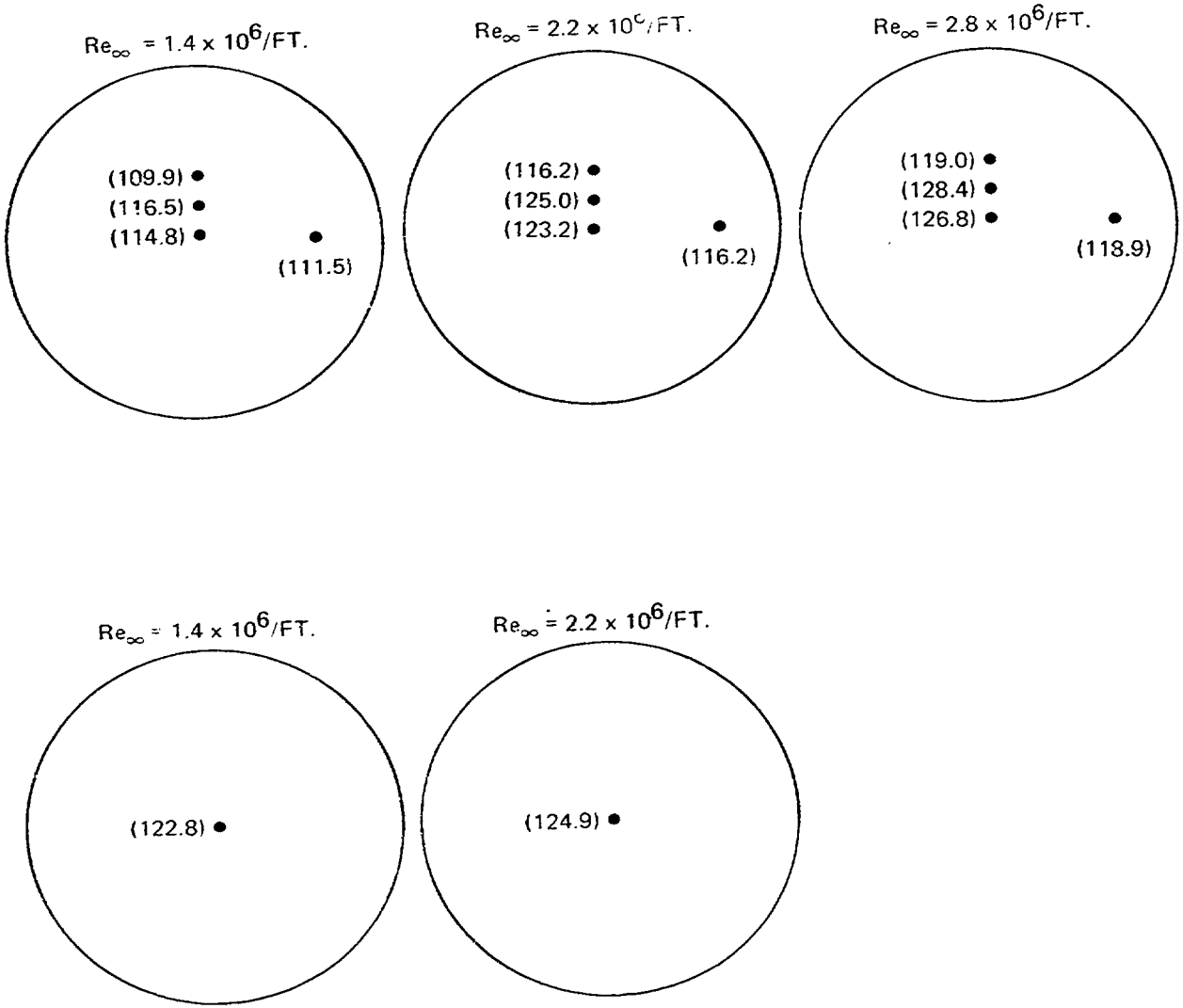

Figure 48. Base Acoustic Intensity Distribution (dB) at Various Reynolds Numbers and Mach Numbers (α = 0°)

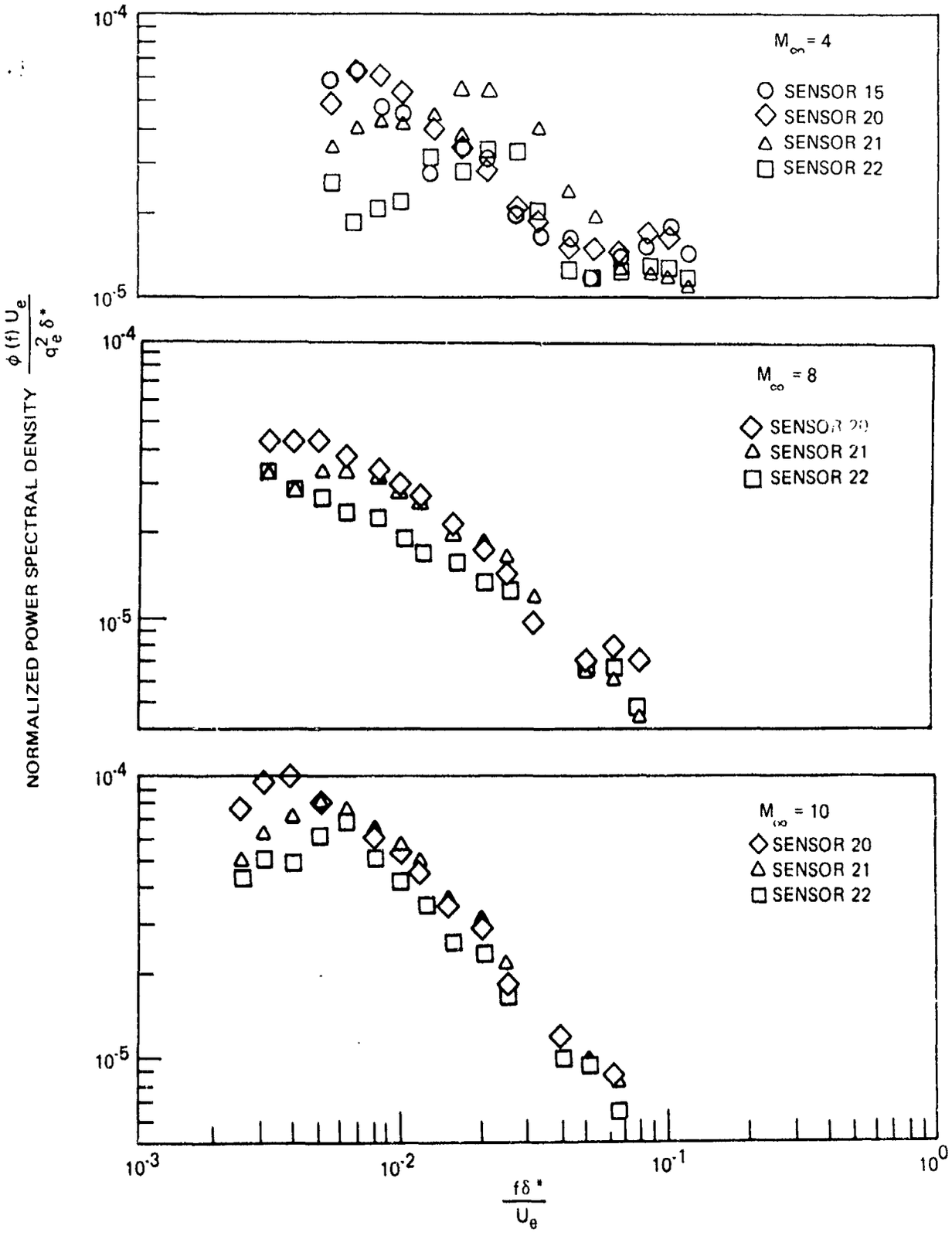

Figure 49. Normalized Turbulent Flow Spectra for Various Mach Numbers

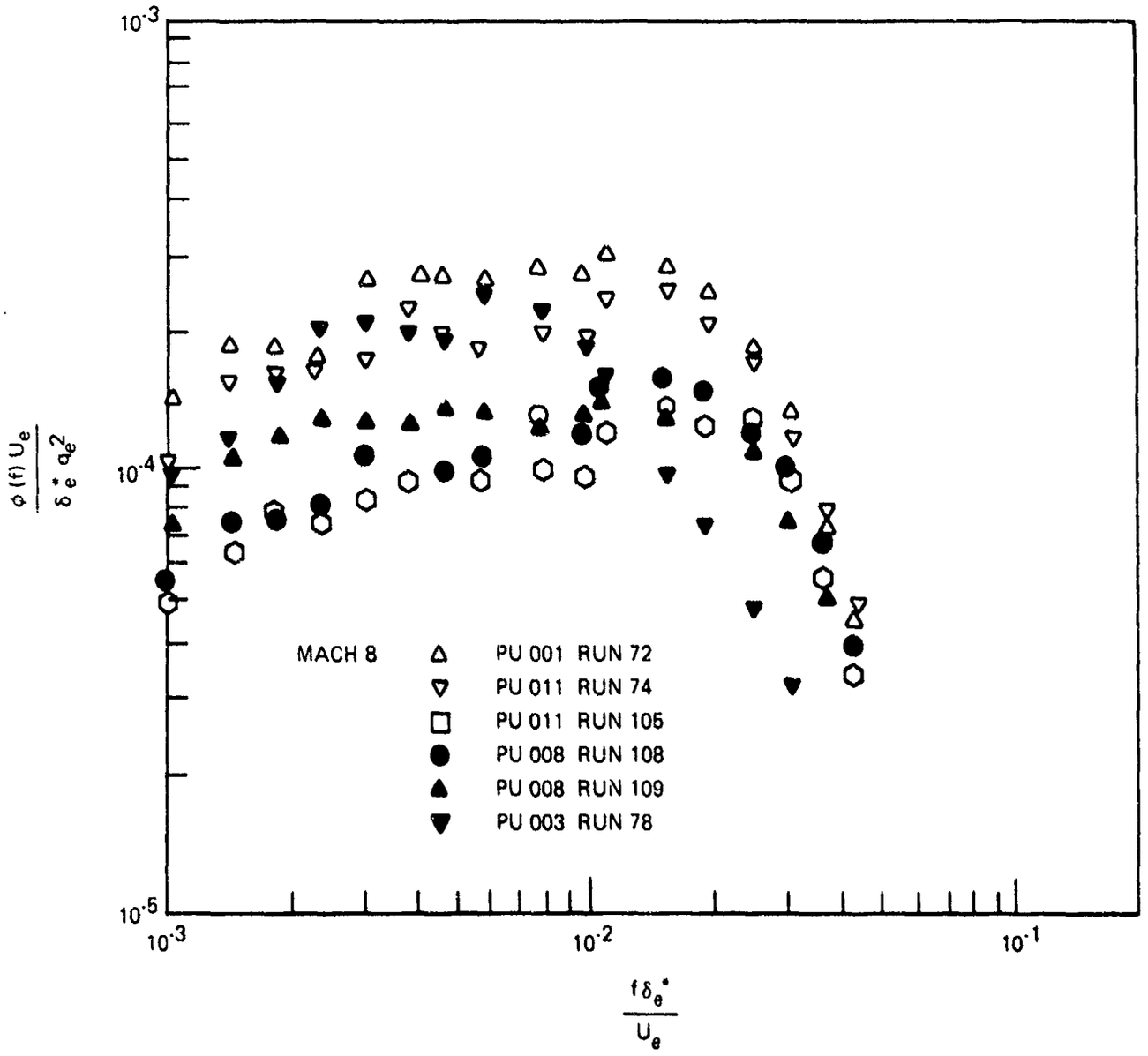

Figure 50. Normalized Power Spectral Density Distribution for Transitional Flow $M_\infty = 8$

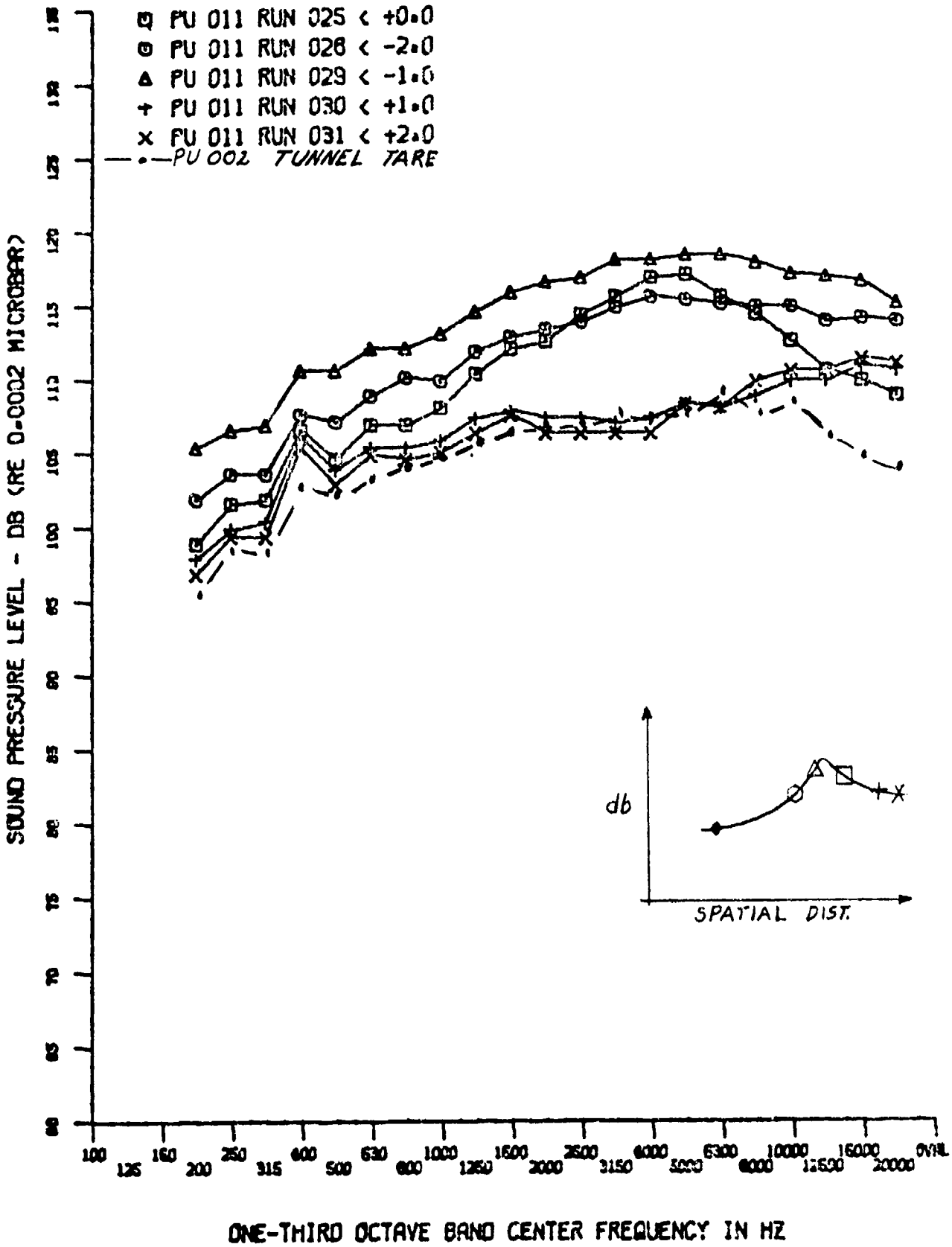

Figure 51. Variation of Transition Spectra in Transition Zone ($M_\infty = 4$, $Re_\infty = 1.4 \times 10^6$, $R_N = 0$)

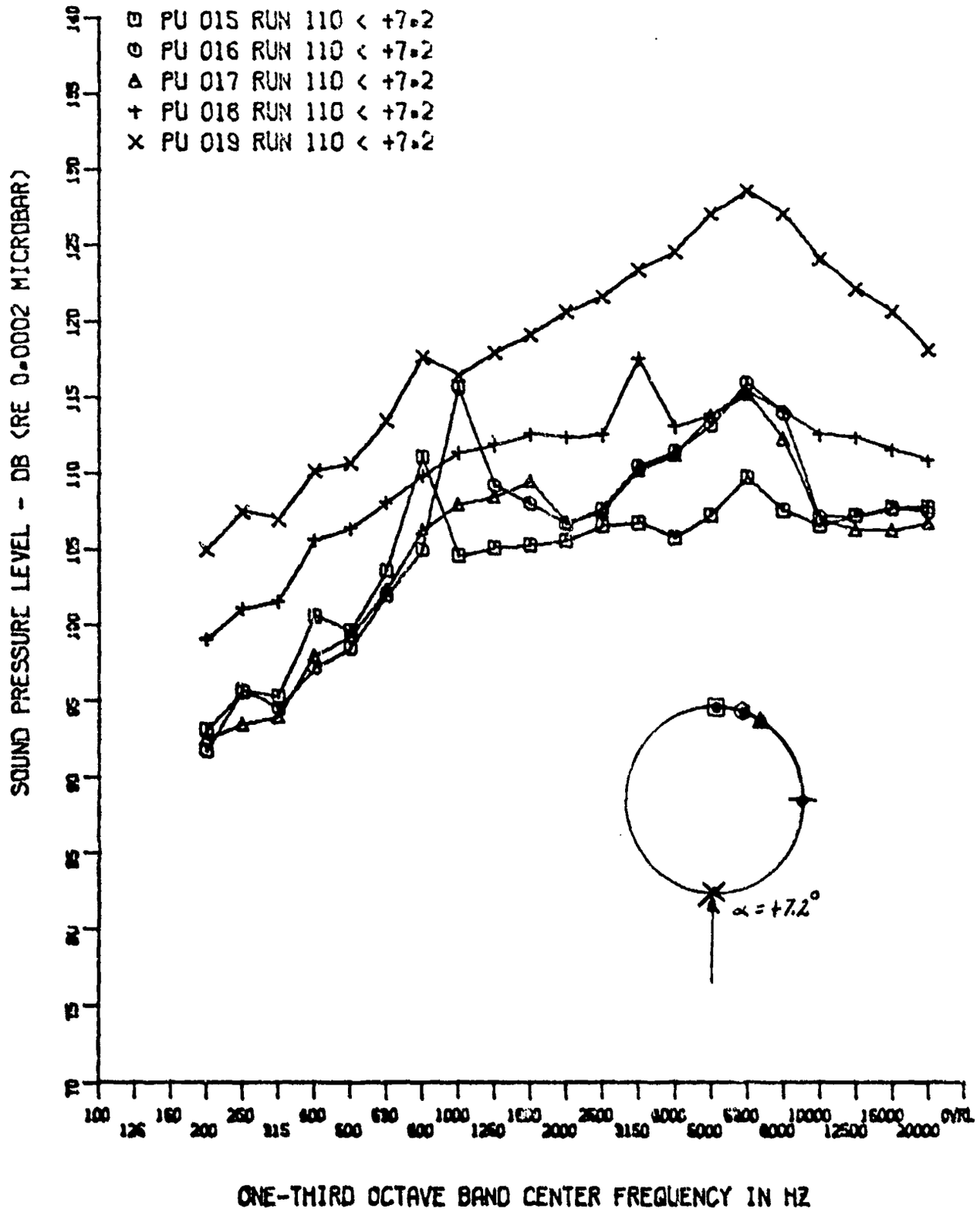

Figure 52. Comparison of Pressure Spectra in Circumferential Direction (Separated Flow Leeward Sensors), $M_\infty = 8$, $Re_\infty = 2.8 \times 10^6$

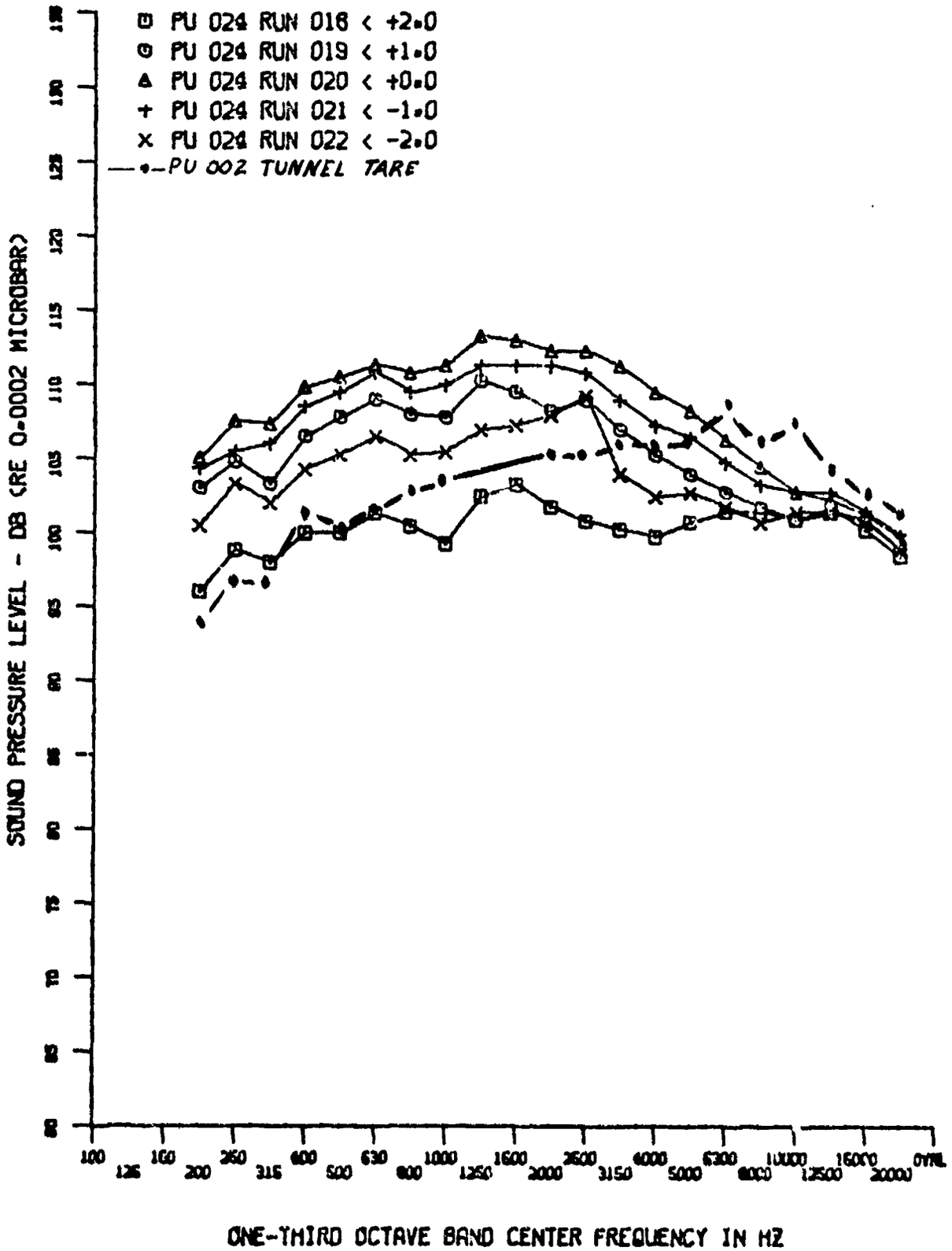

Figure 53. Comparison of Base Flow Pressure Spectra for Various α (Base Center), $M_\infty = 4$, $Re_\infty = 2.2 \times 10^6$

3. CROSS CORRELATION FUNCTIONS

Space-time correlation functions representing turbulent, transitional and separated flow are shown in Figure 54. The typical decrease and broadening of peaks for increasing separation distance are attributed to decay of high frequency turbulent eddies as they progress downstream. The only significant difference between turbulent and transitional flow is in the convective velocity. Correlation functions obtained at high Mach numbers (8, 10) tend to be broad for small separation distances. This effect is thought to be caused by tunnel noise. No correlation was evident for base flow.

4. CONVECTION VELOCITY

Convection velocities in transitional flow were approximately 0.6 times that for turbulent flow. Figure 55 compares broad band convection velocities for transitional and turbulent flow for various separation distances. Turbulent flow convection velocities measured are typical to that of other experimenters discussed in Section 4.

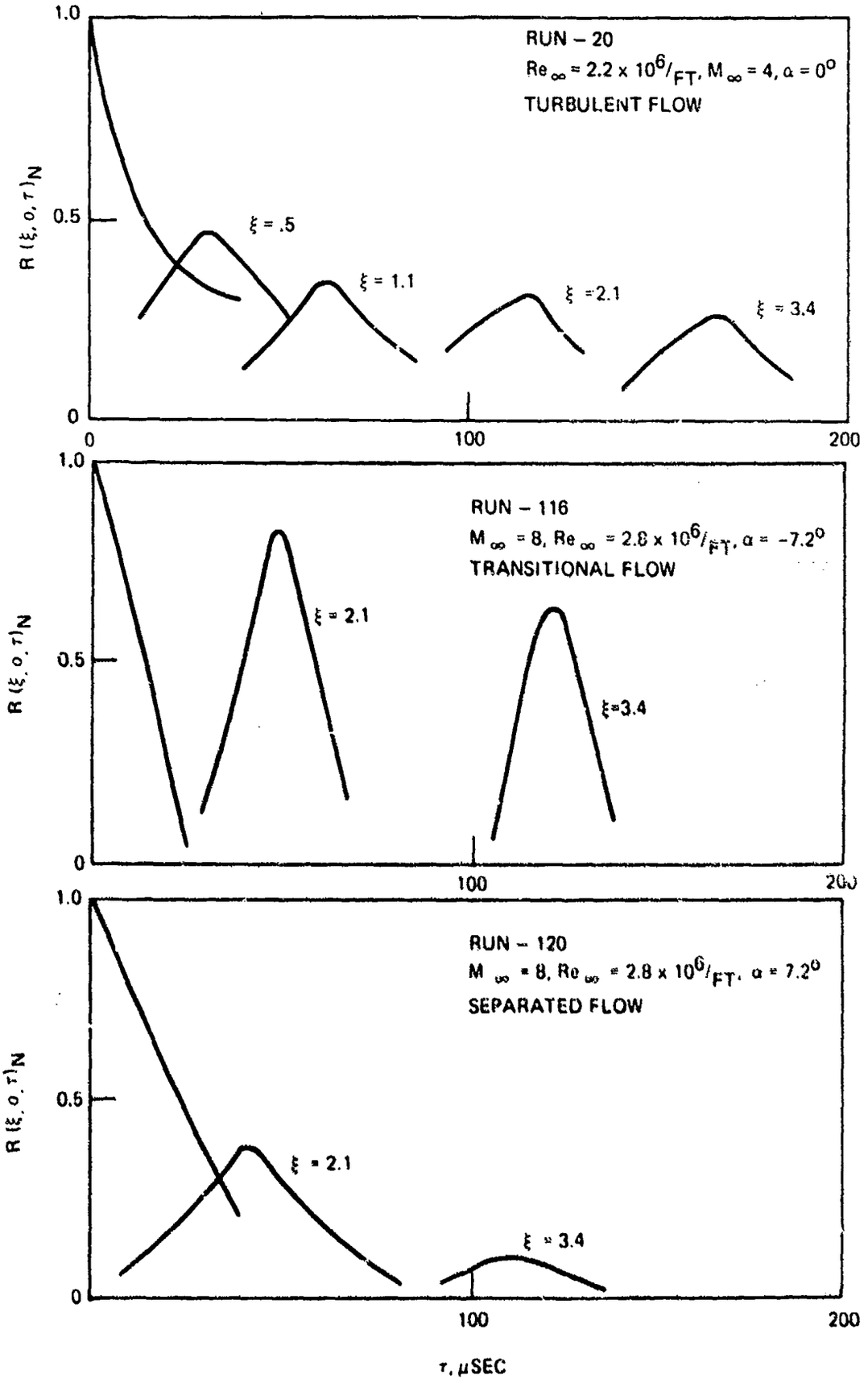

Figure 54. Broad Band Correlation Functions for Various Flow Conditions

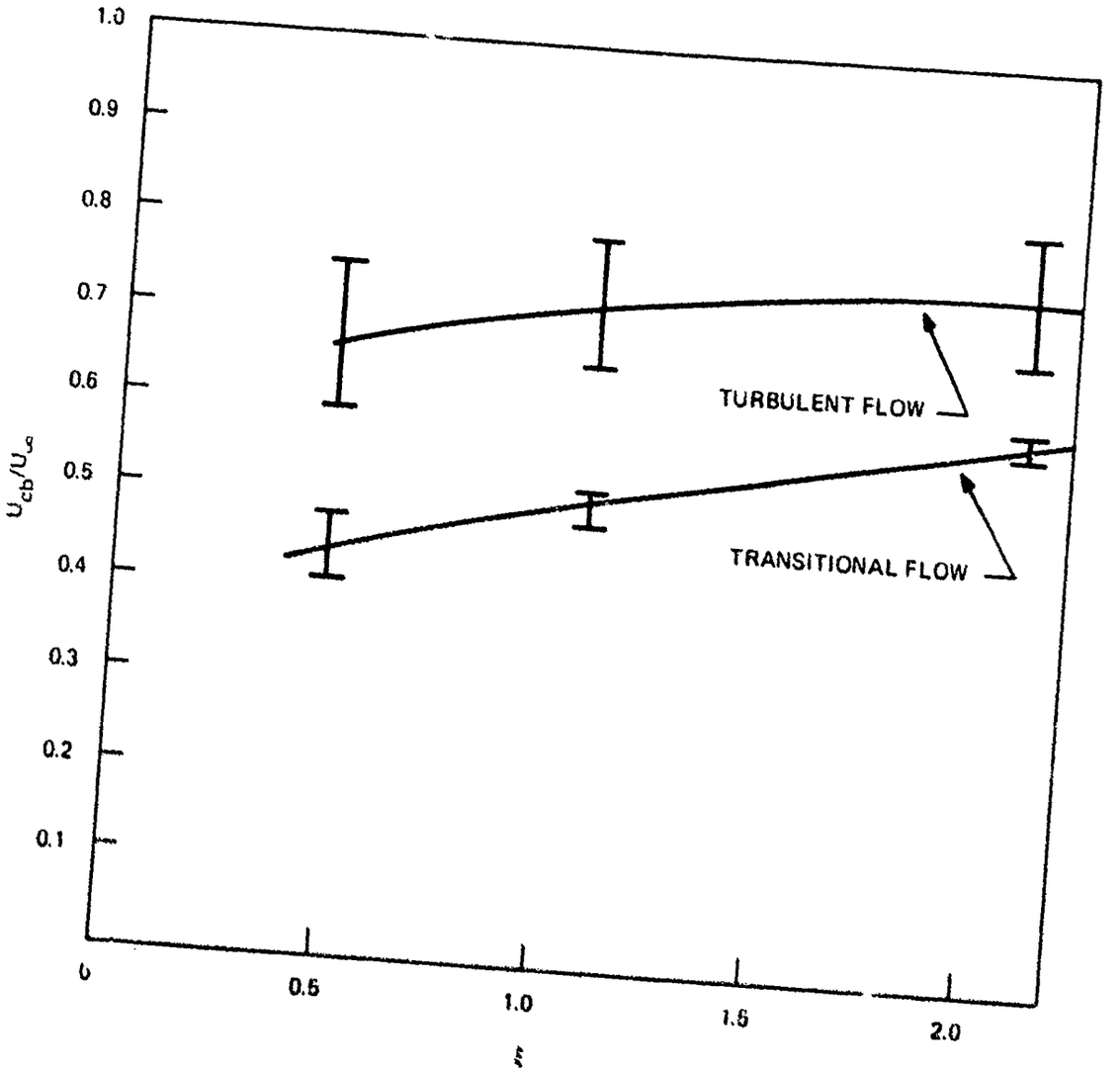

Figure 55. Comparison Between Turbulent and Transitional Broad Band Convection Velocity

SECTION VI

PREDICTION METHODS REFINEMENT

Utilizing existing data summarized in Section II, and data obtained in this tunnel program as presented in Section V, Volumes I and II, Volume II, recommendations for the aerodynamic properties necessary to describe the aeroacoustic loading environment are given. The criteria for recommended methods were based upon the most reasonable fit of experimental data and their practicality in design use.

Attempts to develop narrow-band cross correlation functions have resulted in wide scatter over the frequency spectrum of interest. This apparent erratic behavior in the narrow band results has been traced to limitations in the Fast Fourier Transform technique used to analyze the data. While not totally understood, indications are that the limiting process utilized in the digital program, while rigorously correct, is not compatible with the finite sample size associated with the data of this study. This is the only plausible explanation for the apparent nontypical behavior in the narrow-band correlation plots. Hence, this information is not included in the results of this study.

1. ATTACHED TURBULENT BOUNDARY LAYER FLOW

a. Acoustic Magnitude

Figure 56 summarizes equations used for acoustic magnitude, as proposed by various experimenters. These are compared with test data including data obtained in the present test program. Figure 57 presents the data of other experimenters including present data extrapolated out to infinity, for purposes of comparison. Lowson's expression compares well with available data below Mach 5 and tends to underpredict for higher Mach numbers. This is due to the available test data trend to group at two levels (0.006 for $M \leq 2$ and 0.0015 for $4 < M < 10$). In order to be representative at both levels, a variable Mach number coefficient in the denominator of Lowson's expression becomes necessary. Houbolt's refined equation accounts for this by use of a coefficient, r_e, which is a function of temperature and local velocity. Table VII compares the present test data with predictions using Houbolt's refined expression for acoustic magnitude. These values differ from those presented in Figure 56 in that actual test conditions were used to determine the recovery factor r_1 in the expression for r_e, where in Figure 56 a value of unity for the recovery factor (r_1) was assumed to calculate r_e.

Houbolt's expression (repeated below) for acoustic magnitude is therefore recommended for general use.

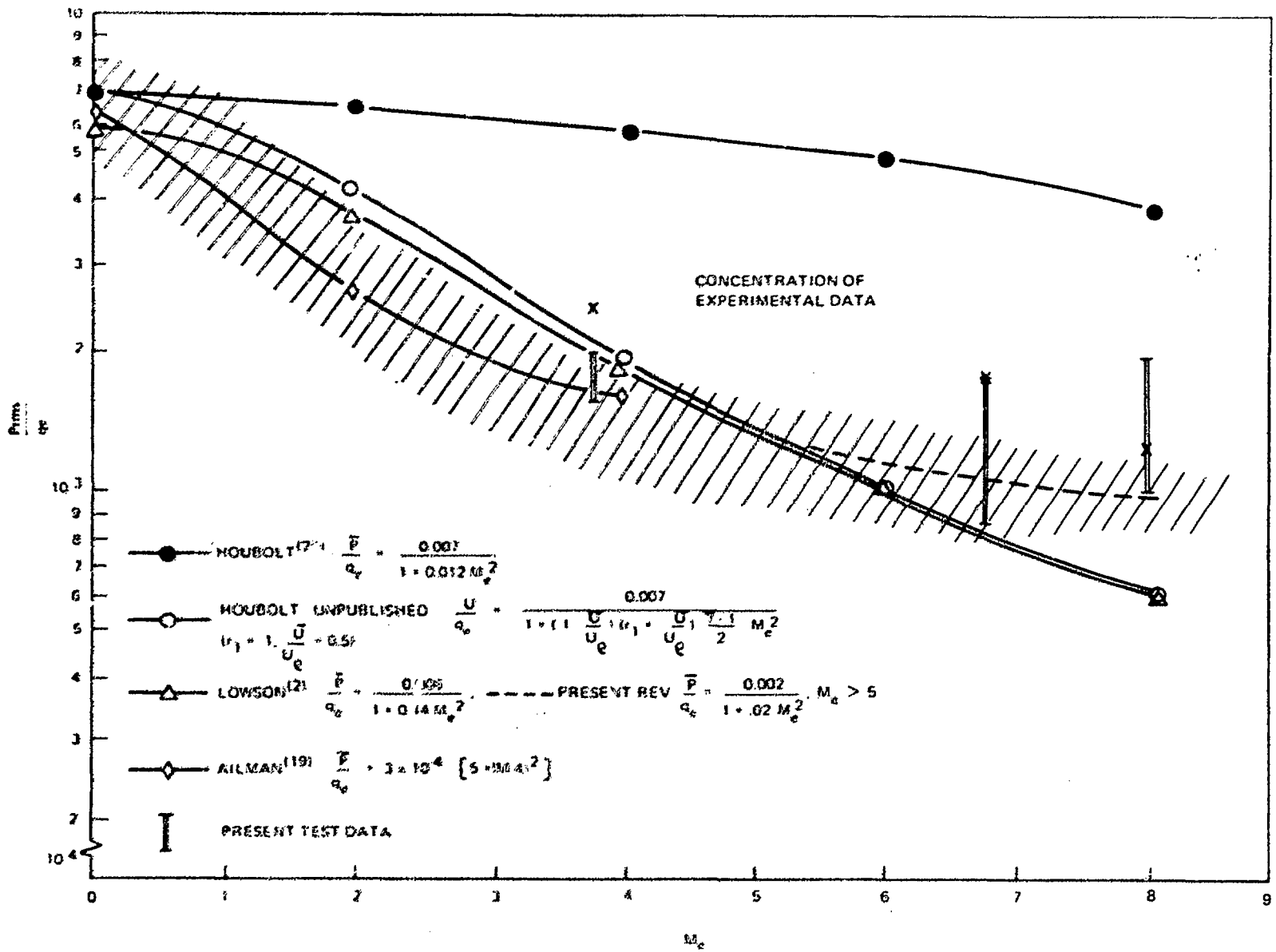

Figure 56. Comparison of Overall Acoustic Magnitude Prediction Methods to Experimental Data

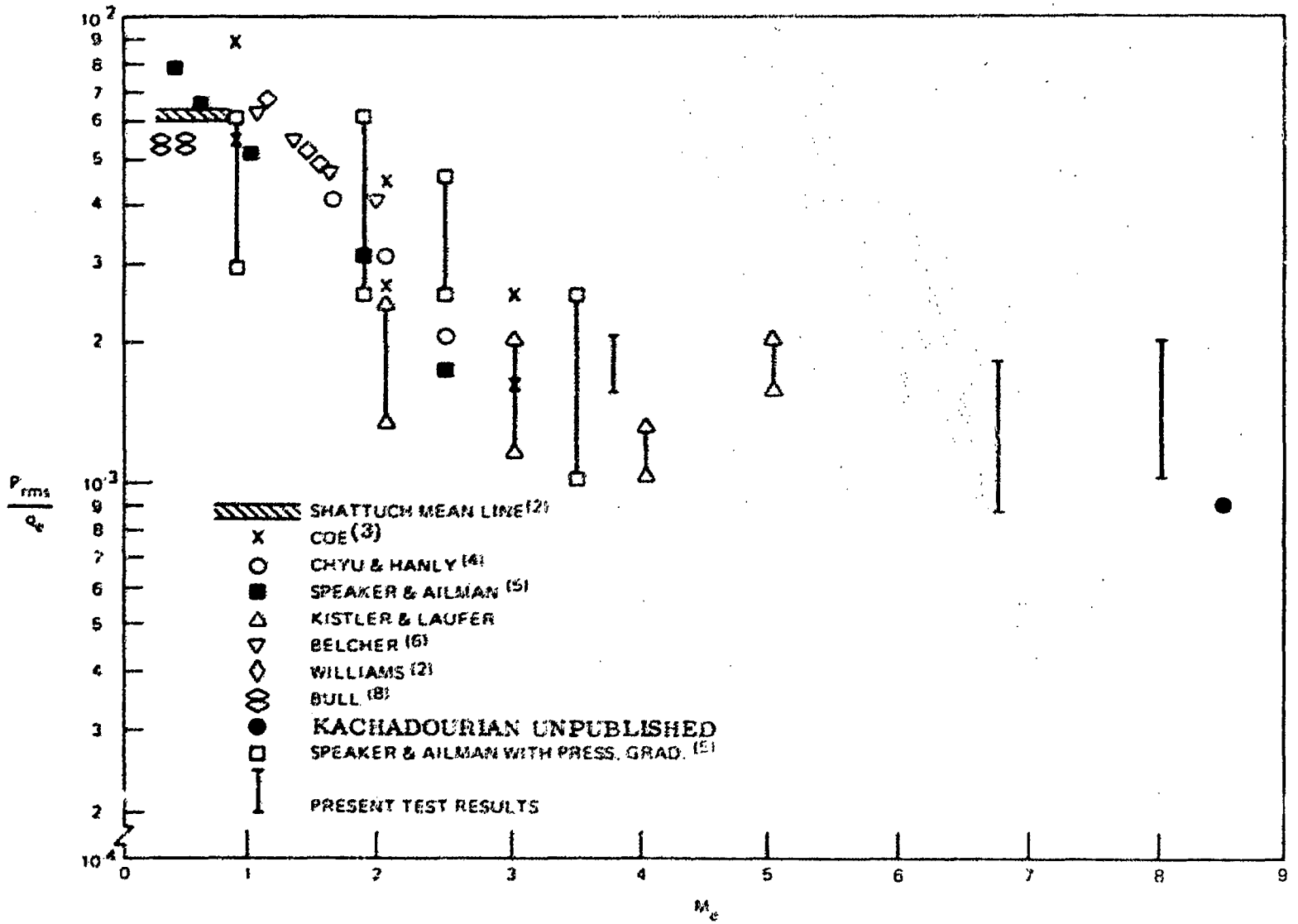

Figure 57. Root Mean Square Pressure Fluctuation Vs Mach Number for Attached Turbulent Flow

$$\frac{P_{rms}}{q_e} = \frac{0.007}{1 + r_e\left(\frac{\gamma - 1}{2}\right) M_e^2} \tag{3}$$

where

$$r_e = \left(1 - \frac{\bar{U}}{U_e}\right) \left(r_1 + \frac{\bar{U}}{U_e}\right) \tag{4}$$

and

$$\frac{T_w}{T_e} = 1 + r_1 \left(\frac{\gamma - 1}{2}\right) M_e^2 \tag{5}$$

Because of its simplicity and close fit to experimental data ($M \leq 5$) Lowson's equation (Equation 1) can also be applied. Above Mach 5, the equation should be adjusted to:

$$\frac{P_{rms}}{q_e} = \frac{0.002}{1 + 0.02 M_e^2} \quad M \geq 5 \tag{4a}$$

$$\frac{P_{rms}}{q_e} = \frac{0.006}{1 + 0.14 M_e^2} \quad M \leq 5 \tag{6}$$

TABLE VII. PREDICTION VS. TEST ACOUSTIC MAGNITUDE (TURBULENT FLOW)

Free Stream Mach No.	$P_{rms}/q_e \times 10^3$	
	Test Data*	Predicted (Equation 3)
4	1.53 to 1.9	2.5
8	0.835 to 1.58	1.5
10	1.08 to 2.04	1.2

*Test data adjusted to overall value for comparison with Equation 11 and previous data.

b. Acoustic Power Spectral Density

The criteria used in defining an expression for power spectral density function were that the integral of the function is equal to the root mean pressure squared ($\int_{-\infty}^{\infty} \phi(f)\, df = P^2_{rms}$), the function remain finite, and that the function be symmetric about zero, a requirement due to its Fourier transform relationship with the autocorrelation function. Figures 58, 59, and 60 compare Houbolt's and Lowson's equations. Both expressions compare well with

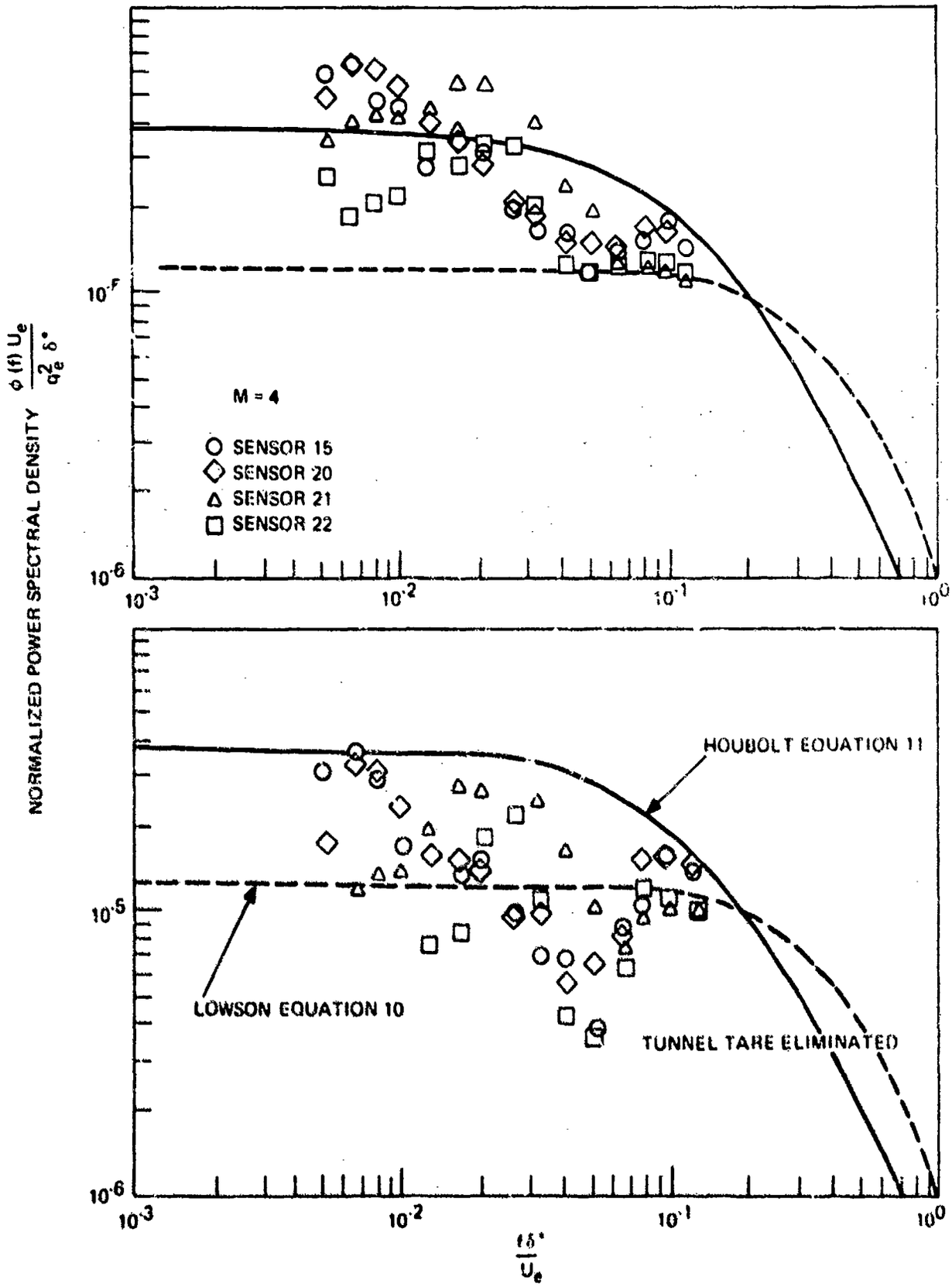

Figure 58. Normalized Power Spectral Density Distribution for Turbulent Flow $M_\infty = 4.0$

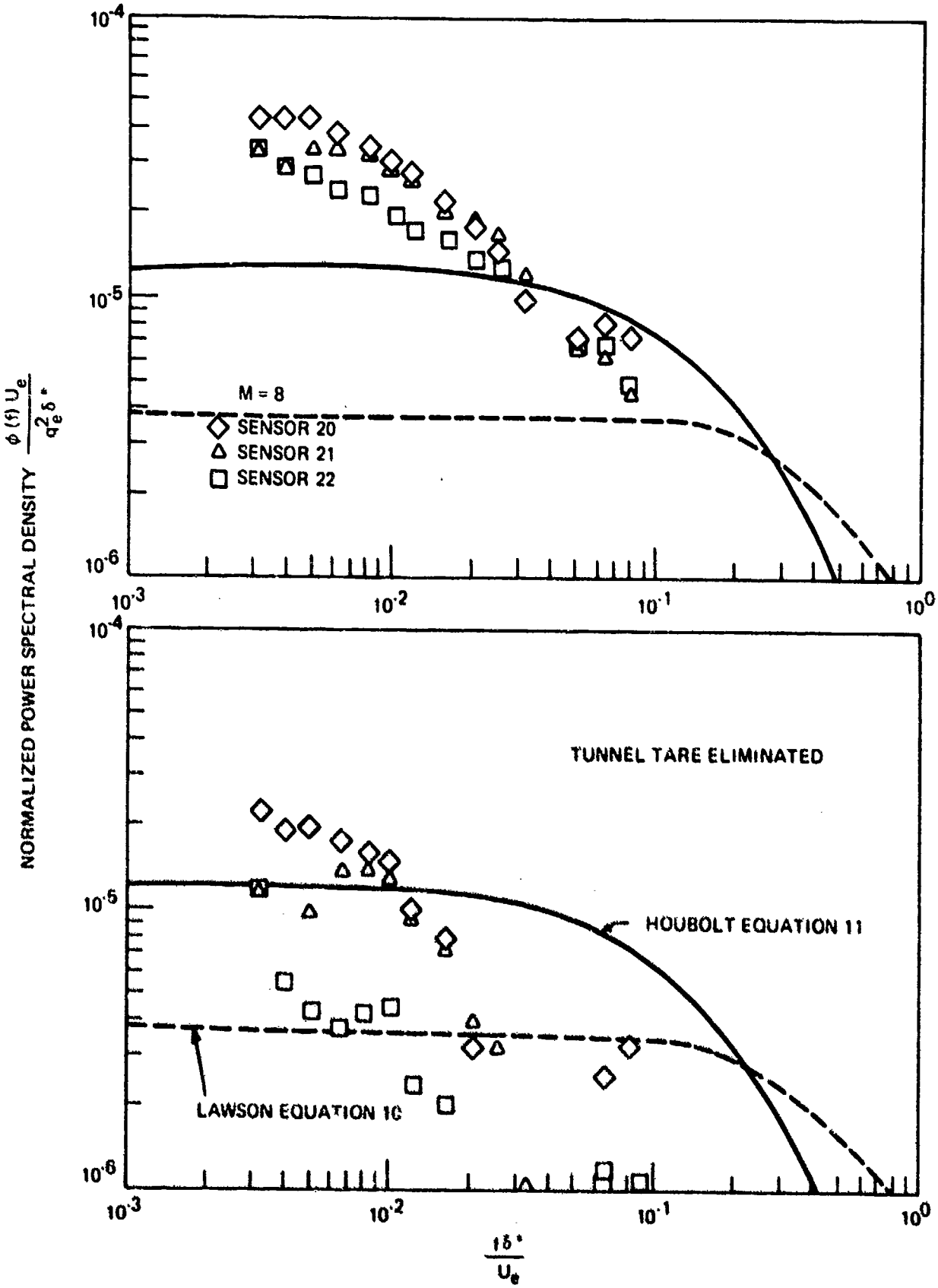

Figure 59. Normalized Power Spectral Density Distribution for Turbulent Flow $M_\infty = 8.0$

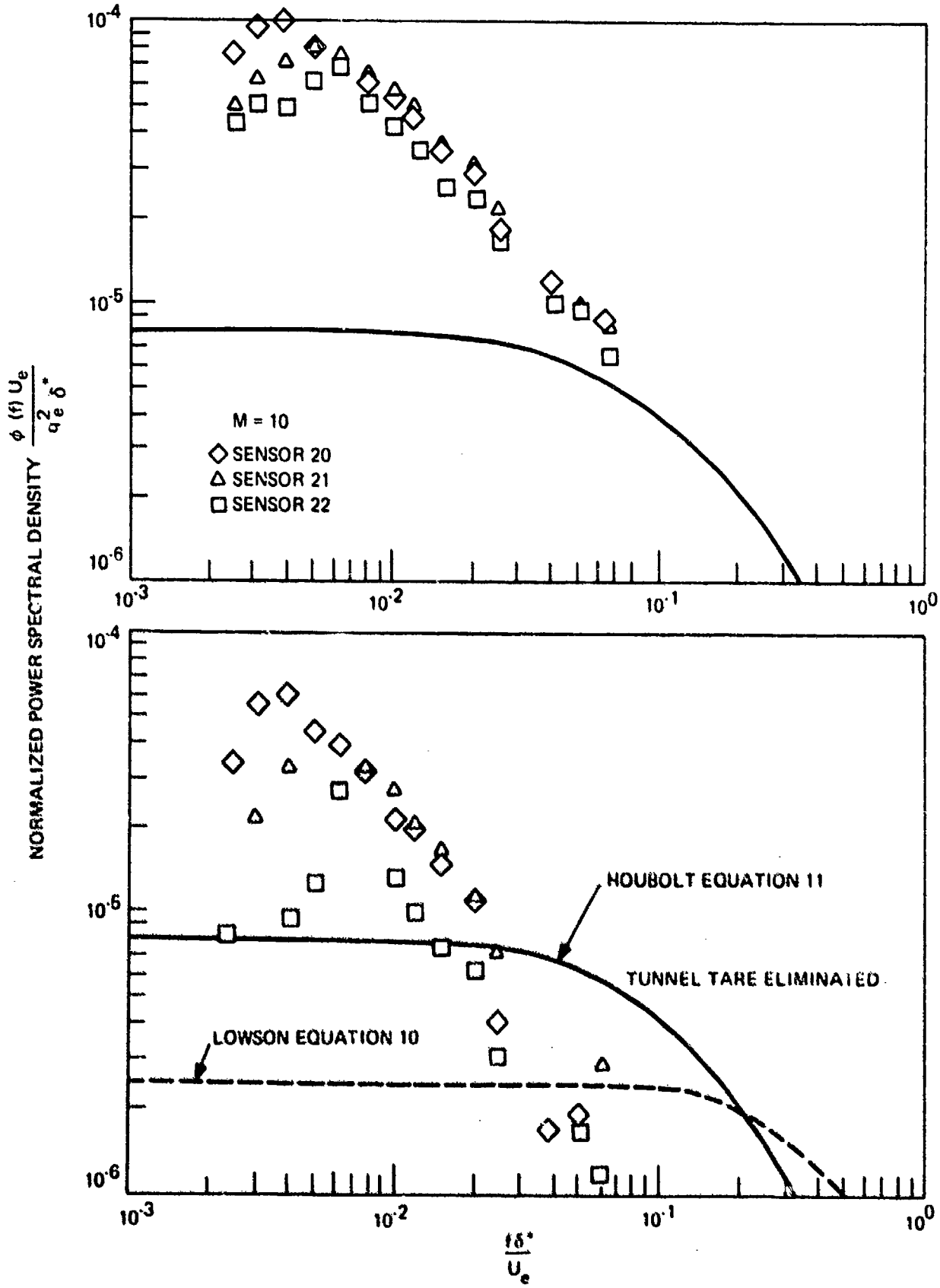

Figure 60. Normalized Power Spectral Density Distribution for Turbulent Flow $M_\infty = 10.0$

present data (except at Mach 10) with Houbolt's (Equation 10) expression being reasonably conservative in the low frequency range of primary interest. Since Lowson's spectral equation (Equation 11) is defined in terms of boundary layer thickness (δ) it was necessary to express δ in terms of the boundary layer displacement thickness given in Table III of Section V. Present data ($M_\infty = 4, 8$) are also shown in Figure 61 with data obtained by other experimenters. Good correlation was obtained.

Of the relationships discussed in Section IV, Houbolt's expression (Equation 10) given below is recommended for general use because of its ease of application and degree of conservatism.

$$\phi(\omega) = \frac{2\delta^*}{\pi U_c} P^2_{rms} \frac{1}{1 + \left(\frac{\omega\delta^*}{U_c}\right)^2} \tag{11}$$

c. Cross-Correlation Functions

Due to the inability to derive representative narrow-band cross correlation functions from the wind tunnel data, recourse was made to the literature for typical expressions applicable to supersonic flow. Available data in the Mach 0.3 to 2.5 region indicate the form of the functions to be as given in the following equations:

$$\phi_R(\xi, 0, \omega) = A_\xi(\xi, \omega) \cos\frac{\omega\xi}{U_c} \left[\phi_{\xi_1}[\omega]\, \phi_{\xi_2}[\omega]\right]^{1/2} \tag{16}$$

$$\phi_R(0, \eta, \omega) = A_\eta(\eta, \omega) \left[\phi_{\eta_1}[\omega]\, \phi_{\eta_2}[\omega]\right]^{1/2} \tag{17}$$

Lowson[2] and Robertson[1] using data obtained by Bull[4] and Chyu and Hanly[9] defined the coefficients for the above equations to be:

$$A_\eta(\eta, \omega) = \exp\left(-0.72|\eta|\frac{\omega}{U_c}\right) \exp\left(-2.0\frac{|\eta|}{\delta}\right) \tag{18}$$

$$A_\xi(\xi, \omega) = \exp\left(-0.1|\xi|\frac{\omega}{U_c}\right) \exp\left(-0.27\frac{|\xi|}{\delta}\right) \tag{19}$$

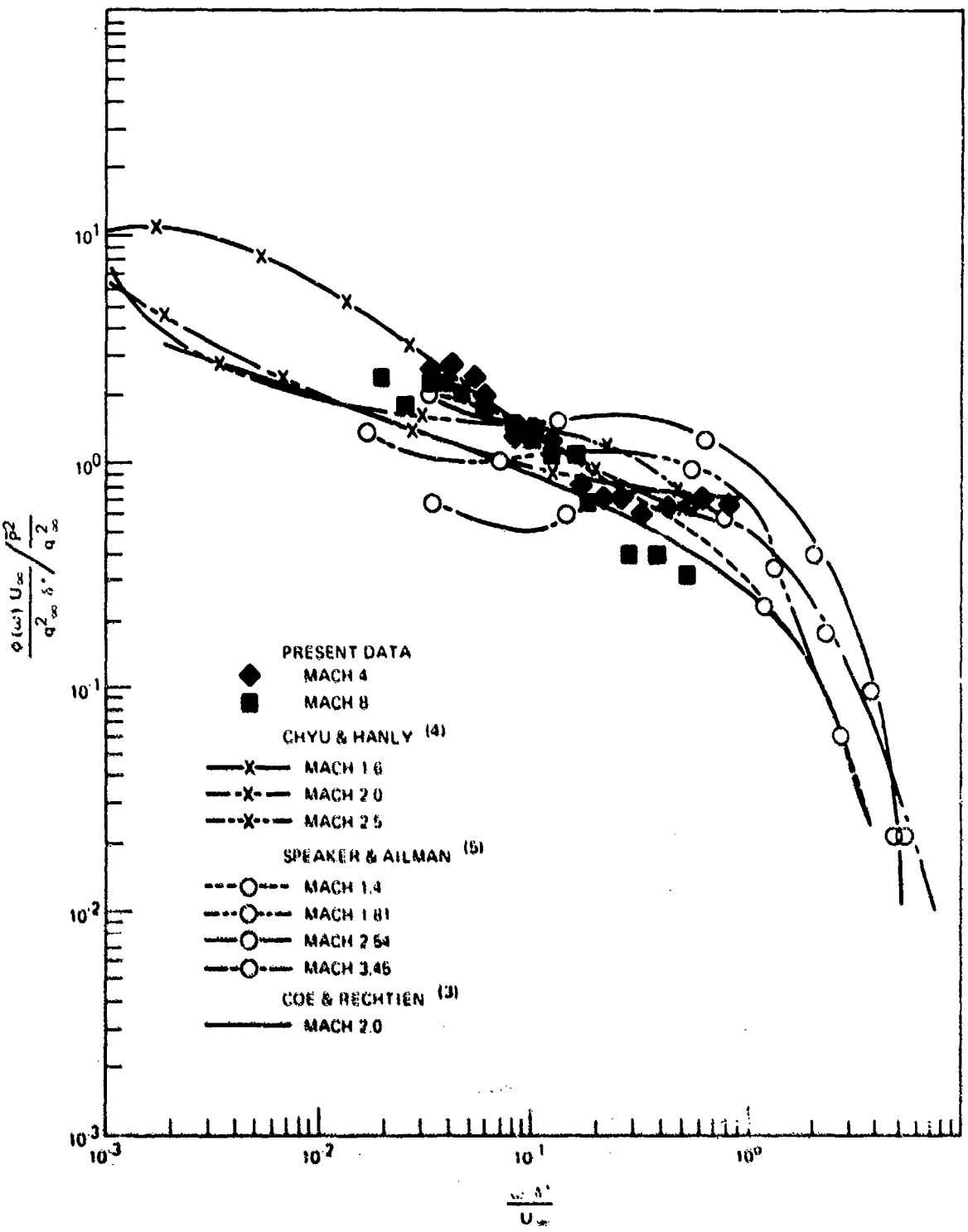

Figure 61. Comparison of Present Normalized Power Spectral Density to that of Other Experimenters

The above expressions (Equations 18 and 19) may also be written in terms of the boundary layer displacement thickness parameter as:

$$A_\eta(\eta, \omega) = \exp\left(-0.72|\eta|\frac{\omega}{U_c}\right)\left[0.3 + 0.7\exp\left(-0.5\frac{|\eta|}{\delta^*}\right)\right] \tag{20}$$

$$A_\xi(\xi, \omega) = \exp\left(-0.1\frac{|\xi|}{U_c}\omega\right)\exp\left(-0.034\frac{|\xi|}{\delta^*}\right) \tag{21}$$

Equations 16 through 21 are recommended in defining the cross-power spectra for turbulent flow.

d. Convection Velocity

Broad band convection velocities obtained in the present test program ($M_\infty = 4$ to 10) were typical of those observed by other experimenters ($M_\infty = 0.3$ to 2.5), therefore Equation 24 developed by Lowson[2] for the narrow band convection velocity in turbulent flow is considered representative.

$$\frac{U_c}{U_\infty} = 0.075 + 0.3\exp\left(-0.11\frac{\omega\delta}{U_\infty}\right) - 0.25\exp\left(-1.2\frac{\xi}{\delta}\right) \tag{24}$$

2. TRANSITIONAL BOUNDARY LAYER FLOW

Figure 46 gave typical acoustic definition of the fully developed turbulent boundary layer (TBL) and transitional aerodynamic flow regions for the various wind tunnel conditions and model orientations investigated in this program. Curves which connect the data points presented therein were generated in conjunction with aerodynamic prediction of the transition region and represent the estimated shape of the sound pressure level (SPL) profile. For the purpose of evaluating acoustic data near the peak of transition, analysis was restricted to those specific cases where the transducer registered within 2 dB of the peak transitional fluctuating pressure level. Once normalized values of the acoustic magnitude (P_{rms}) and power spectral density functions ($\phi(f)$) had been obtained for these cases, the multiplicative factors given in Table VIII were utilized to calculate values representative of peak transition. When the data point location on the SPL profile is at the estimated peak no adjustment was required.

Note: Contributions from tunnel tare noise (Sensor 2) are sufficiently lower than measured values of transitional spectra and acoustic magnitude that these noise contributions are considered negligible in the analysis of transitional data which follows.

TABLE VIII. LIST OF APPLICABLE TRANSITION CASES

Mach No.	Run	Sensor	dB Below Apparent Peak	Adjustment Factor for $\phi(f)$ and P^2_{rms}
4	11	22	0	1.0
	20	11	2	1.58
	20	13	0	1.0
	29	11	2	1.58
	28	13	0	1.0
	30	8	1	1.26
	11	21	0	1.0
8	72	11	2	1.58
	74	13	0	1.0
	105	11	0	1.0
	108	8	0	1.0
	109	8	0	1.0
	78	3	1	1.26
10	144	11	1	1.26
	145	11	0	1.0
	144	9	1	1.26
	142	8	1	1.26
	143	8	1	1.26
	144	8	1	1.26
	144	7	1	1.26

a. Acoustic Intensity

The value of P_{rms} (0 to 20 kHz) for a given condition is typically presented by normalizing with respect to either free stream or local dynamic pressure (q_∞, q_e) It was determined that a tighter collapse of the present data resulted from a q_e normalization. However, for comparison with other transition data, the measured values depicted in Figure 62 were normalized (after adjustment per Table VIII) with respect to the free stream dynamic pressure. Using q_e as the normalizing parameter, Figure 63 reveals how the measured values of P_{rms}/q_e near peak transition exceed those determined for turbulent boundary layer flow. In order to develop a refined acoustic intensity prediction technique for transitional pressure data, an attempt was made to extend the frequency range of analysis out to infinity. This was accomplished by employing the equation for acoustic power spectral density derived in Section VI.2.b to fit the spectral data, i.e.

$$\phi(f) = \frac{2.0 \times 10^{-4} \, \delta^* \, q_e^2 / U_e}{1 + \left[C(M_e) \, \delta^* \, f/U_e \right]^2} \tag{51}$$

where $C(M_e)$ is given by Equation 50.

Therefore integrating both sides of Equation 51 from zero to infinity yields the following formula for the mean square acoustic pressure in terms of the local dynamic pressure q_e:

$$p^2_{RMS} = \frac{3.14 \times 10^{-4} \, q_e^2}{C(M_e)} \tag{45}$$

The plotted results are shown in Figure 64 which indicates P^2_{RMS}/q_e versus local Mach number as predicted from the spectral data using Equations 51 and 45.

Values for transitional acoustic magnitude given in this figure reveal a generally shallow data trend for $4.0 < M_\infty < 10.0$. The equation for rms pressure which describes these plotted values in the Mach number range investigated is

$$P_{RMS} = \frac{0.0041 q_e}{1 + 0.013 \, M_e^2} \qquad (3.7 \leq M_e \leq 8.1) \tag{46}$$

The above expression is quite similar in form to Lowson's equation for intensity of fully turbulent flow $P_{RMS}/q_e = 0.006/(1 + 0.14 \, M^2_e)$. An assumption that these two equations are both applicable at low Mach numbers would imply a cross-over of P_{RMS}/q_e values for transitional and fully turbulent aerodynamic conditions as $M_e \rightarrow 0$. However, it is evident

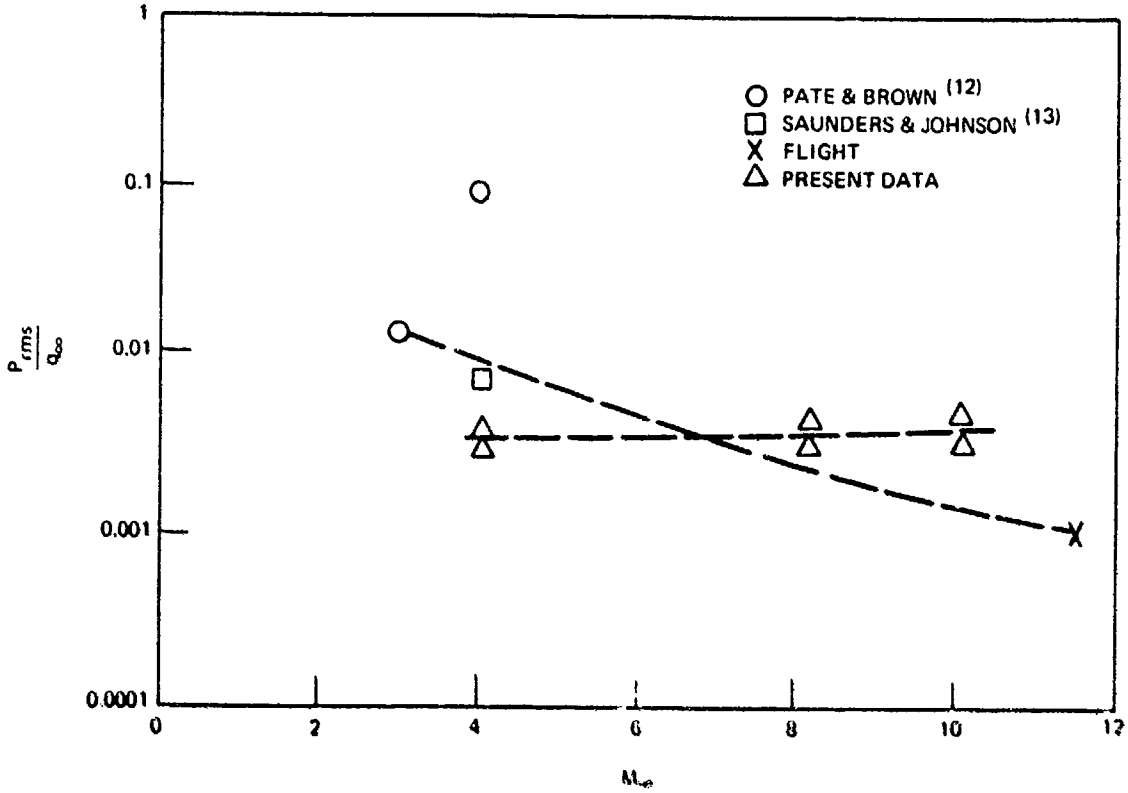

Figure 62. Root Mean Square Pressure Fluctuations vs. Free Stream Mach Number - Transitional Flow

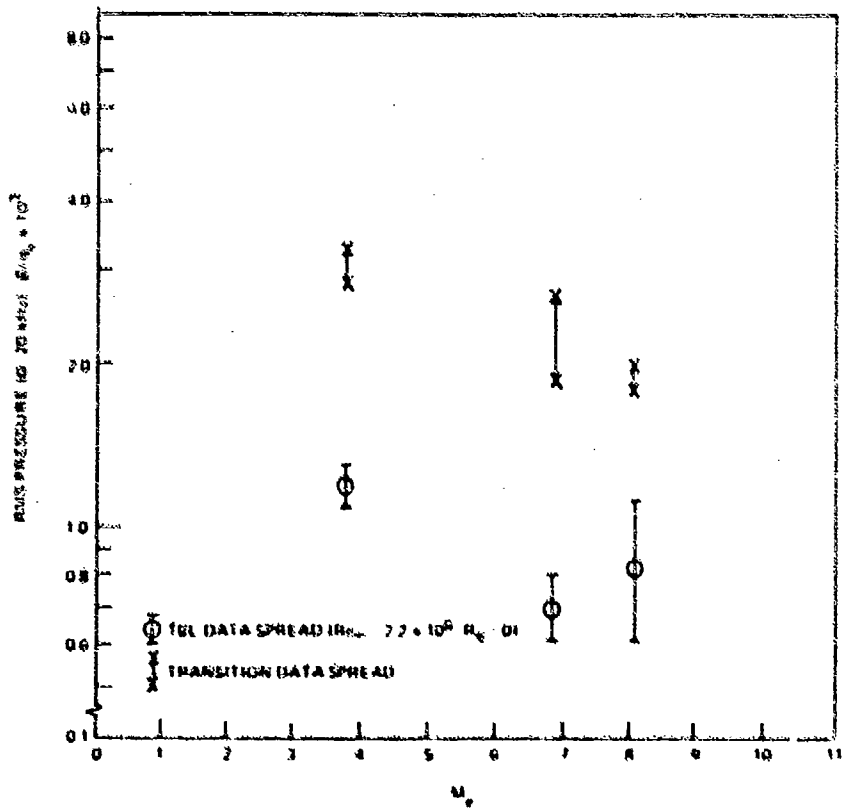

Figure 63. Comparison of Transitional and Full Turbulent RMS Pressure Fluctuations vs. Mach Number

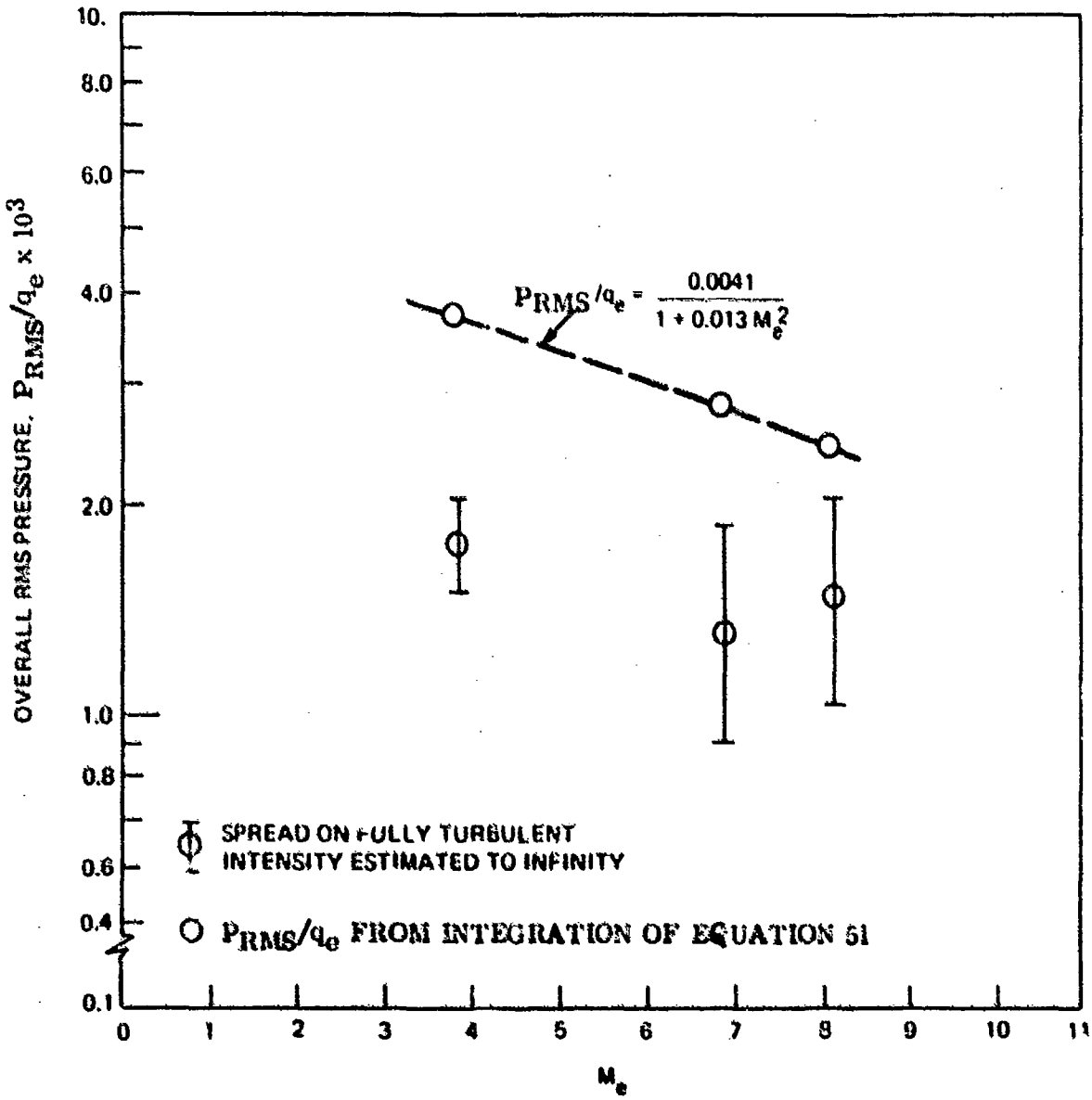

Figure 64. Transitional Acoustic Magnitude vs. Local Mach Number

from Figure 56 that normalized values of fully turbulent acoustic magnitude follow different trends for Mach numbers less than and greater than approximately four. Therefore, expressions similar to Lowson's must be qualified with the applicable Mach number range. This suggests that the same trend holds for transitional data, such that an equation somewhat different from Equation 46 would have to be employed for transitional intensity at low Mach number. Quantitative effects of transition at subsonic and transonic velocities should therefore be the subject of further investigation. However, for high-beta re-entry vehicles transition is associated with high Mach numbers and expressions derived in this section defining the acoustic properties of transitional flow are directly applicable to vehicles of this type.

b. Acoustic Power Spectral Density

For those cases of transitional flow listed in Table VIII, the one-third octave band SPL data were employed to calculate spectral values versus frequency out to 20,000 Hz. These values of Φ were normalized to the local aerodynamic TBL parameters U_e, δ^*, and q_e. Spectral values are shown plotted in Figures 65 to 67 as functions of the non-dimensional frequency parameter $f' = f\delta^*/U_e$ (Strouhal number) for the various test Mach numbers. No clearly identifiable spectral shape difference was noted between apparent peak transition PSD's and those estimated to be within 2 dB of the apparent peak. Therefore levels of Φ were adjusted uniformly throughout the 20 kHz frequency range using the factors given in the preceding section. From Figures 65, 66 and 67, it can be seen that a reasonable collapse of the resulting normalized data is obtained and that a definite trend in the data is apparent. It is postulated that the data curl up at high frequency exhibited by Mach $_\infty$ = 4 spectra results from an overcorrection for sensor size effects in that limited frequency range.

A comparison of these figures reveals that normalized spectral values for a Strouhal number less than 10^{-2} tend to be independent of Mach number, but that the nondimensional cut off frequency f_c' is less for $M_\infty = 10$ than for $M_\infty = 8$ and 4. These facts are taken into account below in developing prediction equations for P_{RMS}/q_e and Φ.

Figure 68 is a plot of a typical $M_\infty = 4$ PSD from the present investigation superimposed on the spectral data from Figure 15. As mentioned in Section III, the high levels seen at low frequency in the previously obtained data may be due to tunnel noise and electrical effects.

Previous techniques for determining predicted levels for a transition environment involved using the turbulent boundary layer acoustic prediction corresponding to given aerodynamic flow conditions as a baseline. Then the limited transition data available was employed to scale up the TBL spectral levels to estimated peak transition values. Therefore it is important to use a comparison of TBL and transitional spectra from the present data to verify and/or refine this prediction procedure. As an example, Figure 69 depicts normalized transitional PSD's (Sensors 11, 13 adjusted to apparent peak) and compares these data to turbulent boundary layer PSD's for Run 20 at $M_\infty = 4$. Normalized spectra for this case exceed TBL values by approximately 1 decade (10 dB).

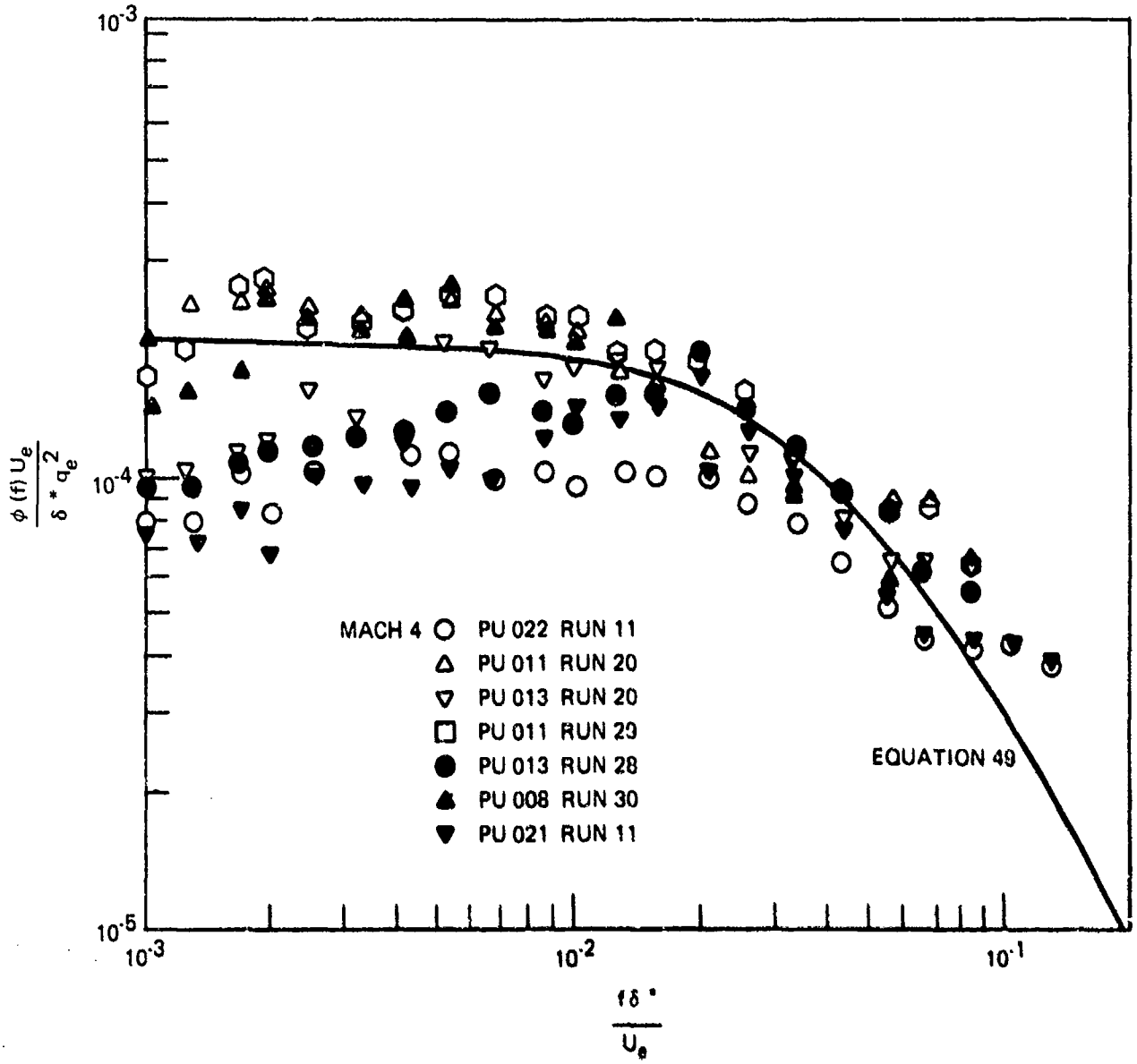

Figure 65. Normalized Power Spectral Density Distribution for Transitional Flow $M_\infty = 4$

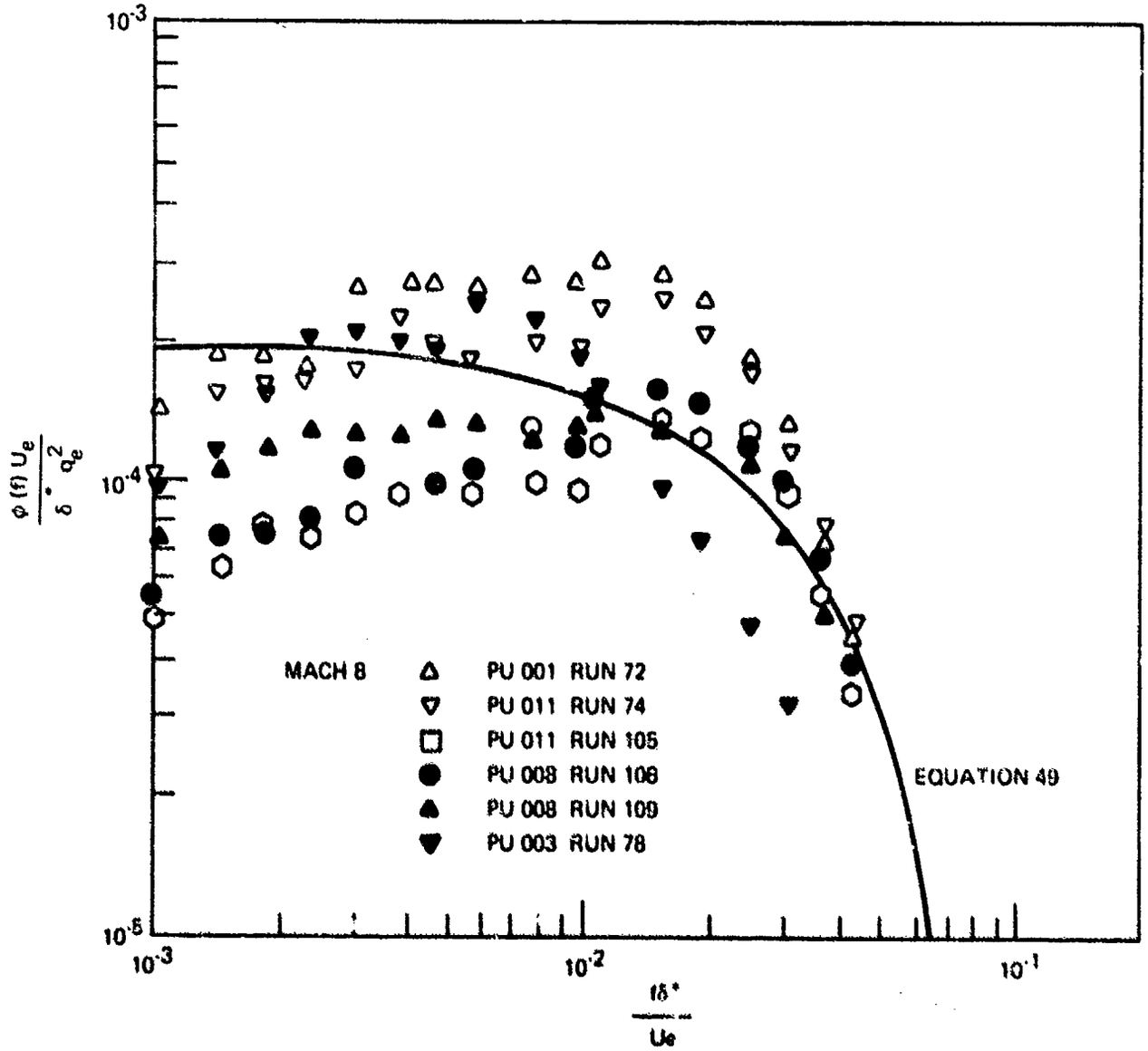

Figure 66. Normalized Power Spectral Density Distribution for Transitional Flow $M_\infty = 8$

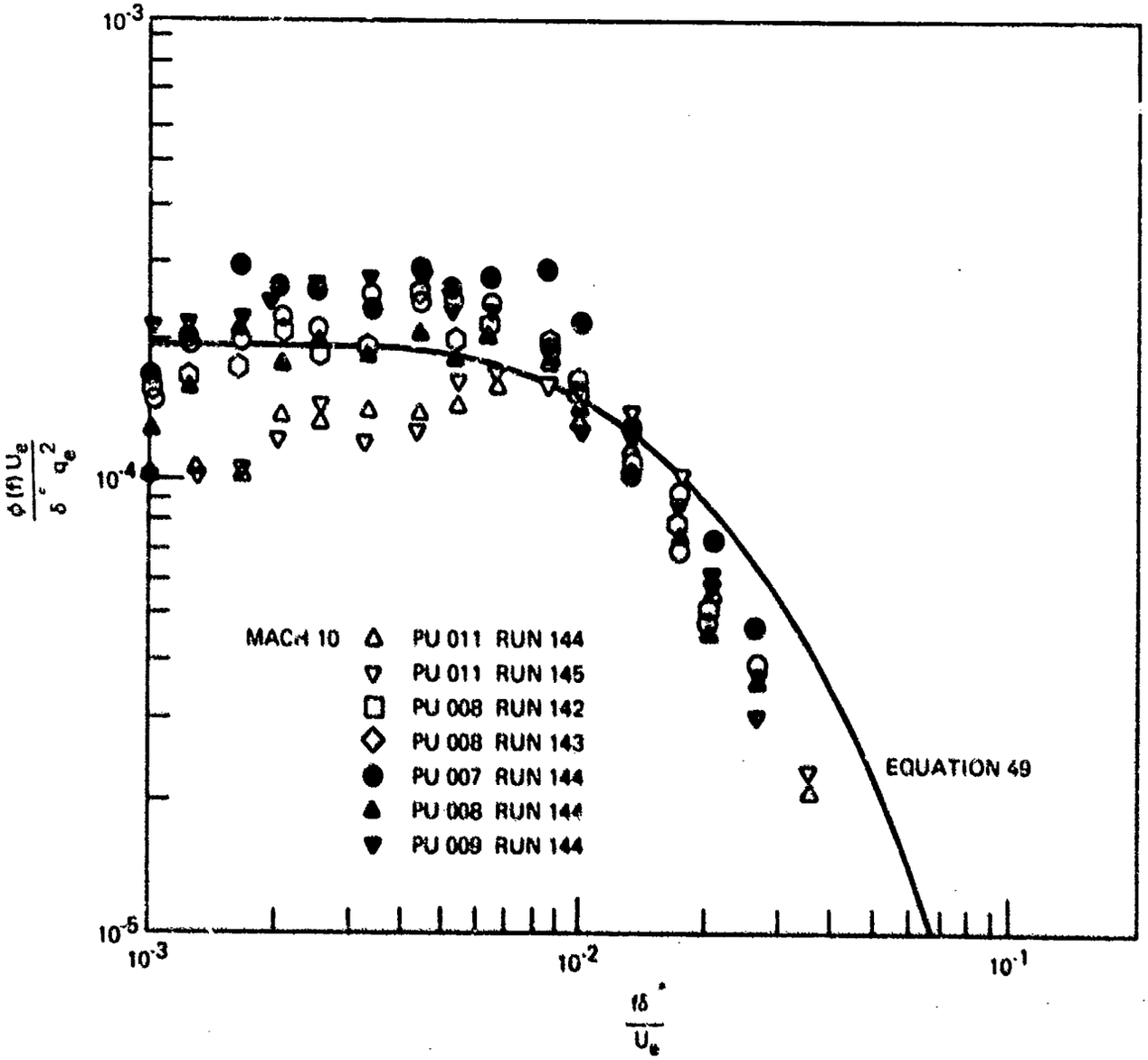

Figure 67. Normalized Power Spectral Density Distribution for Transitional Flow $M_\infty = 10$

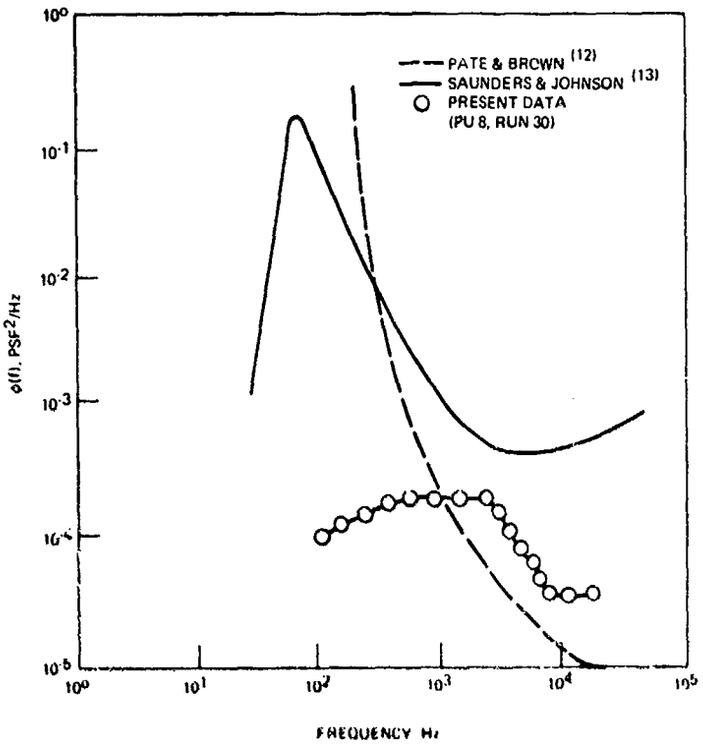

Figure 68. Transitional Flow Spectral Distribution Obtained in Wind Tunnel Experiments (M_∞ = 4)

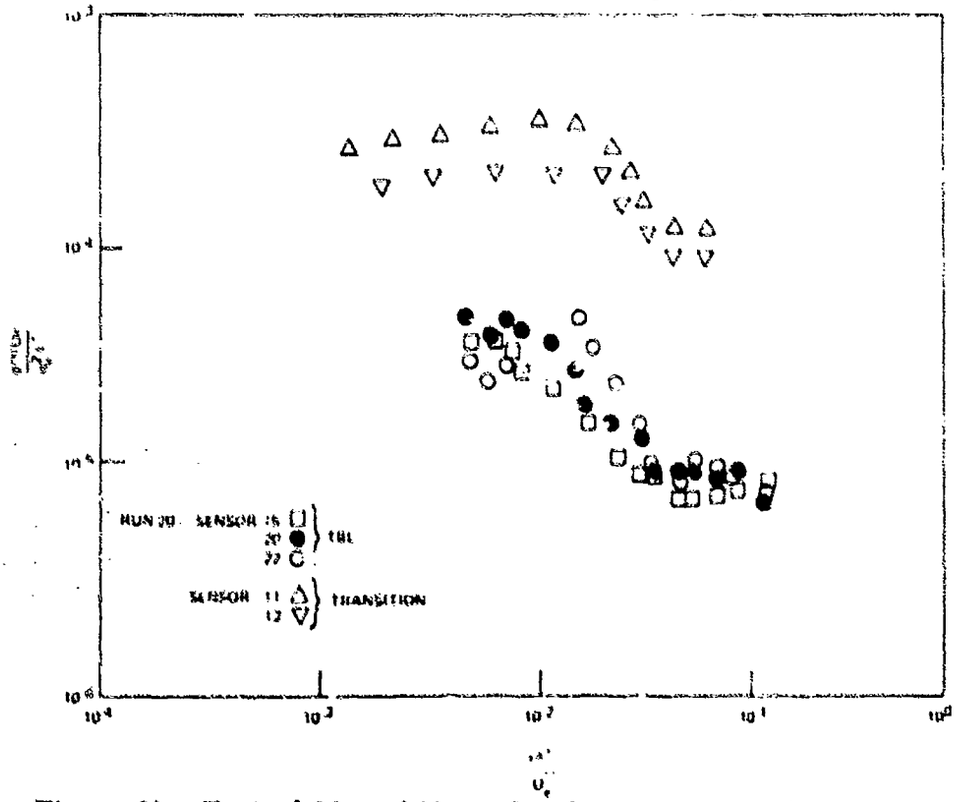

Figure 69. Typical M_∞ = 4 Normalized Spectra for Fully Turbulent and Transitional Flow

It is the intent of this section to derive a method for prediction of transitional quantities more precise than the previous indirect approach, but using a formal development quite similar to that of turbulent acoustic analysis. Attempts at generating an empirical equation to describe TBL spectra have generally assumed that the PSD level as a function of frequency has a form similar to

$$\phi(f) = \frac{K_1 P^2_{RMS}}{1 + (K_2 f)^2} \tag{47}$$

such that $\phi(f) \rightarrow K_1 p^2$ for low frequencies. Values of K_1 are dependent on aerodynamic parameters of velocity, boundary layer displacement thickness and dynamic pressure. Examination of Figures 65 and 67 suggests that peak transition spectral data may be described by an equation of similar form, with P^2_{RMS} replaced by q_e^2. Therefore defining nondimensional quantities

$$\phi' \equiv \phi U_e / \delta^* q_e^2 \quad \text{and} \quad f' = f\delta^*/U_e$$

we get

$$\phi'(f') = \frac{C_o}{1 + [Cf']^2} \tag{48}$$

where the character of the undetermined coefficients are defined by a best fit of the data.

An equation for ϕ' which provides a relatively good fit to the normalized data is the following:

$$\phi'(f') = \frac{2.00 \times 10^{-4}}{1 + [C(M_e) f']^2} \tag{49}$$

where

$$C(M_e) = 18.6 (1 + 0.013 M_e^2)^2 \tag{50}$$

Figures 65, 66 and 67 present Equation 49 superimposed on the normalized spectra.

In terms of absolute quantities, Equation 49 becomes

$$\phi(f) = \frac{2.0 \times 10^{-4} \delta^* q_e^2/U_e}{1 + \left[C(M_e)\delta^* f/U_e\right]^2} \tag{51}$$

The particular form of $C(M_e)$ in Equations 49 and 51 was chosen for compatibility with Equation 46, such that performing an integration of Equation 51 from 0 to infinity and taking the square root yields

$$P_{RMS}/q_e = \frac{1.78 \times 10^{-2}}{\sqrt{C(M_e)}} = \frac{0.0041}{1 + 0.013\, M_e^2}$$

which is identically Equation 46.

Further insight into the implications of Equation 51 can be gained by examining the identity

$$P_{RMS}^2 \equiv \int_0^\infty \phi(f)\, df = \frac{2.0 \times 10^{-4} q_e^2 \quad \pi/2}{C(M_e)} \tag{52}$$

which implies

$$2.0 \times 10^{-4} q_e^2 = \frac{2P_{RMS}^2 C(M_e)}{\pi} \tag{53}$$

Substituting this into Equation 51, the expression for transitional acoustic spectra in terms of TBL aerodynamic parameters becomes

$$\phi(f) = \frac{4 \dfrac{C(M_e)}{2\pi}\left(\delta^*/U_e\right)\bar{p}^2}{1 + \left[2\pi \dfrac{C(M_e)}{2\pi}\delta^* f/U_e\right]^2} \tag{54}$$

Now define a fictitious transitional flow length parameter δ_t (analogous to the turbulent boundary layer displacement thickness), by

$$\delta_t \equiv \frac{C(M_e)}{2\pi}\delta^* \qquad 3.7 \le M_e \le 8.1 \tag{55}$$

Equation 54 hence becomes

$$\phi(f) = \frac{4\,(\delta_t\,/U_e)\,\bar{p}^2}{1 + \left[2\pi f \delta_t\,/U_e\right]^2} \qquad 3.7 \leq M_e \leq 8.1 \tag{56}$$

which is Equation 11 for TBL spectra expressed in the frequency domain except δ^* and U_c have been respectively replaced with δ_t and U_e. The similarity in form further ensures that both sides of Equation 56 integrate identically to p^2_{RMS}. Therefore it is postulated herein that transitional spectra in the range $3.7 < M_e < 8.1$ can be defined using a prediction technique completely analogous to fully turbulent procedures, using Equations 55 and 56. Figure 70 describes the dependence of the ratio $\delta_t\,/\delta^*$ on local Mach number.

c. Cross Correlation Functions

As previously discussed, narrow band cross correlation functions were not obtained. Since the spectral distribution for transitional flow measured in the present test program was similar to that of turbulent flow it appears reasonable that the Cross Correlation Function remain the same. Until further resolution of this area is made, it is recommended that the

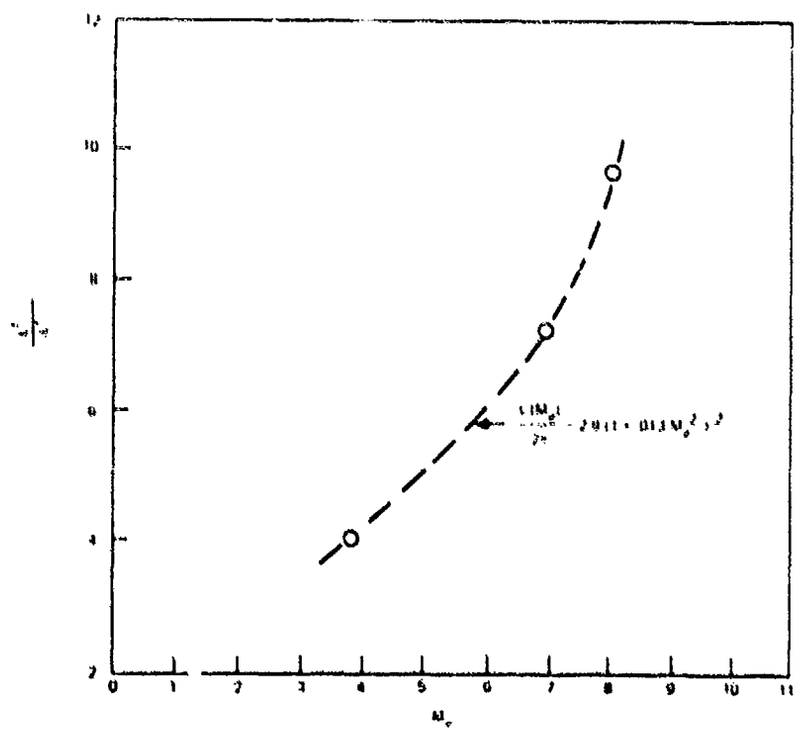

Figure 70. Functional Relationship of Transitional and Fully Turbulent Characteristic Length Parameters

correlation functions for fully developed turbulent flow be used as a first approximation. Equations 20 and 21 are therefore recommended to define the cross correlation coefficients for transitional flow.

$$A_\eta(\eta, \omega) = \exp\left(\frac{-0.72|\eta|\omega}{U_c}\right)\left[0.3 + 0.7\exp\left(\frac{-0.5|\eta|}{\delta^*}\right)\right] \tag{20}$$

$$A_\xi(\xi, \omega) = \exp\left(\frac{-0.1|\xi|\omega}{U_c}\right)\exp\left(\frac{-0.034|\xi|}{\delta^*}\right) \tag{21}$$

d. Convection Velocity

Broad band convection velocities for transitional flow determined from data obtained in the present test program were approximately 0.6 of that in turbulent flow; therefore, the following expression is recommended for transitional flow

$$\frac{U_c}{U_\infty} = 0.045 + 0.18\exp\left(\frac{-0.11\,\omega\delta}{U_\infty}\right) - 0.15\exp\left(\frac{-1.2\xi}{\delta}\right) \tag{57}$$

3. BASE FLOW

a. Acoustic Magnitude

Houbolt[20] was the only source found which defined expressions for the acoustic environment acting on the base of a re-entry vehicle. Based upon engineering logic and the knowledge of turbulent flow, the following expression was derived relating base pressure fluctuations to the static pressure

$$P_{rms_b} = \frac{0.01\,M_b^2}{1 + .18\,M_b^2}\,P_b \tag{38}$$

This relationship agreed well with data obtained by Eldred[18] for subsonic flow but as stated in Houbolt's report, verification of the coefficients in the above equation was in order for supersonic flow. Figure 71 compares Equation 38 to data obtained in this study at zero angle of attack for Mach numbers associated with the wake boundary of 6.2 and 13.6 (M_∞ = 4 and 10 respectively). Predicted levels are lower than measured values indicating that adjustments to the denominator in the expression given by equation 38 are required. No adjustment to the numerator coefficient is required since it agrees with

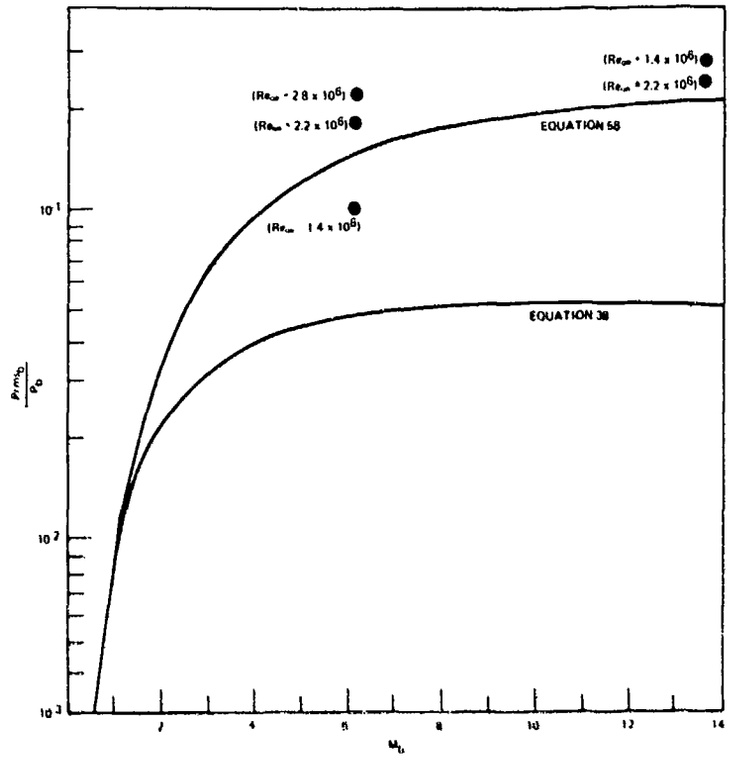

Figure 71. Overall Acoustic Intensity for Base Flow (Prediction vs Test)

Eldred's subsonic results. Using a coefficient of 0.04 in the denominator as given in Equation 58 agrees well with data. Figure 71 is a plot of Equation 58 and the tunnel data.

$$P_{rms_b} = \frac{0.01\, M_b^2}{1 + 0.04\, M_b^2}\, P_b \tag{58}$$

At large Mach numbers, Equation 58 suggests that the rms pressure level is dependent simply on the base static pressure, reaching an asymptotic value of $0.25\, P_b$.

b. Acoustic Power Spectral Density and Correlation Function

In order to arrive at the power spectral density for base flow Houbolt assumed a correlation function of the form

$$R(\tau) = P^2_{rms_b}\, e^{-(V_T/L)t} \tag{39}$$

where V_T was an effective transport velocity and L the scale of turbulence. Assuming that the transport velocity was related to the transverse component of the wake boundary velocity ($V_T = V_b \sin\theta$ where θ is the half cone angle of the wake cone) and the scale of turbulence (L) proportional to the base radius, Equation 59 was developed for the base power spectral density:

$$\phi(\omega) = \frac{2\,P^2_{rms_b}\,L}{\pi\,V_T}\,\frac{1}{1+\left(\frac{L\omega}{V_T}\right)^2} = \frac{2\,P^2_{rms_b}\,r_b}{\pi U_b \sin\theta}\,\frac{1}{1+\left(\frac{r_b\,\omega}{U_b \sin\theta}\right)^2} \tag{59}$$

Equation 59 is compared with normalized test data ($M_\infty = 4$, $R_{e_\infty} = 1.4 \times 10^6$, 2.2×10^6, 2.8×10^6) in Figure 72. It is evident that this equation is conservative at low Strouhal numbers. Figure 73 compares the same Mach 4 data with Equation 60 which assumes that the transport velocity is equal to the wake boundary velocity. Good agreement is attained with test data therefore Equation 60 and its associated correlation function, Equation 61 are recommended to define acoustic environments for base flow. Figure 74 compare the recommended equation to data obtained at $M_\infty = 10$ reasonably good correlation is attained:

$$\phi(f) = \frac{2d\,P^2_{rms_b}}{U_b\left[1+\left(\frac{d\pi f}{U_b}\right)^2\right]} \tag{60}$$

$$R(\tau) = P^2_{rms_b}\,e^{-(U_b/d)\tau} \tag{61}$$

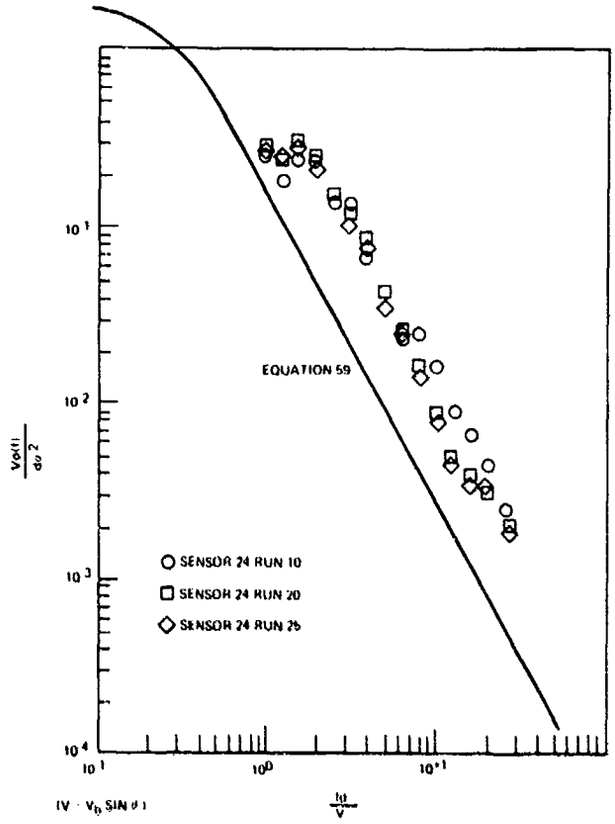

Figure 72. Normalized Base Acoustic Spectra ($M_\infty = 4$)

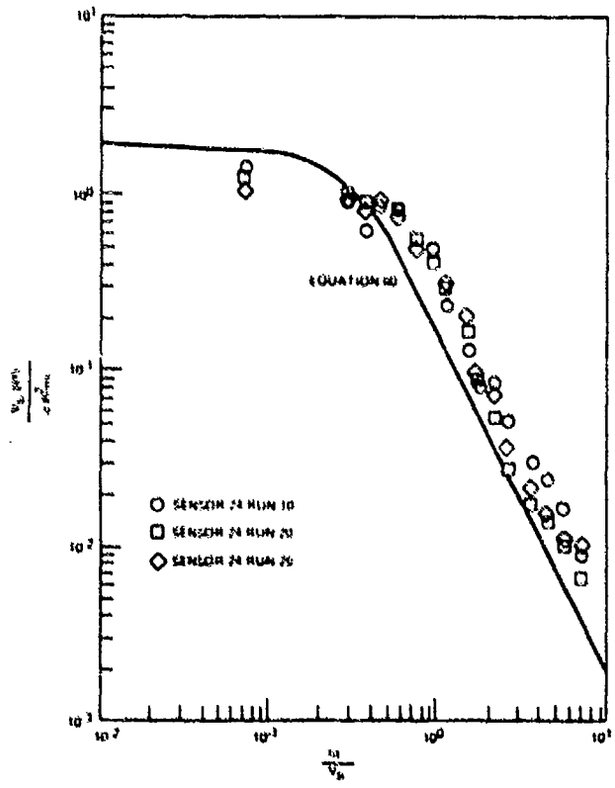

Figure 73. Normalized Base Acoustic Spectra ($M_\infty = 4$)

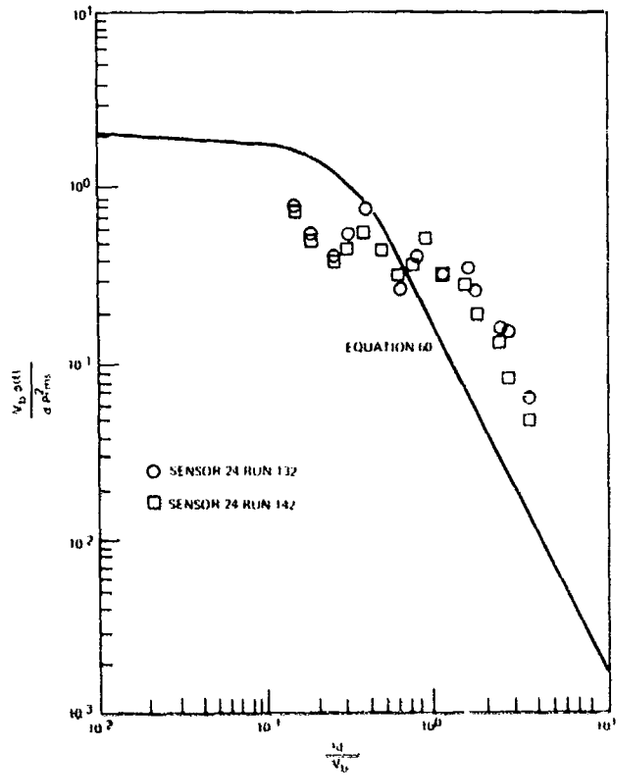

Figure 74. Normalized Base Acoustic Spectra (M_∞ = 8)

SECTION VII

REFERENCES

1. Robertson, J. E., "Prediction of In-Flight Fluctuating Pressure Environments Including Protuberance Induced Flow", Wyle Laboratories Research Report, WR 71-10, March 1971.

2. Lowson, M. V., "Prediction of Boundary Layer Pressure Fluctuations", AFFDL-TR-67-167, April 1968.

3. Coe, C. F., "Surface Pressure Fluctuations Associated with Aerodynamic Noise", NASA SP-207, July 1969.

4. Chyu, W. J., Hanly, R. D., "Power-and-Cross-Spectra and Space-Time Correlations of Surface Fluctuating Pressures at Mach Numbers Between 1.6 and 2.5", NASA TN D-5440, September 1969.

5. Speaker, W. V., Ailman, C. M., "Spectra and Space-Time Correlations of the Fluctuating Pressures at a Wall Beneath a Supersonic Turbulent Boundary Layer Perturbed by Steps and Shock Waves", NASA CR-486, May 1969.

6. Belcher, P. M., "Prediction of Boundary Layer Turbulence Spectra and Correlation for Supersonic Flight", September 1965.

7. Williams, D. J. M., "Measurements of the Surface Pressure Fluctuations in Turbulent Boundary Layer", Univ. of Southampton, A.A.S.U. Report 162, December 1960.

8. Bull, M. K., Wilby, J. F., and Blackman, D. R., "Wall Pressure Fluctuations in Boundary Layer Flow and Response of Simple Structures to Random Pressure Fields", AASU Report No. 243, July 1963.

9. Maestrello, L.,"Radiation From and Panel Response to a Supersonic Turbulent Boundary Layer", Boeing Scientific Research Laboratories, D1-82-0719, September 1968.

10. Serafini, J. S., "Wall Pressure Fluctuations and Pressure-Velocity Correlations in a Turbulent Boundary Layer, NASA-TR-R-165, 1963.

11. White, R. W., Predicted Vibration Responses of Apollo Structure and Effects of Pressure Correlation Lengths on Response", Wyle Laboratories Research Report, WR 67-4, March 1967.

12. Pate, S. R., Brown, M. D., "Acoustic Measurements in Supersonic Transitional Boundary Layers", AEDC-TR-69-182, October 1969.

13. Saunders, H., Johnson, R. I., and MaCourek, M. N., "Boundary Layer Acoustic Measurements in Transitional and Turbulent Flow at M = 4.0", AIAA presentation at Fourth Aerodynamic Testing Conference, April 1969.

14. Houbolt, J. C., "On the Estimation of Pressure Fluctuations in Boundary Layers and Wakes", GE-TIS 66SD296, April 1966.

15. Saunders, H., "Evaluation and Data Analysis of PDV/SA2 Vehicle During Re-entry Flight", GE Document 9333-J1-390, September 1969.

16. Rechtien, R. D., "A Study of the Fluctuating Pressure Field in Regions of Induced Flow Separation at Supersonic Speeds", University of Missouri, Rolla UMR Research Report, May 1970.

17. Hilton, D. A., "In-Flight Aerodynamic Noise Measurements on a Scout Launch Vehicle", NASA TN D-1818, July 1963.

18. Eldred, K., Roberts, W., and White, R., "Structural Vibrations in Space Vehicles", WADD Technical Report 61-62, December 1961.

19. Allman, C. M., "On Predicting Fluctuating Pressures at a Wall Beneath a Turbulent Boundary Layer", Douglas Paper No. 4331, April 1967.

20. Houbolt, J. C., "Structural Response of Re-entry Vehicles to Boundary Layer Noise", GE-TIS 65SD223A, March 1965.

21. Bull, M. K. and Willis, J. I., "Some Results of Experimental Investigations of the Surface Pressure Field to a Turbulent Boundary Layer, ASD-TDR-62-425, August 1962.

22. Bull, M. K., "Wall-Pressure Fluctuations Associated with Subsonic Turbulent Boundary Layer Flow", J. Fluid Mech., Vol. 28, Part 4, 1967.

23. Crocker, M. J., "The Response of Supersonic Transport Fuselage to Boundary Layer and to Reverberant Noise", J. Sound Vib., (1969) 9 (1) 6-20.

APPENDIX

ENGINEERING RELATIONS /GRAPHS FOR THE DETERMINATION OF LOCAL FLOW PROPERTIES ON SHARP BODIES

A. MARTELLUCCI

Within the body of this report, the measured acoustic data have been normalized with various aerodynamic flow properties such as the boundary layer edge dynamic pressure, $q_e \equiv 1/2\ \rho_e u_e^2$, the boundary layer displacement thickness, δ^*, the local static pressure, $P_w \equiv P_e$, etc. It is the purpose of this appendix to provide the reader, who may not have ready access to viscous flow computer programs or who may be unfamiliar with the equations/techniques necessary to compute the viscous properties, with simplified equations and charts with which to determine some of the more fundamental local flow properties.

In general, for blunted bodies, the determination of the properties within the viscous layer involves the numerical solution of the boundary layer equations using, for example a finite difference scheme. Another common approach involves casting the equations in an integral form resulting in integro-differential equations which are solved by integration along the body surface to the station(s) in question. As a result, computer programs have been formulated to solve these systems of equations. Programs exist for the solution of the laminar and turbulent boundary layer flows, however, when the boundary layer on the body is laminar - transitional-turbulent, special devices or techniques must be employed to solve this class of problem. In the finite difference solution scheme, in which a forward marching solution is employed, one customarily lets the viscosity vary in the transitional boundary layer region (which must be known a priori) from the molecular value at transition onset to the turbulent effective value at the end of transition using, say, a gaussian distribution.

The integral form of the viscous layer equations are more commonly used in vehicle design. In this type of scheme, it is quite common to treat the transitional region as a point, that is, the viscous layer is treated as laminar to this point and downstream of this point the turbulent flow relations are used. To pass through this region one must establish the constants of integration for the turbulent solution (i.e., the so-called "effective origin" concept). This is customarily performed by equating the laminar momentum thickness, θ_L, to turbulent value, θ_T, thereby establishing an artificial origin to the turbulent solution such that at that particular station of matching (usually transition onset) the value of $\theta_L = \theta_T$. The remaining turbulent properties can then be determined. This information is by way of background. I will attempt to present simplified laminar and turbulent boundary layer equations valid for pointed cones or sharp flat plates. Furthermore, graphs will be presented from which the inviscid flow (boundary layer edge) properties can be determined. It should again be stressed that the following information is valid only for sharp leading edge bodies. Strictly speaking, for blunted bodies the integral equations must be solved. Thus the following information provides a means of estimating approximate values or estimates of parameters which are valid for blunt body stations far from the leading edge.

INVISCID FLOW

In this section, a series of graphs will be presented which can be used to define the inviscid perfect gas ($\gamma = 1.40$) flow properties on pointed cones and wedges. Listed below are the Figure numbers and the flow properties presented in each chart.

FIGURE		PROPERTY
CONE	WEDGE	
A-1	A-5, 6	Wall Pressure Ratio, $P_w/P_\infty = P_e/P_\infty$, vs M_∞ for various θ_c
A-2	A-7	Edge Temperature Ratio, T_e/T_∞ vs M_∞ for various θ_c
A-3	A-8	Edge Mach number, M_e vs M_∞ for various θ_c
A-4	A-9	Local unit Reynolds number ratio, R_e/R_{e_∞} vs θ_c for various M_∞

With the free stream conditions known, the local dynamic pressure on the body, q_e, can be determined from the following:

$$q_e \cong 1/2\, \rho_e\, u_e^2 = \frac{\gamma}{2} \left(\frac{P_e}{P_\infty}\right) P_\infty\, M_e^2 \qquad (1)$$

where $\gamma/2 = 0.7$

The relation for the local velocity is:

$$u_e = M_e\, a_e = M_e \sqrt{\gamma R T_e} = 49.01\, M_e \sqrt{\left(\frac{T_e}{T_\infty}\right) T_\infty} \text{ (fps)} \qquad (2)$$

The local wetted length Reynolds number at a distance, s, along the body surface can be determined from Figure A-4 or A-9 and the following:

$$R_{e_s} \cong \left(R_e/R_{e_\infty}\right) R_{e_\infty}\, S$$ where $R_{e_\infty} = \rho_\infty\, u_\infty/\mu_\infty$ is the free stream unit Reynolds number. (3)

BOUNDARY LAYER EQUATIONS - Compressible Flow/Ideal Gas

Viscous layer equations will be presented here to enable the reader to calculate the momentum or displacement thickness for a cone or wedge with either all laminar, all turbulent, or a laminar-turbulent boundary layer (using the matched momentum thickness approach).

LAMINAR FLOW

Boundary Layer velocity thickness:

$$\delta_L = \frac{5.3\, S \left[\left(\mu^*/\mu_e \right) \Big/ \left(T_e/T^* \right) \right]^{0.5}}{3^{K/2} \sqrt{R_{e_s}} \left(T^*/T_e \right)^{0.18}} \tag{4}$$

where

$K = 0$ flat plate, $K = 1$ cone

Reference Temperature:

$$T^* = 0.5\, T_w + (0.5 - 0.22\, r)\, T_e + 0.22\, r\, T_{0_\infty} \tag{5}$$

Recovery Temperature:

$$T_r = r\, T_{0_\infty} + (1-r)\, T_e \tag{6}$$

Viscosity:

$$\mu = 2.270 \frac{T^{3/2}}{T + 198.6} \times 10^{-8} \frac{\text{LB-Sec}}{\text{ft}^2} \tag{7}$$

r = recovery factor = 0.848 (laminar)

recovery factor = (.896) (turbulent)

and T_w = model wall temperature

The ratio of the boundary layer displacement to velocity thickness is given by:

$$\frac{\delta_L^*}{\delta_L} = \frac{u_e^2/2h_e + 3.36\ T_w/T_e - 0.376}{u_e^2/2h_e + 3.36\ T_w/T_e + 5.79} \tag{8}$$

where

$$h_e = C_p\ T_e \tag{9}$$

$$C_p = 6006\ \frac{ft^2}{sec^2\ {}^oR} \qquad \text{(for air)}$$

The ratio of the boundary layer momentum to velocity thickness is given by:

$$\frac{\theta_L}{\delta_L} = 0.125 \left(\frac{T^*}{T_e}\right)^{0.18} \tag{10}$$

Through the use of equations (4) through (10), the local viscous parameters δ_L, δ_L^*, and θ_L can be determined.

TURBULENT FLOW

The momentum thickness can be expressed as:

$$\theta_T = \frac{0.037\ \epsilon\ S}{1.913^K\ Re_s^{\ 0.2}} \tag{11}$$

where

$$\epsilon = \left(\frac{\mu^*}{\mu_e}\right)^{0.2} \left(\frac{T_e}{T^*}\right)^{0.8}$$

The boundary layer displacement thickness can be obtained from the following relations, in conjunction with equation (11):

$$\frac{\delta_T^*}{\theta_T} = -1 + \left(1.29\ \frac{T_w}{T_r} + 1\right) \left[1 + 2.08\ (M_e^2 / 5)\right] \text{for } M_e > 4.5 \tag{12}$$

$$\frac{\delta_T^*}{\theta_T} = -1 + \left(1.29 \frac{T_w}{T_r} + 1\right)\left[1.04\left(1 + \frac{M_e^2}{5}\right) - .04\right] \tag{13}$$

for $M_e \leq 4.5$

LAMINAR-TURBULENT FLOW

The growth of the momentum and displacement thicknesses along a body for the case where the flow is laminar to a point (such as the transition onset point) then is turbulent thereafter may be obtained as follows:

(1) δ_L^* is determined from equations (8) and (4)

(2) θ_L is determined from equations (10) and (4)

(3) Let $\theta_L = \theta_T$ at $S = S_{TR}$

That is, from equation (11) establish the value of S_e (effective origin argument) which pertains to the prescribed value of θ_L. It should be noted that at $S_e = 0$ the value of S (from the vehicle origin) is non-zero. This is illustrated in the sketch below:

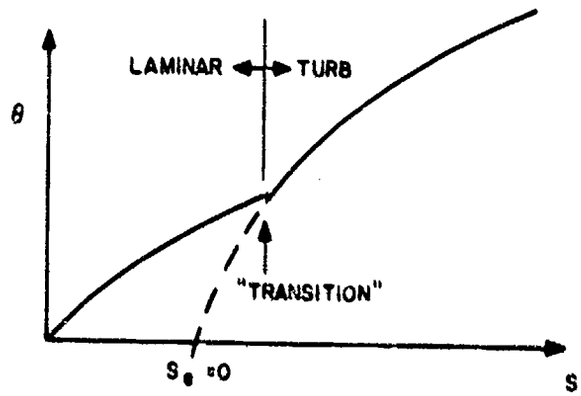

(4) Evaluate $\dot{\theta}_T$ as a function of S_e

(5) Determine δ_T^* from equation (12) or (13) whichever pertains.

Thus, through the use of Figures (A-1) through (A-9) in conjunction with equations (1) through (13) those local properties employed in the normalization of the forebody acoustic measurements can be estimated.

BASE PRESSURE CORRELATION

The RMS acoustic pressure on the base of conical bodies is normalized with the base pressure. When the flow at the cone base is transitional-turbulent, experimental data have shown that the pressure across the base is approximately constant. A correlation of available flight and wind tunnel cone data, results in the line shown in Figure A-10, where P_b/P_w is plotted against M_e. P_w and M_e can be determined from Figures A-1 and A-3, respectively.

FLIGHT EXAMPLE ON THE USE OF THE APPENDIX:

Let us assume that one wishes to determine the acoustic magnitude levels and the power spectra for a conical re-entry vehicle at an altitude of 10,000 feet. The vehicle in this case is 6° half angle cone which is 6 feet long and has a nose to base bluntness ratio $R_N/R_B < .02$ (hence a sharp cone approximation for this case will be valid). Let us further assume that at H = 10 Kft, $M_\infty = 15$ and $T_w = 3000^oR$.

From standard altitude tables (e.g. 1962) one can establish

$$P_\infty = 1455.6 \text{ PSFa}$$

$$T_\infty = 483^oR$$

$$T_{o_\infty} = 22{,}555^oR^*$$

$$R_{e_\infty}/\text{ft} = 8.025 \times 10^7$$

Thus the geometry and free stream conditions are set, and are summarized below:

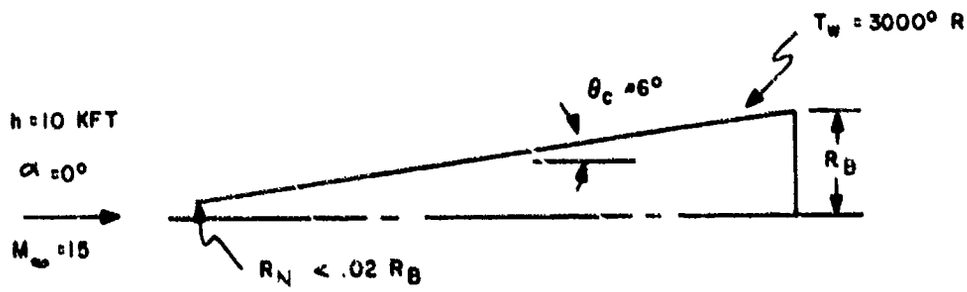

*It should be noted here that for the flight case, the freestream stagnation properties must be obtained from a Mollier Diagram. For simplicity here, ideal gas relations were used.

The local inviscid flow properties can be determined from Figures A-1 to A-4 and are listed below:

Fig. A-1	$P_w/P_\infty = 5.0$	$P_w = 7278$ psf
Fig. A-2	$T_e/T_\infty = 1.73$	$T_e = 835.6^\circ R$
Fig. A-3		$M_e = 11.4$
Fig. A-4	$R_e/R_{e_\infty} = 1.86$	$R_e/ft = 1.49 \times 10^8$

$$q_e = \gamma/2\ M_e^2\ P_w = 662{,}000 \text{ psf}$$

Using the acoustic intensity prediction suggested in the body of this report for fully developed turbulent flow, i.e.,

$$P_{rms}/q_e = 0.002 \Big/ \left(1 + 0.02\ M_e^2\right) = 0.000555$$

which corresponds to 179 dB.

For the fully developed turbulent flow case presented here, one can readily compute the displacement thickness using the equations presented. The procedure would be as follows:

Given T_w, T_e, and the freestream conditions one can determine T^* and T_r from equations (5) and (6), respectively. That is

$$T^* = 0.5(3000) + \left[.5 - .22(.896)\right] 835.6 + 0.22(.896)\ (22{,}555)$$

$$T^* = 6{,}199^\circ R$$

$$T_r = 0.896\ (22{,}555) + (1 - .896)\ 835.6$$

$$T_r = 20{,}296^\circ R$$

Before computing θ_T from equation (11), one must first determine

$$\epsilon = \left(\frac{\mu^*}{\mu_e}\right)^{0.2} \left(\frac{Te}{T^*}\right)^{0.8}$$

$$= \left[\left(\frac{16833}{835.6}\right)^{3/2} \left(\frac{835.6 + 198.6}{6199 + 198.6}\right)\right]^{0.2} \left[\frac{835.6}{6199}\right]^{0.8}$$

$$\epsilon = 0.255$$

Thus from equation (11) at S = 6'

$$\theta_T = \frac{0.037\,(.255)\,(6)}{1.913 \left[1.49\text{x}10^8)\,(6)\right]^{0.2}}$$

$$\theta_T = 0.000479 \text{ Ft.}$$

Then from equation (12)

$$\delta^*_T = 0.000479 \left[-1+\left(\frac{1.29(3000)}{20296} +1\right) \left\{1+2.08 \frac{(11.4)^2}{5}\right\}\right]$$

$$\delta^*_T = 0.0309 \text{ Ft.}$$

This value would be used in the acoustic power spectral density relation $\phi(w)$ as defined in the body of the report.

This numerical example serves as an illustration in determining the normalization parameters utilized in the body of the report. It should be recognized that for the flight case real gas flow tables should be employed. For wind tunnel cases, ideal gas flow relations and tables are generally adequate.

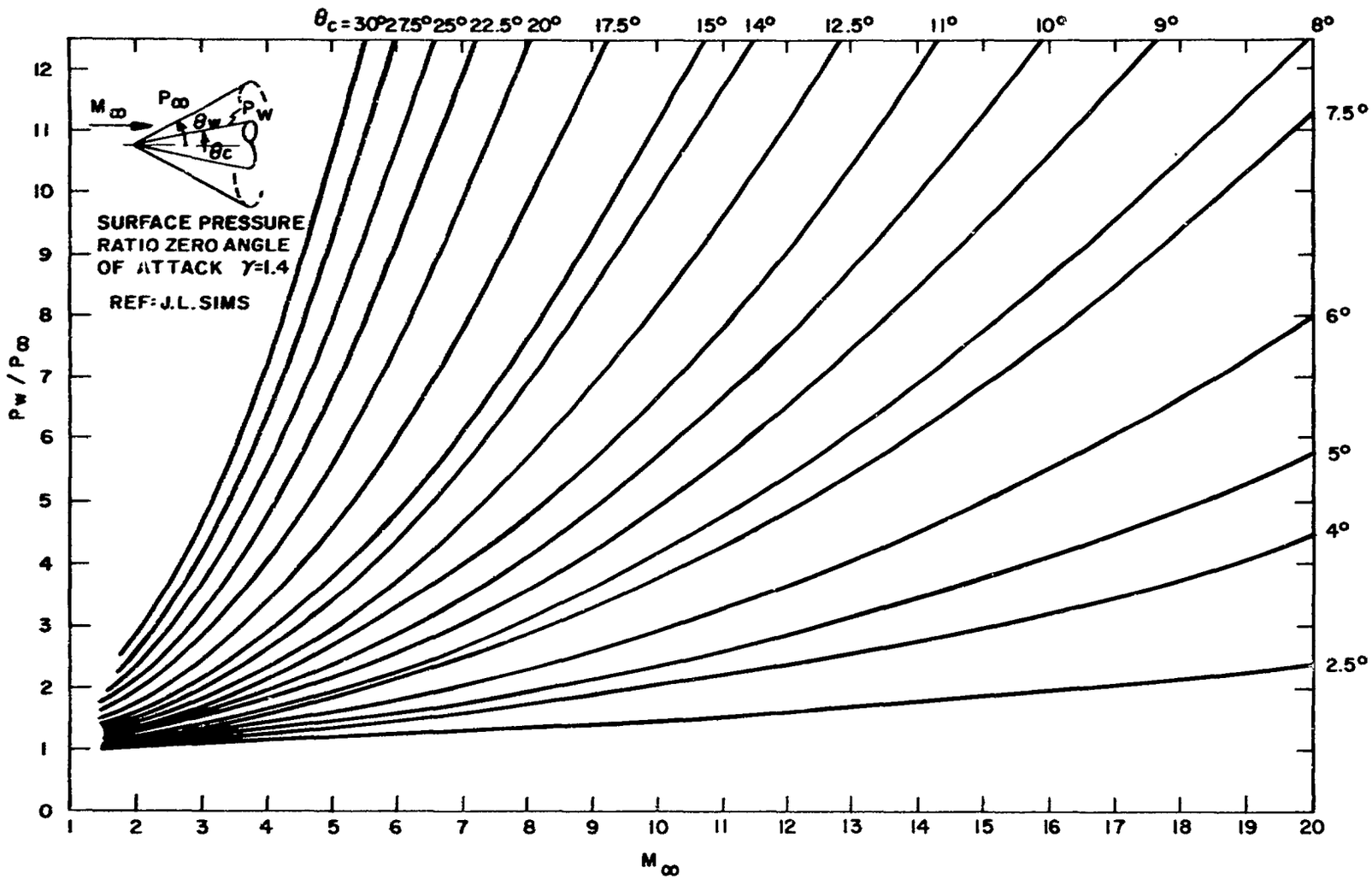
θ_c = 30° 27.5° 25° 22.5° 20° 17.5° 15° 14° 12.5° 11° 10° 9° 8°
7.5°
6°
5°
4°
2.5°
M_∞
P_∞
θ_w
P_w
θ_c
SURFACE PRESSURE RATIO ZERO ANGLE OF ATTACK γ=1.4
REF: J.L. SIMS
P_w / P_∞
M_∞

Figure A-1

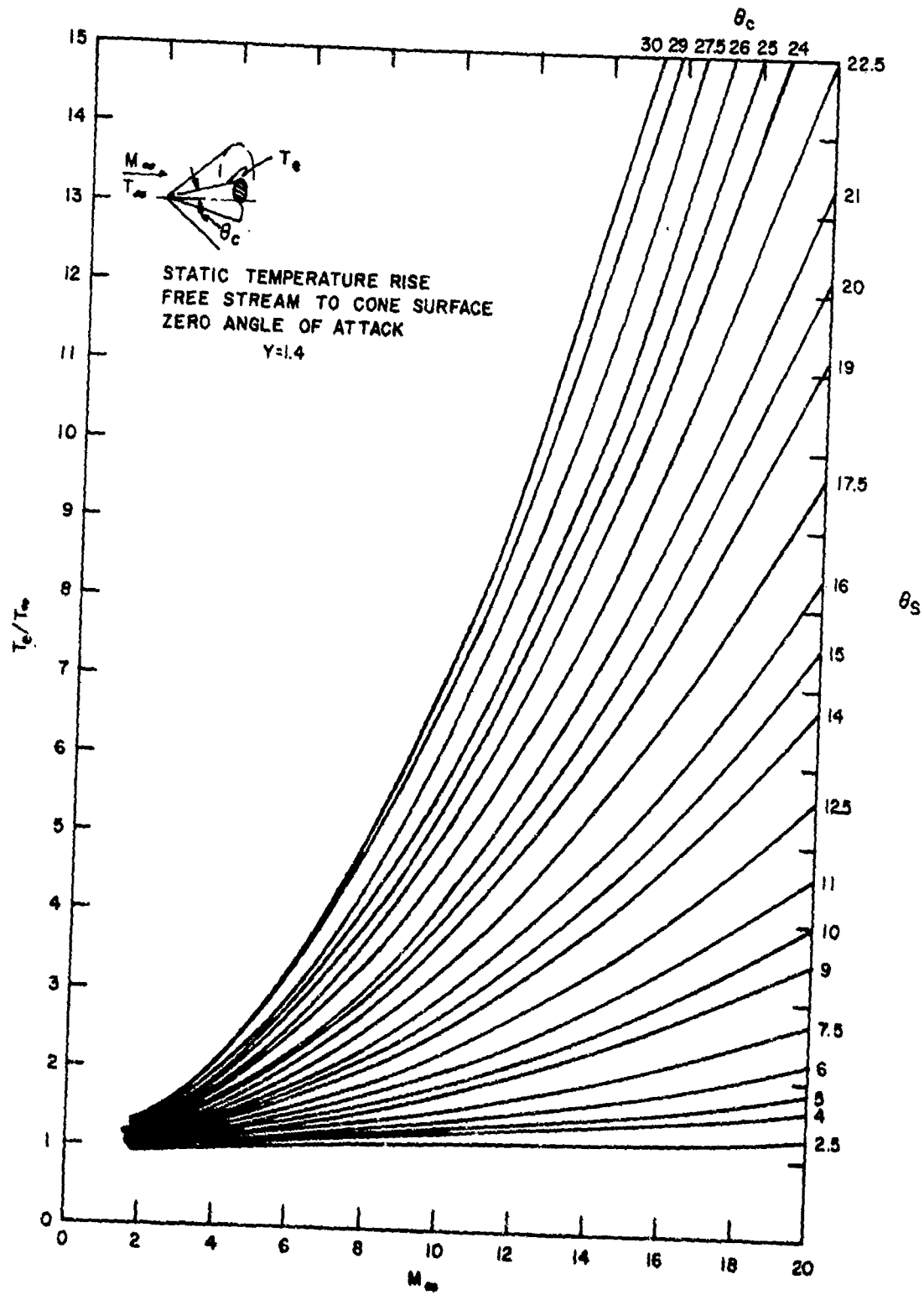
STATIC TEMPERATURE RISE
FREE STREAM TO CONE SURFACE
ZERO ANGLE OF ATTACK
γ=1.4
T_e/T_∞
M_∞
θ_c
θ_s
T_e
30 29 27.5 26 25 24
22.5
21
20
19
17.5
16
15
14
12.5
11
10
9
7.5
6
5
4
2.5

Figure A-2

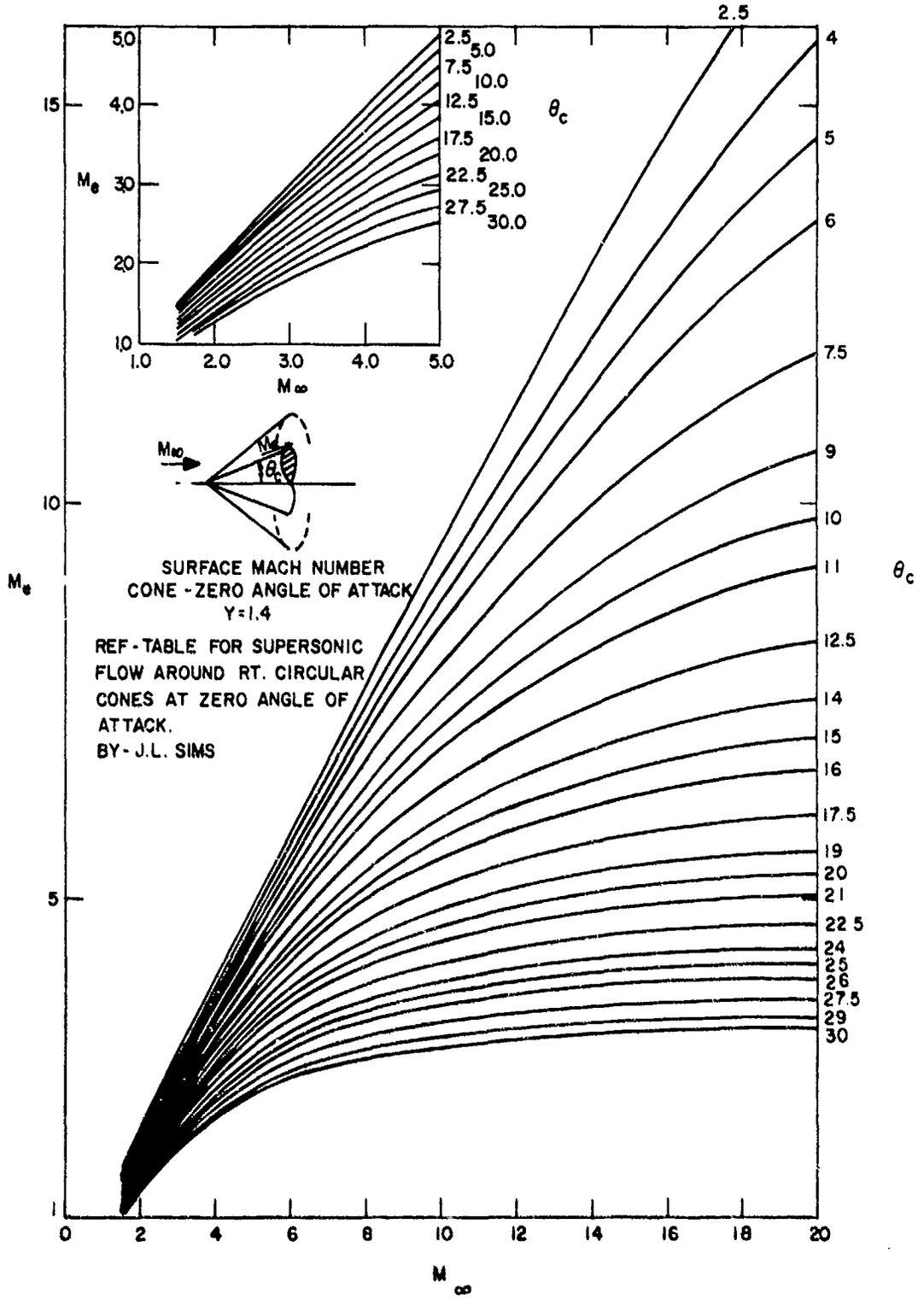
SURFACE MACH NUMBER
CONE - ZERO ANGLE OF ATTACK
γ = 1.4
REF - TABLE FOR SUPERSONIC
FLOW AROUND RT. CIRCULAR
CONES AT ZERO ANGLE OF
ATTACK.
BY - J.L. SIMS
M_e
M_∞
θ_c
M_{∞}
M_e
θ_c

Figure A-3

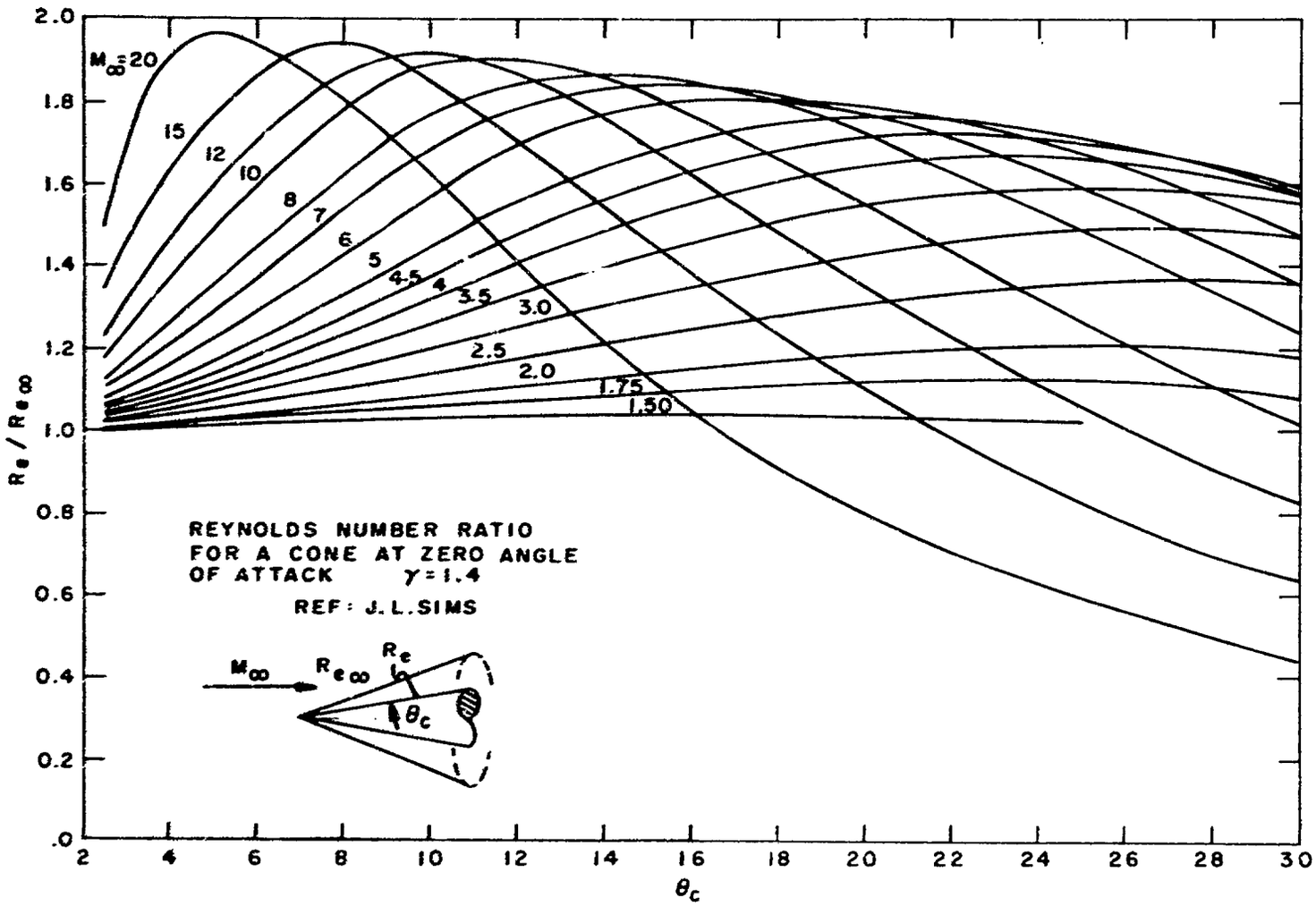
$M_\infty = 20$
15
12
10
8
7
6
5
4.5
4
3.5
3.0
2.5
2.0
1.75
1.50
REYNOLDS NUMBER RATIO
FOR A CONE AT ZERO ANGLE
OF ATTACK $\gamma = 1.4$
REF: J. L. SIMS
M_∞
$R_{e\infty}$
R_e
θ_c
$R_e / R_{e\infty}$
θ_c
2.0
1.8
1.6
1.4
1.2
1.0
0.8
0.6
0.4
0.2
.0
2
4
6
8
10
12
14
16
18
20
22
24
26
28
30

Figure A-4

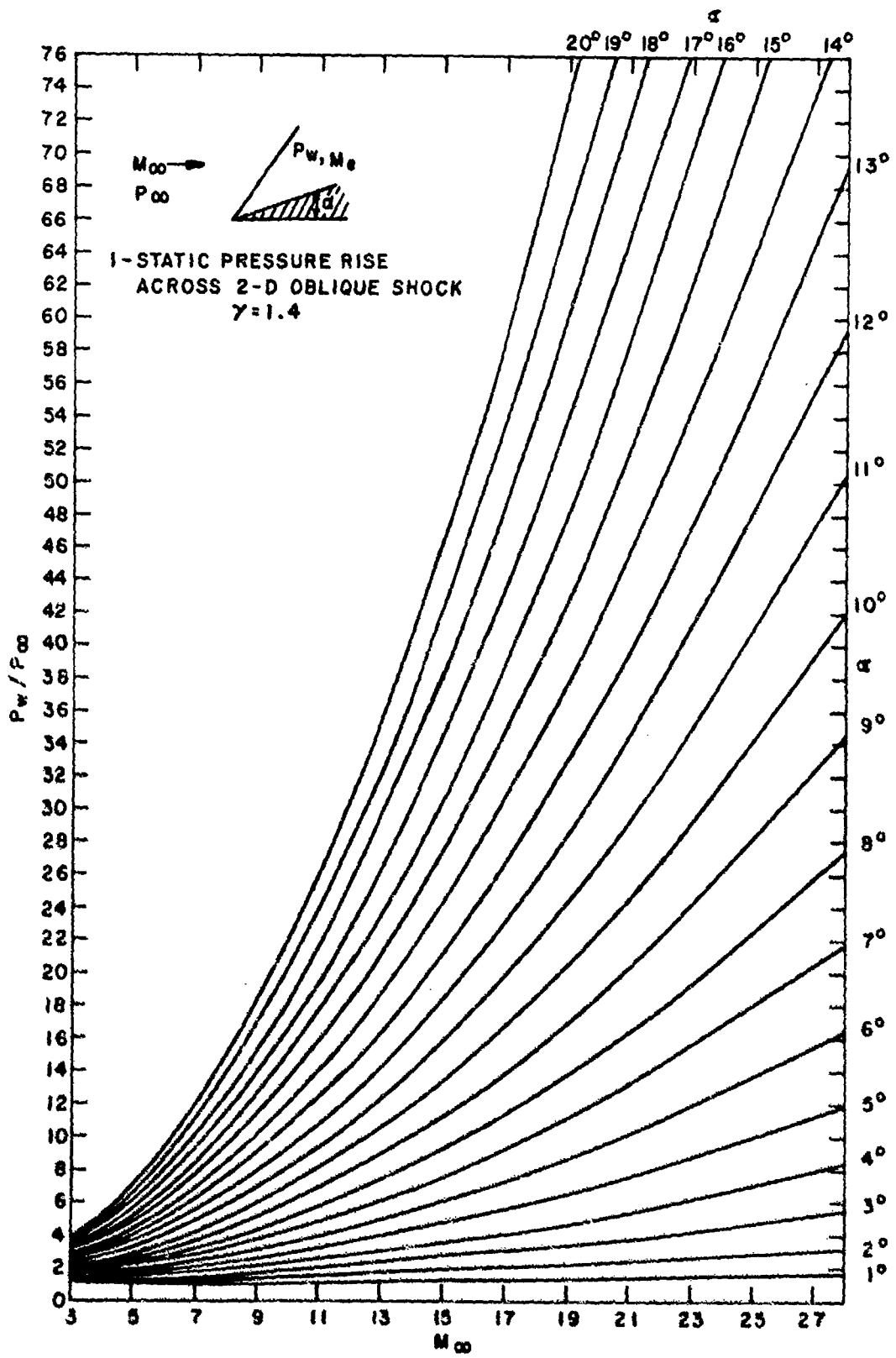
α
20° 19° 18° 17° 16° 15° 14°
13°
12°
11°
10°
9°
8°
7°
6°
5°
4°
3°
2°
1°
α
M_∞
P_∞
P_w, M_e
α
1-STATIC PRESSURE RISE
ACROSS 2-D OBLIQUE SHOCK
γ=1.4
P_w/P_∞
0 2 4 6 8 10 12 14 16 18 20 22 24 26 28 30 32 34 36 38 40 42 44 46 48 50 52 54 56 58 60 62 64 66 68 70 72 74 76
3 5 7 9 11 13 15 17 19 21 23 25 27
M_∞

Figure A-5

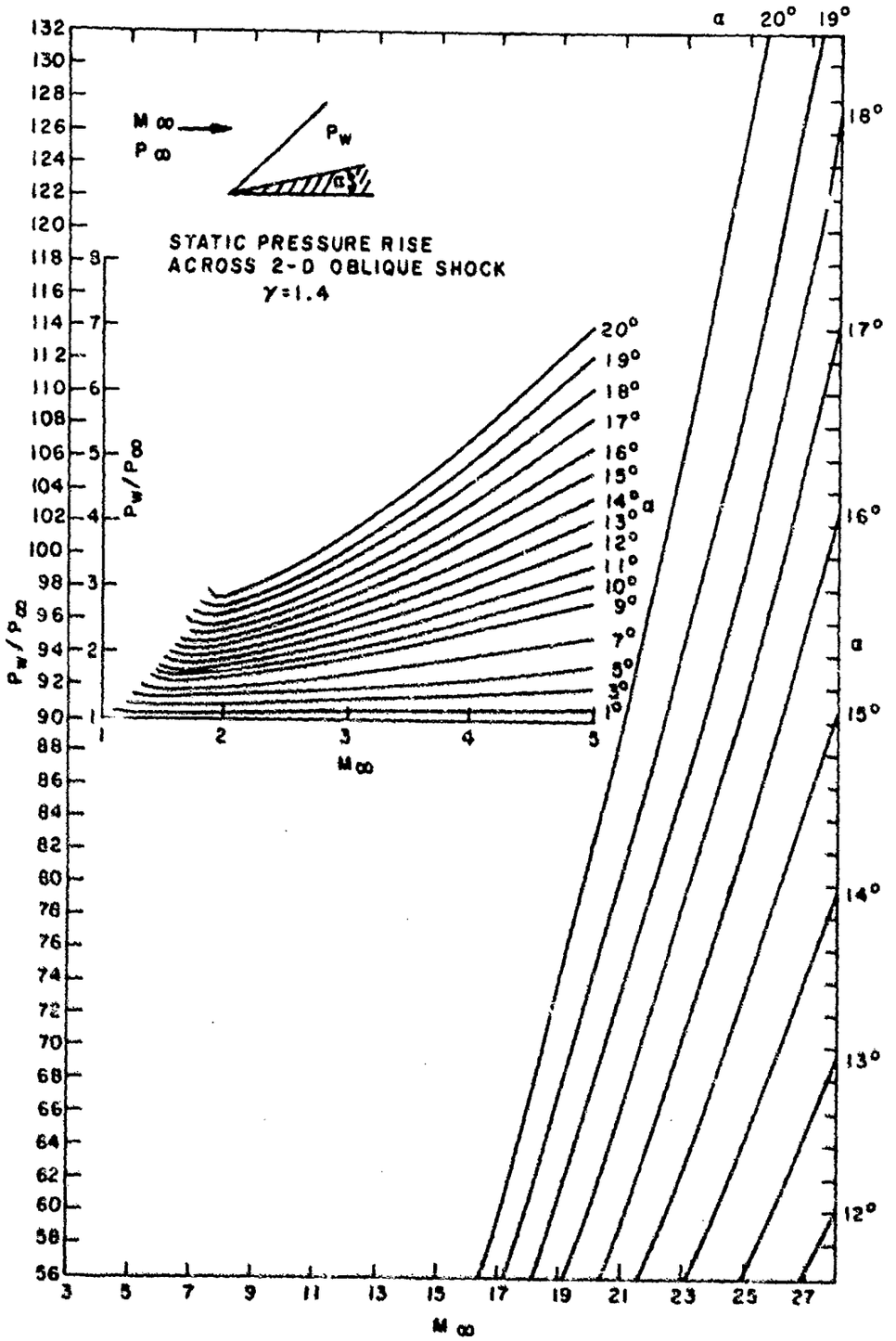
STATIC PRESSURE RISE
ACROSS 2-D OBLIQUE SHOCK
γ=1.4
M∞
P∞
Pw
α
Pw/P∞
M∞

Figure A-6

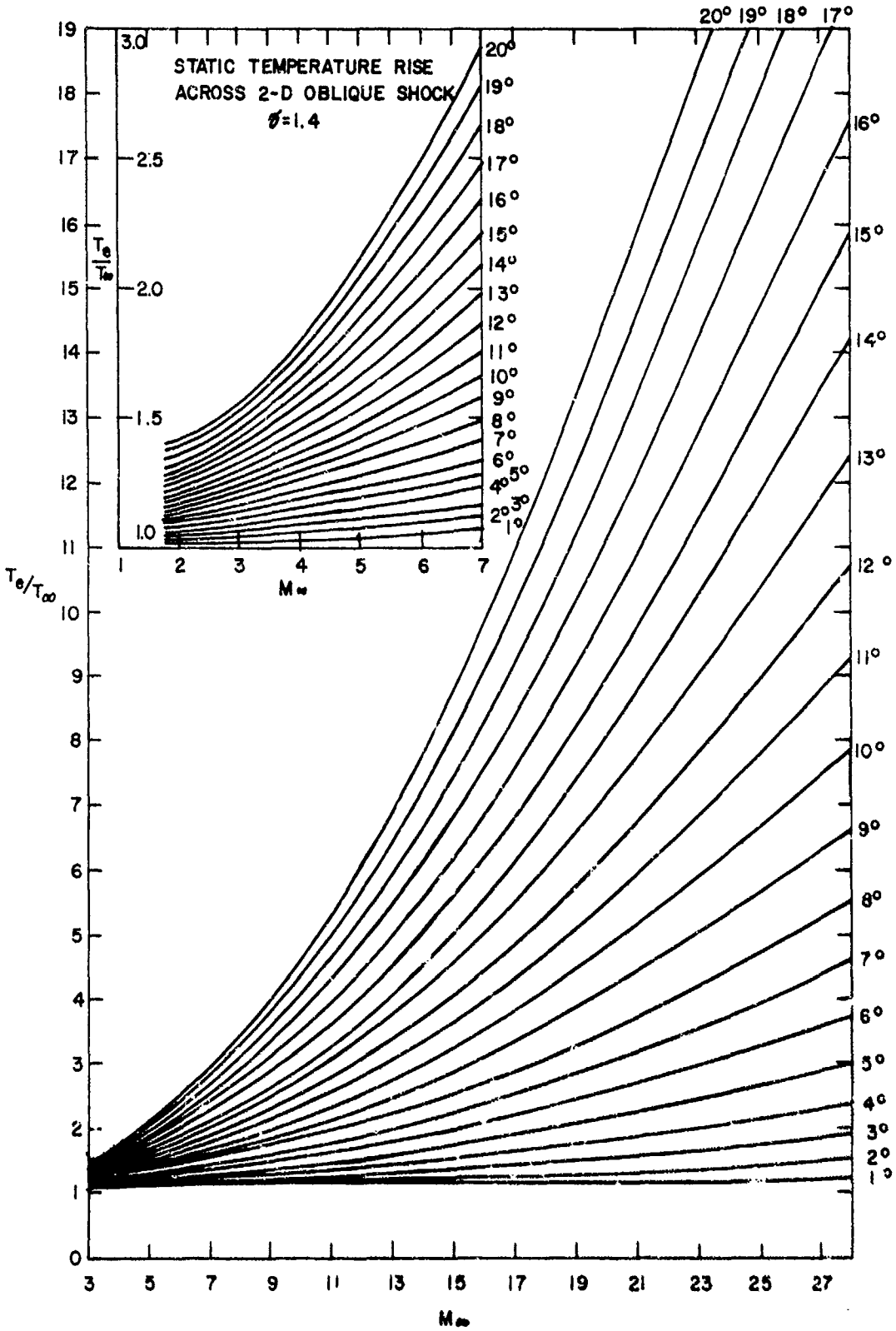
STATIC TEMPERATURE RISE
ACROSS 2-D OBLIQUE SHOCK
γ=1.4
T_e/T_∞
M_∞
20° 19° 18° 17°
16°
15°
14°
13°
12°
11°
10°
9°
8°
7°
6°
5°
4°
3°
2°
1°

Figure A-7

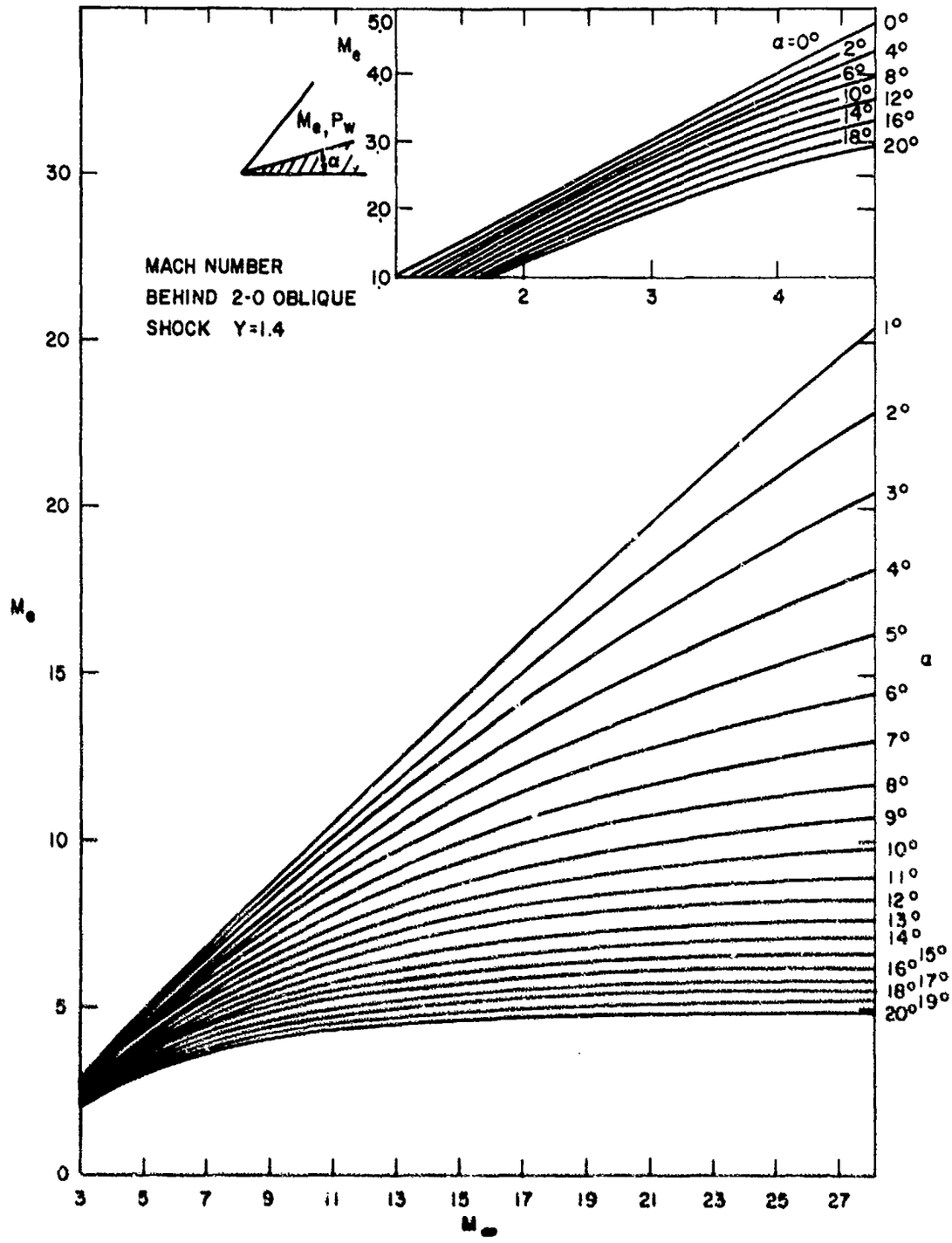
MACH NUMBER
BEHIND 2-0 OBLIQUE
SHOCK γ=1.4
M_e
M_e, P_w
α
α=0°
2°
4°
6°
8°
10°
12°
14°
16°
18°
20°
1°
3°
5°
7°
9°
11°
13°
15°
17°
19°
M_∞

Figure A-8

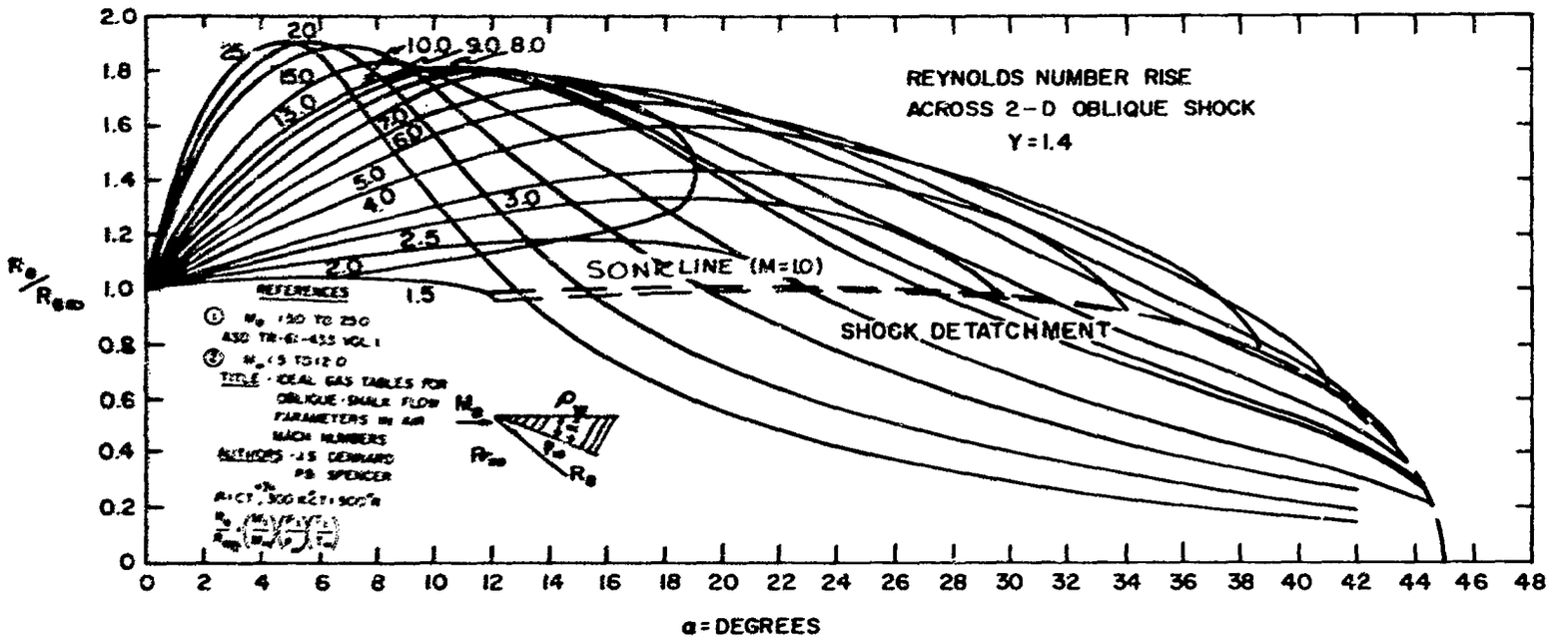
REYNOLDS NUMBER RISE
ACROSS 2-D OBLIQUE SHOCK
γ = 1.4
SONIC LINE (M=1.0)
SHOCK DETATCHMENT
$R_e/R_{e\infty}$
α = DEGREES
REFERENCES
TITLE · IDEAL GAS TABLES FOR OBLIQUE-SHOCK FLOW PARAMETERS IN AIR MACH NUMBERS
AUTHORS · J.S. DENNARD P.S. SPENCER

Figure A-9

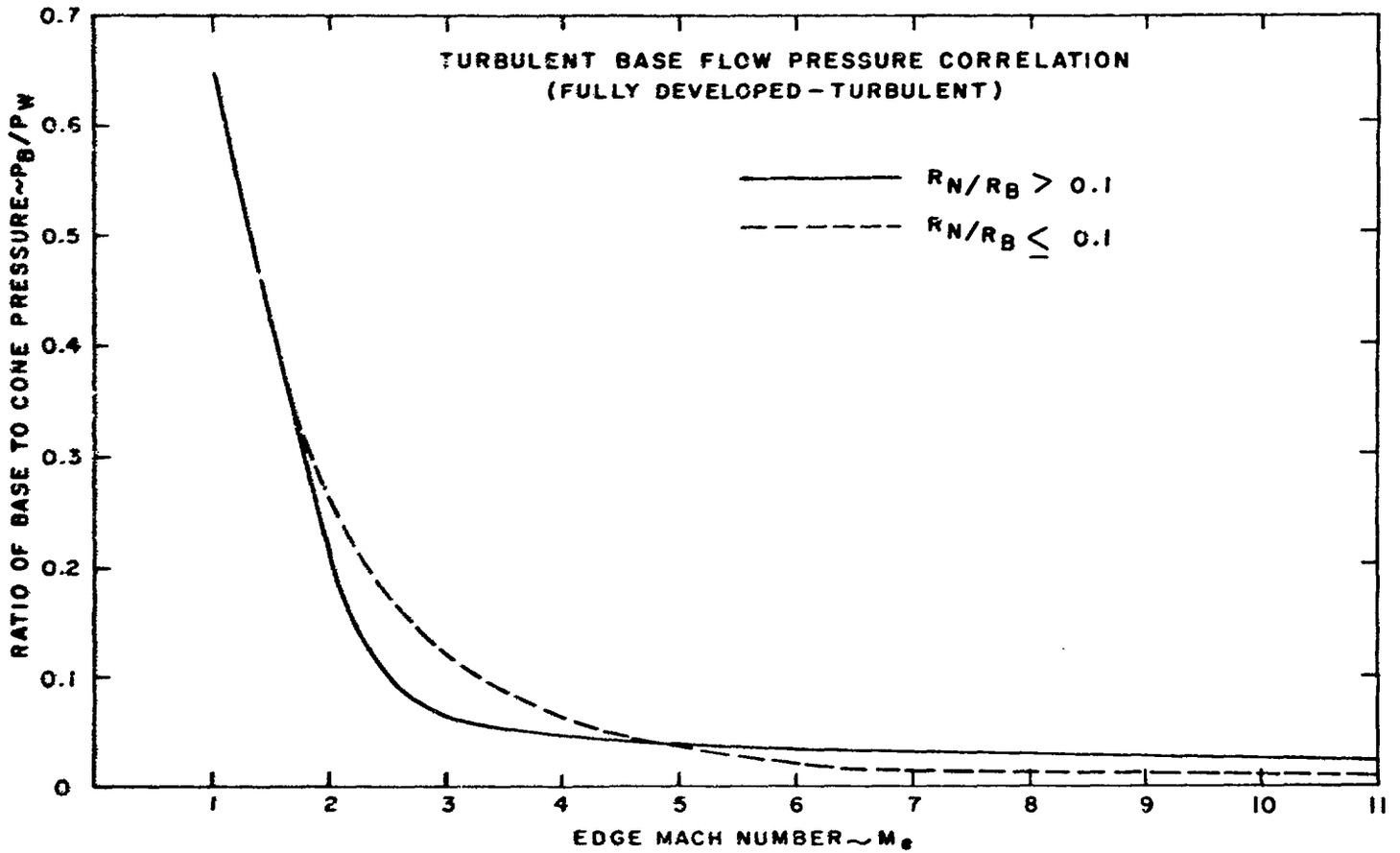
TURBULENT BASE FLOW PRESSURE CORRELATION
(FULLY DEVELOPED - TURBULENT)
$R_N/R_B > 0.1$
$R_N/R_B \leq 0.1$
RATIO OF BASE TO CONE PRESSURE ~ P_B/P_W
0.7
0.6
0.5
0.4
0.3
0.2
0.1
0
1
2
3
4
5
6
7
8
9
10
11
EDGE MACH NUMBER ~ M_e

Figure A-10

UNCLASSIFIED

Security Classification

DOCUMENT CONTROL DATA - R&D

(Security classification of title, body of abstract and indexing annotation must be entered when the overall report is classified)

1 ORIGINATING ACTIVITY (Corporate author)

General Electric - RESD
32nd and Chestnut Streets
Philadelphia, Penna. 19101

2a REPORT SECURITY CLASSIFICATION
Unclassified

2b GROUP

3 REPORT TITLE

AERO ACOUSTIC LOADS ASSOCIATED WITH HIGH-BETA RE-ENTRY VEHICLES

4 DESCRIPTIVE NOTES (Type of report and inclusive dates)

Final - February 1971 to October 1972

5 AUTHOR(S) (Last name, first name, initial)

Chaump, Louis E., Martellucci, Anthony, Monfort, Alan

6 REPORT DATE
May 1973

7a TOTAL NO. OF PAGES
147

7b NO. OF REFS
23

8a CONTRACT OR GRANT NO
F33615-71-C-1245

b PROJECT NO
147102

9a ORIGINATOR'S REPORT NUMBER(S)

9b OTHER REPORT NO(S) (Any other numbers that may be assigned this report)
AFFDL-TR-72-138, Vol. I.

10 AVAILABILITY/LIMITATION NOTICES

Distribution limited to U.S. Government agencies only; test and evaluation; statement applied 28 November 1972. Other requests for this document must be referred to AF Flight Dynamics Laboratory, (FY), Wright-Patterson AFB, Ohio 45433.

11 SUPPLEMENTARY NOTES

12 SPONSORING MILITARY ACTIVITY

Air Force Flight Dynamic Laboratory
Wright-Patterson AFB, Ohio 45433

13 ABSTRACT

Conical shaped vehicles with high ballistic coefficients are subjected during re-entry, to intense fluctuating air pressures which result in high internal sound and vibration levels. As a result of these high vibration levels internal components can be adversely affected. In order to insure reliability, vibration, test criteria are predicted based on limited experimental data at high Mach numbers and generally result in conservatism of the design. This program using prior experimental data and high Mach number data obtained in the present contract, reviews existing analytical expressions necessary to define aeroacoustic loads associated with high beta re-entry vehicles and recommends analytical expressions for transitional, fully developed turbulent, separated and base flow.

DD FORM 1473

Unclassified

Security Classification

UNCLASSIFIED

Security Classification

14. KEY WORDS	LINK A ROLE	LINK A WT	LINK B ROLE	LINK B WT	LINK C ROLE	LINK C WT
Aeroacoustic Environments						
Re-entry Vehicle						
Turbulent Flow						
Base Flow						
Transitional Flow						

INSTRUCTIONS

1. ORIGINATING ACTIVITY: Enter the name and address of the contractor, subcontractor, grantee, Department of Defense activity or other organization *(corporate author)* issuing the report.

2a. REPORT SECURITY CLASSIFICATION: Enter the overall security classification of the report. Indicate whether "Restricted Data" is included. Marking is to be in accordance with appropriate security regulations.

2b. GROUP: Automatic downgrading is specified in DoD Directive 5200.10 and Armed Forces Industrial Manual. Enter the group number. Also, when applicable, show that optional markings have been used for Group 3 and Group 4 as authorized.

3. REPORT TITLE: Enter the complete report title in all capital letters. Titles in all cases should be unclassified. If a meaningful title cannot be selected without classification, show title classification in all capitals in parenthesis immediately following the title.

4. DESCRIPTIVE NOTES: If appropriate, enter the type of report, e.g., interim, progress, summary, annual, or final. Give the inclusive dates when a specific reporting period is covered.

5. AUTHOR(S): Enter the name(s) of author(s) as shown on or in the report. Enter last name, first name, middle initial. If military, show rank and branch of service. The name of the principal author is an absolute minimum requirement.

6. REPORT DATE: Enter the date of the report as day, month, year, or month, year. If more than one date appears on the report, use date of publication.

7a. TOTAL NUMBER OF PAGES: The total page count should follow normal pagination procedures, i.e., enter the number of pages containing information.

7b. NUMBER OF REFERENCES: Enter the total number of references cited in the report.

8a. CONTRACT OR GRANT NUMBER: If appropriate, enter the applicable number of the contract or grant under which the report was written.

8b, 8c, & 8d. PROJECT NUMBER: Enter the appropriate military department identification, such as project number, subproject number, system numbers, task number, etc.

9a. ORIGINATOR'S REPORT NUMBER(S): Enter the official report number by which the document will be identified and controlled by the originating activity. This number must be unique to this report.

9b. OTHER REPORT NUMBER(S): If the report has been assigned any other report numbers *(either by the originator or by the sponsor)*, also enter this number(s).

10. AVAILABILITY/LIMITATION NOTICES: Enter any limitations on further dissemination of the report, other than those imposed by security classification, using standard statements such as:

(1) "Qualified requesters may obtain copies of this report from DDC."

(2) "Foreign announcement and dissemination of this report by DDC is not authorized."

(3) "U. S. Government agencies may obtain copies of this report directly from DDC. Other qualified DDC users shall request through _____."

(4) "U. S. military agencies may obtain copies of this report directly from DDC. Other qualified users shall request through _____."

(5) "All distribution of this report is controlled. Qualified DDC users shall request through _____."

If the report has been furnished to the Office of Technical Services, Department of Commerce, for sale to the public, indicate this fact and enter the price, if known.

11. SUPPLEMENTARY NOTES: Use for additional explanatory notes.

12. SPONSORING MILITARY ACTIVITY: Enter the name of the departmental project office or laboratory sponsoring *(paying for)* the research and development. Include address.

13. ABSTRACT: Enter an abstract giving a brief and factual summary of the document indicative of the report, even though it may also appear elsewhere in the body of the technical report. If additional space is required, a continuation sheet shall be attached.

It is highly desirable that the abstract of classified reports be unclassified. Each paragraph of the abstract shall end with an indication of the military security classification of the information in the paragraph, represented as (TS), (S), (C), or (U).

There is no limitation on the length of the abstract. However, the suggested length is from 150 to 225 words.

14. KEY WORDS: Key words are technically meaningful terms or short phrases that characterize a report and may be used as index entries for cataloging the report. Key words must be selected so that no security classification is required. Identifiers, such as equipment model designation, trade name, military project code name, geographic location, may be used as key words but will be followed by an indication of technical context. The assignment of links, rules, and weights is optional.

*U.S.Government Printing Office: 1973 — 759-494/592

Unclassified

Security Classification